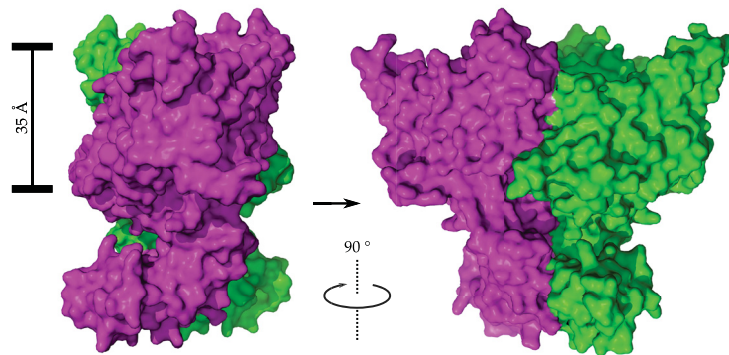




HEINRICH HEINE  
UNIVERSITÄT DÜSSELDORF

# CLC CHLORIDE CHANNELS IN INHERITED DEAFNESS AND HYPERALDOSTERONISM



INAUGURAL-DISSERTATION ZUR ERLANGUNG DES DOKTORGRADES DER MATHEMATISCH-  
NATURWISSENSCHAFTLICHEN FAKULTÄT DER HEINRICH-HEINE-UNIVERSITÄT DÜSSELDORF

VORGELEGT VON

HUA TAN (譚華)

AUS HENGYANG, HUNAN, CHINA

DÜSSELDORF · JÜLICH, MAI 2018

aus dem Institut für Zelluläre Biophysik (ICS-4)  
des Forschungszentrum Jülich  
und der Mathematisch-Naturwissenschaftlichen Fakultät  
der Heinrich-Heine-Universität Düsseldorf

Gedruckt mit der Genehmigung der  
Mathematisch-Naturwissenschaftlichen Fakultät der  
Heinrich-Heine-Universität Düsseldorf

Berichterstatter:

1. Prof. Dr. med. Christoph Fahlke
2. Prof. Dr. Henrike Heise

Tag der mündlichen Prüfung:

# *Acknowledgements*

In the middle of April 2014 I got an answer from Christoph that he offered me a PhD job position in his lab. I don't know how much he has regretted his decision since then. But life has no regrets! As time flies and this journey is approaching the end and I'm getting close to a time point to say goodbye, I want to thank him, not (just) out of an expectation of a decent mark for this thesis, but (also) for his supervision, support and tolerance to my idleness. However, one of the best gifts from Christoph is his designating Gabriel as my co-supervisor in ICS-4.

It was a big fortune for me to work with Gabriel in the past years. Gabriel is not only a great supervisor that helped me learn to do science, but also a friend and a big brother to me. For a PhD student who comes from such a different country and stays alone in Germany, the tough challenges are often not from work, but from outside of work. I sincerely appreciate that on those frigid overcast days Gabriel gave me tremendous support, strength and courage, and made me finally come through. These unforgettable memories will still give me strength and courage many years later in my life.

Many thanks to Prof. Heise to be the mentor of my PhD project.

I thank all the colleagues in ICS-4 institute, particular the technicians, your support provided me terrific convenience for my work. It was a pleasure to work with you.

I wanted to thank my parents. Even though since I moved to the other side of this planet you two never called me first (I always believe it is not the reason that the international phone call is pretty expensive), I believe most of the time you are aware that you still have a lovely son, somewhere.

Again, I greatly appreciate the days that I spent with Christoph and Gabriel in ICS-4. These experiences must become the most unforgettable ones in my life.



# *Abstract*

The CLC chloride channel family is responsible for the transmembrane movement of the most abundant anion in the human body,  $\text{Cl}^-$ . Proteins from this family are involved in many physiological functions, such as proper transport of chloride across epithelia, maintenance of cytoplasmic or vesicular  $\text{Cl}^-$  and  $\text{H}^+$  concentrations as well as regulating cellular excitability. Mutations of CLCs have been identified in many genetic diseases. Unraveling the underlying pathology often helped to also better understand the physiology of these channels and transporters. In this thesis we characterized several naturally occurring mutations in *CLC-K/barttin* and *CLC-2* channels in different diseases to facilitate such understanding.

*CLC-Ka* and *-Kb* channels are found in nephron epithelia and in the marginal cells of the inner ears. They play a pivotal role in renal urine concentration and hearing. Barttin is the  $\beta$ -subunit of *CLC-K* channels, essential for maturation, proper sorting and gating of the channel. Loss-of-function of barttin typically abolishes function of *CLC-K* channels and leads to Bartter syndrome type IV, with symptoms such as renal failure and hearing loss. In the first part of this thesis, we characterized the barttin V33L mutation, which only led to the isolated occurrence of deafness but not renal disease in a Pakistani family. We conclude that the only partly decreased *CLC-K* membrane conductance may account for this particular phenotype.

*CLC-2* is widely expressed in many tissues. It has been suggested to be important for maintenance of cytosolic  $\text{Cl}^-$  levels and the resting membrane potential. In the second part of this thesis we studied several mutations within the coding region of the *CLCN2* gene. These mutations were identified in patients suffering from primary hyperaldosteronism. We discovered that these mutations increased the open probability of the channel in HEK293T cells, resulting in a gain-of-function. HAC15 cells expressing mutant *CLC-2* were found to be constitutively depolarized resulting in an enhanced expression of aldosterone synthase. We concluded that the gain-of-function of these *CLC-2* mutants likely increases the resting potential of native zona glomerulosa, ending up with excessive and unregulated production of aldosterone.



# Contents

<b>Acknowledgements</b>	<b>I</b>
<b>Abstract</b>	<b>III</b>
<b>1 Introduction</b>	<b>1</b>
1.1 Overview of Human CLC Family . . . . .	1
1.2 Physiology of CLC . . . . .	3
1.2.1 CLC-K/barttin . . . . .	3
1.2.2 CLC-2 . . . . .	6
1.2.3 Other Members of the CLC Family . . . . .	8
<b>2 Publications</b>	<b>11</b>
2.1 Reduced Membrane Insertion of CLC-K by V33L Barttin Results in Loss of Hearing, but Leaves Kidney Function Intact . . . . .	12
2.2 CLCN2 Chloride Channel Mutations in Familial Hyperaldosteronism Type II . . . . .	23
<b>3 Discussion</b>	<b>91</b>
3.1 Contribution from Our Studies . . . . .	91
3.2 Genetic Mutations Impair Behavior and Phenotype of CLC-K/barttin and CLC-2 Ion Channels . . . . .	92
3.2.1 Loss of Channel Activity and Phenotype . . . . .	92
3.2.2 Gain-of-Function . . . . .	94
<b>Bibliography</b>	<b>97</b>
<b>Zusammenfassung</b>	<b>103</b>
<b>Erklärung</b>	<b>105</b>



# Chapter 1

## Introduction

### 1.1 Overview of Human CLC Family

The chloride ion ( $\text{Cl}^-$ ) is an essential anion of life, playing an important role in the maintenance of cellular homeostasis and signal propagation. Chloride ions may cross the lipid bilayer of cells through specific chloride channels or transporters, some well known examples of which are the CLC family<sup>[1]</sup>, the CFTR (Cystic Fibrosis Transmembrane Conductance Regulator) family<sup>[2]</sup> and the ligand-gated  $\text{GABA}_A$  receptor family<sup>[3]</sup>.

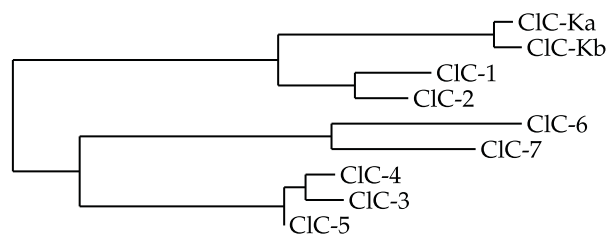


**Figure 1.1:** The phylogenetic tree of the human CLC family. The tree was generated using Phylogeny.fr<sup>[4,5]</sup> based on the canonical sequence of each protein. The UniProt accession numbers are P51800 for CLC-Ka, P51801 for CLC-Kb, P35523 for CLC-1, P51788 for CLC-2, P51790 for CLC-3, P51793 for CLC-4, P51795 for CLC-5, P51797 for CLC-6 and P51798 for CLC-7.

The first member of the CLC family, named CLC-0, was cloned from the electric organ of *Torpedo marmorata* in 1990<sup>[6]</sup>. Since then, nine homologs of CLC-0 (Figure 1.1) have been identified in the human genome. CLC-1, -2, -Ka and -Kb have been demonstrated to form chloride channels<sup>[7-9]</sup>, while CLC-3 to -7 were surprisingly identified as  $\text{Cl}^-/\text{H}^+$  exchange transporters (antiporters)<sup>[10-14]</sup>. Different from ion channels, they mediate transport of chloride ions coupled stoichiometrically with the transport of protons in the opposite direction. While the channels of the human CLC family mostly contribute to the chloride conductance of the plasma membrane, antiporters are typically localized in intracellular vesicles regulating pH and intravesicular  $\text{Cl}^-$  concentrations.

Based on single channel recordings, it has been known that CLC proteins contain two separate conduction pathways, long before the molecular identity of these channels was



## 1.2 Physiology of CLC

### 1.2.1 ClC-K/barttin

The human chloride channels ClC-Ka and -Kb are encoded by the separate genes *CLC-NKA* and *CLCNKB*. Nevertheless, their sequences are 91% identical and their expression pattern is strongly overlapping. They were labeled as “ClC-K” because they were first identified in the nephron epithelia of kidneys<sup>[7,28–30]</sup>. Immunostaining of ClC-K2 (homolog of the human ClC-Kb) in ClC-K1 (homolog of ClC-Ka) knockout mice showed that the ClC-K2 channel was widely expressed in the basolateral membrane of the ascending limb of the loop of Henle, the distal tubule and the cortical collecting duct<sup>[31]</sup>. Immunostainings further indicated that ClC-K channels are also expressed in marginal cells within the stria vascularis of the inner ear<sup>[7]</sup>. Both, ClC-Ka and ClC-Kb belong to the chloride channel group of the CLC family showing strong preference for expression in the basolateral plasma membrane of epithelial cells<sup>[7,30]</sup>. The formation of functional ClC-K channels in human cells requires the essential  $\beta$ -subunit, barttin, which is encoded by the *BSND* (Bartter syndrome with sensorineural deafness) gene. Barttin modulates the gating and targets ClC-K channels to their proper subcellular localization<sup>[7,32,33]</sup>. In comparison with ClC-1 and ClC-2<sup>[34]</sup>, ClC-Ka/barttin has an unusually high single channel conductance ( $\sim 40$  pS, more than ten times larger than the single channel conductance of ClC-1 and ClC-2) and a high open probability that is almost voltage-independent under physiological conditions<sup>[35–37]</sup>. Such single channel properties will render lipid membranes very conductive to  $\text{Cl}^-$ , suggesting that ClC-Ka-expressing cells may mediate rapid transepithelial transport of  $\text{Cl}^-$ . The function of this transepithelial transport could be increased or decreased by changing the availability of functional ClC-Ka/barttin channels in the surface membrane.

### Bartter Syndrome

The kidney is an important excretory organ in the human body. Its smallest functional unit is the nephron, thousands of which can be found within the organ. In the nephron (Figure 1.3A), the initial urine forms via hemofiltration from the capillaries in Bowman’s capsule and flows sequentially through the proximal convoluted tubule, the loop of Henle, the distal convoluted tubule and the collecting duct from where the final urine leaves the kidney and is further transported towards the bladder. The initial urine contains a large amount of amino acids, sugars and salts. During the flow of the urine along the tubules of the nephron, the vast majority of nutrients and water are reabsorbed into the blood. This process of reabsorption requires ion channels and transporters which show specific expression patterns along the epithelia of the nephron tubules. Most water, organic compounds and ions are already reabsorbed in the proximal convoluted tubule. In the loop of Henle, the fluid is further concentrated in the descending limb through a selective reabsorption of water, resulting in an increase in the osmolarity of the fluid, and NaCl being subsequently reabsorbed in the ascending limb. The distal convoluted tubule and the collecting duct then determine the final

concentrations of salts, pH and water in urine and body. Components that are not reabsorbed, including metabolic waste, toxicants and small amount of inorganic salts are excreted along with the residual water in the final urine.

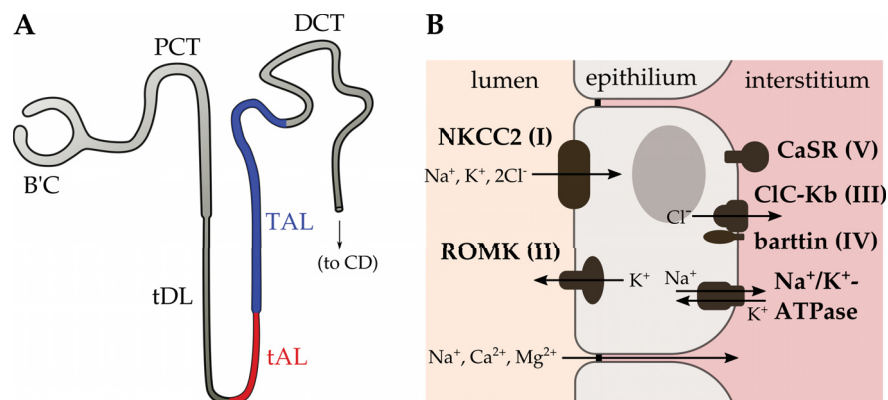


**Figure 1.3:** (A): Structure of human nephron. B'C, Bowman's capsule; PCT, proximal convoluted tubule; tDL, thin descending limb of Henle's loop; tAL, thin ascending limb of Henle's loop, indicated in red, where CIC-Ka is mostly expressed; TAL, thick ascending limb of Henle's loop, indicated in blue, where CIC-Kb is predominantly expressed; DCT, distal convoluted tubule; CD, collection duct. (B): The disease-causing proteins in epithelia of TAL involved in Bartter syndrome, with the corresponding type indicated in the parenthesis.

**Table 1.1:** An overview of different types of Bartter syndrome.

Type	Defect gene	Defect protein	Featuring phenotype
I	<i>SLC12A1</i> <sup>[38]</sup>	SLC12A1 (NKCC2)	neonatal, hypocalcemia
II	<i>KCNJ1</i> <sup>[39]</sup>	ROMK (Kir1.1 / KCNJ1)	neonatal, hypocalcemia
III	<i>CLCNKB</i> <sup>[40]</sup>	CIC-Kb	postnatal, growth retardation
IVa	<i>BSND</i> <sup>[41]</sup>	barttin	prenatal, deafness
IVb	<i>CLCNKA</i> & <i>-KB</i> <sup>[42]</sup>	CIC-Ka & -Kb	prenatal, deafness
V	<i>CASR</i> <sup>[43,44]</sup>	CaSR	hypocalcemia

Bartter syndrome refers to a class of disorders in salt reabsorption along the thick ascending limb of loop of Henle with symptoms including pronounced salt wasting, hypokalemic metabolic alkalosis and hypercalciuria. The first case was reported by F. Bartter and his colleagues in 1962<sup>[45]</sup>. To date, five types of Bartter syndrome have been described (Table 1.1) and each of them has been associated to mutations in a specific causative gene<sup>[46]</sup>. Type I is caused by dysfunction of the Na-K-2Cl co-transporter SLC12A1 (NKCC2), type II by the potassium channel ROMK (Kir1.1 or KCNJ1), type III by CIC-Kb, type IV by barttin (IVa) or by simultaneous dysfunction of CIC-Ka and CIC-Kb (IVb) and type V by CaSR (calcium-sensing receptor).

As shown in Figure 1.3, CIC-Kb/barttin channels are a key component in the process of chloride reabsorption. In the epithelium of the thick ascending limb of Henle, Cl<sup>-</sup> is taken up by NKCC2 in the apical side from the lumen and exits the cell on the basolateral side via CIC-Kb into the interstitium. Disruption of CIC-Kb function would lead to accumulation of Cl<sup>-</sup> in the cytoplasm, leading to inhibition of NKCC2,

thereby also prohibiting the uptake of  $K^+$  and  $Na^+$ . Physiologically, because  $K^+$  recycles from the cell via ROMK back into the urine, the uptake of  $Cl^-$  leads to an imbalance in the absorbed charge, generating a transepithelial electric potential. Such potential is necessary for the paracellular transport of  $Na^+$ ,  $Ca^{2+}$  and  $Mg^{2+}$ , as shown in Figure 1.3. Therefore dysfunction of  $ClC-K$ /barttin channels causes not only a loss of  $Cl^-$  but also other electrolytes.

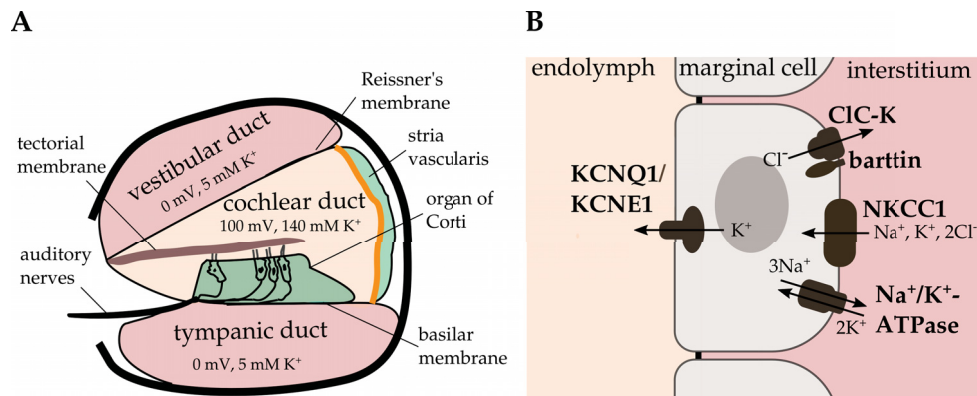


**Figure 1.4:** (A): Illustration of cochlea section. *Stria vascularis* is the narrow area where the high positive endocochlear potential is formed<sup>[47,48]</sup>. It is comprised of multiple layers of cell types with the one facing the endolymph being the marginal cell layer, marked in orange color. (B): The channels and transporters expressed in the marginal cells. Note, both  $ClC-Ka$  and  $-Kb$  are present in marginal cells.

In the cochlea,  $ClC-K$  channels are located in the basolateral membrane of marginal cells of the *stria vascularis* and dark cells<sup>[7]</sup> of the vestibular organs. The cochlea is the core component of hearing, responsible for transducing mechanical sound waves into electrical signals for neuronal propagation. As shown in Figure 1.4A, separated by two membranes, Reissner's membrane and the basilar membrane, the cochlea includes three differentiated chambers or ducts: the vestibular duct (*scala vestibuli*), the tympanic duct (*scala tympani*) and the cochlear duct (*scala media*). The first two ducts contain perilymph while the cochlear duct contains endolymph. Perilymph has an extracellular ionic composition similar to plasma, with high  $Na^+$  and low  $K^+$  concentrations<sup>[49]</sup>. In contrast to perilymph, the endolymph, which is generated in the *stria vascularis*, has a higher concentration of  $K^+$  than  $Na^+$ <sup>[50]</sup> and thus a potential  $\sim 100$  mV more positive than perilymph relative to the surrounding tissue. Such ionic composition and endocochlear potential suits the function of cochlea. Bathed in endolymph, the hair cells take up  $K^+$  from endolymph to depolarize after receiving a sound stimulus. In this process, the high endocochlear potential is the driving force for the uptake of  $K^+$ . The depolarized hair cells release neurotransmitters which are then captured by the synaptic receptors of the auditory neurons, transducing the sound stimuli into neuronal signals. The high  $K^+$  concentration and electric potential are thus necessary for depolarization of the hair cells.  $ClC-K$ /barttin channels have been demonstrated to play a significant role in generating the endocochlear potential<sup>[47,48]</sup>.

Apart from the renal Bartter syndrome phenotype, type IV patients also exhibit impaired hearing, likely because the function of both  $ClC-Ka$  and  $-Kb$  are similarly affected<sup>[41,42,51]</sup>. Assuming that  $ClC-Ka$  and  $-Kb$  channels were both expressed in the marginal cells of the

ear, they could compensate for each other to some degree explaining why dysfunction of CIC-Kb alone does not lead to hearing loss (type III patients do not exhibit deafness). An alternative explanation would be that CIC-Ka, instead of CIC-Kb, dominates in marginal cells, however, there is no direct evidence to support this hypothesis. It has not been reported whether the CIC-K1 knockout mouse is deaf<sup>[52]</sup> and there is no case report about an isolated dysfunction of CIC-Ka. The patients carrying barttin I12T and V33L<sup>[35,37]</sup>, as further reported in this thesis, suffer only from deafness but not kidney disease which corresponds to an impairment of both, CIC-Ka and CIC-Kb, function with a remaining residual activity.

### 1.2.2 CIC-2

Together with CIC-1 (see Section 1.2.3), CIC-2 (encoded by the *CLCN2* gene) belongs to another branch in the CLC family, as shown in Figure 1.1. CIC-2 is an ion channel located in the plasma membrane and produces slowly activating, inwardly rectifying currents with a single channel conductance around 4.5 pS as measured in Flp-In T-rex 293 cells<sup>[34]</sup>. CIC-2 has been found in many epithelia and various cell types of the nervous system<sup>[53,54]</sup>. A well studied physiological example is the basolateral membrane of the distal colon epithelium, where CIC-2 provides a Cl<sup>-</sup> exit pathway facilitating Cl<sup>-</sup> and subsequently water absorption<sup>[55]</sup> similar to the role of CIC-Kb in the basolateral membrane of the thick ascending limb of Henle's loop. In the nervous system, CIC-2 putatively assists Cl<sup>-</sup> extrusion from the cells, stabilizing the membrane potential and modulating cellular excitability<sup>[56]</sup>. In addition, CIC-2 has been proposed to maintain a low intracellular Cl<sup>-</sup> concentration necessary for inhibitory GABA responses<sup>[57]</sup>. Impairment of CIC-2 function has been related to numerous hereditary human diseases such as epilepsy, leukoencephalopathy and now hyperaldosteronism type II<sup>[58-60]</sup>. Complete disruption of *Clcn2* gene in mice leads to degeneration of the retina and the testes as the formation of blood-testis and blood-retina barriers relies CIC-2 function in the corresponding epithelial supporting cells<sup>[61]</sup>. Suggesting a similar role in brain, recent studies demonstrated a localization of CIC-2 in astrocytes along local blood vessels<sup>[62]</sup>.

#### ***CLCN2* As a Candidate Gene for Primary Hyperaldosteronism**

Aldosterone is a mineralocorticoid hormone produced by the cells in the zona glomerulosa layer of the adrenal cortex in the adrenal gland. It mainly binds to the mineralocorticoid receptors in the distal tubules and collecting ducts of the nephron, triggering an increased expression of proteins facilitating the reabsorption of Na<sup>+</sup> from and excretion of K<sup>+</sup> into the urine. The reabsorbed Na<sup>+</sup> increases the osmolarity of the renal medulla and facilitates the reabsorption of water, thereby increasing the blood volume and blood pressure. Therefore, aldosterone is an important modulator of the homeostasis of Na<sup>+</sup>, K<sup>+</sup> and water of the body as well as being able to influence the arterial blood pressure.

Production of aldosterone is the result of a body-wide signalling cascade called the renin-angiotensin system (RAS), or called the renin-angiotensin-aldosterone system

(RAAS), as illustrated in Figure 1.5. The kidney secretes renin when blood flow slows down as in a drop of blood pressure or during states of dehydration. Renin actively cleaves the constitutively produced angiotensinogen (synthesized in the liver) into angiotensin I. This hormone is then converted by the angiotensin-converting enzyme (ACE) in the lung into angiotensin II. Angiotensin II can bind to the angiotensin II G-protein-coupled-receptor which is expressed, among other tissues, on the cell surface of zona glomerulosa leading to a closure of background potassium channels and cell depolarization. Additional stimuli for aldosterone production are an increase in the plasma potassium concentration or, to a lesser extent, factors such as the adrenocorticotrophic hormone (ACTH).

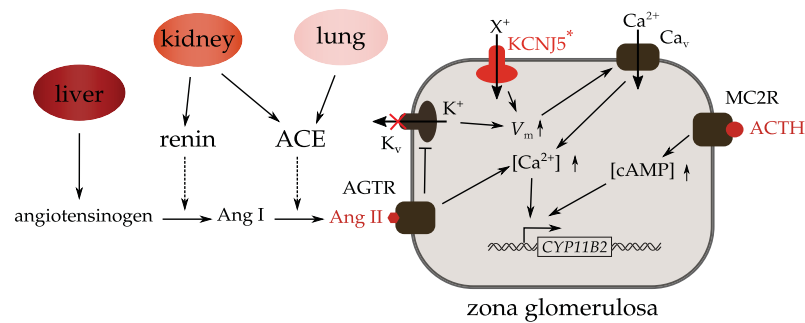


**Figure 1.5:** Regulation of aldosterone production in zona glomerulosa.  $KCNJ5^*$  indicates the  $KCNJ5$  protein that bears the G151R or L168R mutation which abolishes the  $K^+$  selectivity of the channels. The lost selectivity of  $KCNJ5$  increases the membrane permeability to  $Na^+$  and depolarizes the membrane. In contrast, the activated angiotensin II receptor (AGTR) closes the potassium channel, decreases the membrane permeability to  $K^+$  and also depolarizes the membrane. Both processes depolarize the membrane and enhances the production of aldosterone, but the difference is the latter pathway is under control of normal cell signaling. Ang, angiotensin; ACE, angiotensin-converting enzyme; AGTR, angiotensin II receptor;  $V_m$ , membrane potential; ACTH, adrenocorticotrophic hormone; MC2R, melanocortin 2 receptor.

Excessive and unregulated production of aldosterone leads to primary hyperaldosteronism, also called Conn's syndrome, with typical symptoms such as low blood potassium levels and high blood pressure — the opposite conditions that physiologically trigger aldosterone production. Primary hyperaldosteronism is caused either by adrenal tumors or enhancement of aldosterone biosynthesis in — otherwise normal — zona glomerulosa cells. The aldosterone synthase protein encoded by *CYP11B2* is the rate-limiting enzyme in aldosterone synthesis. Because *CYP11B2* transcription and function requires  $Ca^{2+}$  or cAMP<sup>[63,64]</sup>, as shown in Figure 1.5, any factor that results in the constitutive elevation of these second messengers may cause primary hyperaldosteronism. Examples for this concept are mutations of the potassium channel  $KCNJ5$  (Kir3.4) or the calcium channels *CACNA1D* ( $Ca_v1.3$ ) or *CACNA1H* ( $Ca_v3.2$ ). The mutations G151R and L168R in Kir3.4 abolish the  $K^+$  selectivity of the channel, making the channel  $Na^+$ -permeable and resulting in constitutive membrane depolarization. This increase in the membrane potential activates the influx of  $Ca^{2+}$  via L- and T-type calcium channels<sup>[65]</sup>. Mutations in *CACNA1H*<sup>[66]</sup> and *CACNA1D*<sup>[67]</sup> enhance channel activity, particularly close to the resting membrane potential, suggesting higher  $Ca^{2+}$ -influx and thus unregulated aldosterone synthesis.

### 1.2.3 Other Members of the CLC Family

#### CIC-1

CIC-1 modulates the electric excitability of the skeletal muscle cells by mediating Cl<sup>-</sup> transport across the plasma membrane. CIC-1 is mainly located in the plasma membrane, though it has a small single channel conductance (2 – 3 pS)<sup>[34,68,69]</sup>. In fact, CIC-1 is the dominant mediator of the muscle Cl<sup>-</sup> conductance (~80% of the resting conductance), therefore it contributes to maintenance of the resting potential<sup>[70]</sup>. In a surprising addition, expression of CIC-1 was also found in various areas in human brain and heart, suggesting CIC-1 plays a role in these areas<sup>[71]</sup>.

#### CIC-3

CIC-3 is a chloride/proton antiporter widely expressed in many different cell types derived from neuroectoderm. They are found located in the membranes of the intracellular vesicles such as lysosomes, endosomes and synaptic vesicles<sup>[72-75]</sup>. Transfection of CIC-3 HEK293T cells results in small, outwardly rectifying currents in whole cell patch clamp recordings<sup>[75,76]</sup>. *Clcn3*<sup>-/-</sup> mice exhibit a severe postnatal degeneration of hippocampus and retina indicating that CIC-3 may play a pivotal role in the nervous system<sup>[77]</sup>. A recent study suggests CIC-3 may also be involved in a mechanism against myocardial ischemia<sup>[78]</sup>.

#### CIC-4

CIC-4 can be found in many tissues, but predominantly in brain<sup>[79]</sup>. Similar to CIC-3, the heterologously expressed CIC-4 resides mostly in the endoplasmic reticulum although a small fraction of proteins still reach the plasma membrane as indicated by outwardly rectifying currents in *Xenopus* oocytes<sup>[80]</sup> and HEK293T cells<sup>[81]</sup>. In mammalian cells, CIC-4 tends to associate with CIC-3 into heterodimers rather than with another CIC-4 monomer into homodimeric transporters<sup>[82]</sup>. In the presence of CIC-3, CIC-4 is sorted to late endosome/lysosomes or recycling endosomes, dependent on the splice variant of the associated CIC-3<sup>[82]</sup>. This finding indicates CIC-4 may not work independently, but only together with other CLC transporters such as CIC-3. Recently, several CIC-4 mutations were found in cases of X-linked intellectual disability and epilepsy<sup>[83,84]</sup>.

#### CIC-5

CIC-5 can be found in the brain or epithelia of kidney or intestine<sup>[85]</sup>, located in endosomes<sup>[86]</sup>. The outwardly rectifying currents mediated by CIC-5 upon transfection in HEK293T cells indicate significant surface membrane localization of CIC-5 in heterologous expression systems<sup>[80]</sup>. CIC-5 is involved in the acidification and Cl<sup>-</sup> accumulation

of early endosomes<sup>[87]</sup>, which is necessary for proper trafficking of endosomes<sup>[88]</sup>. Impairment of ClC-5 function leads to impairment of endocytosis<sup>[89]</sup>. Being important for endocytosis in the proximal convoluted tubule, ClC-5 impairment causes Dent's disease with symptoms such as recurrent kidney stones and nephrocalcinosis<sup>[90]</sup>.

### ClC-6

ClC-6 protein was exclusively detected in the nervous system, mainly located in late endosomes<sup>[91]</sup>. Heterologous expression experiments indicated ClC-6 as a Cl<sup>-</sup>/H<sup>+</sup> antiporter with outwardly rectifying currents<sup>[13]</sup>. *Clcn6*<sup>-/-</sup> suggested ClC-6 might be involved in a postnatal lysosomal storage disease and a rare form of human neuronal ceroid lipofuscinosis<sup>[91]</sup>. There is no case report so far about involvement of the *CLCN6* gene in human diseases.

### ClC-7

ClC-7 is widely expressed in many tissues and predominantly located in the lysosomal membrane of both native cells and transfected cells<sup>[92,93]</sup>. The *Clcn7*<sup>-/-</sup> mice displayed osteopetrosis, neurodegeneration and lysosomal storage disease but no changes of lysosomal pH in cultured neurons<sup>[92]</sup>. However, the lysosomal Cl<sup>-</sup> concentration in the knockout mice was found to be lower than in wild type mice<sup>[94]</sup>. How the lowered Cl<sup>-</sup> may account for the phenotypes displayed in the knockout mice remains unclear.



## **Chapter 2**

# **Publications**



# Reduced Membrane Insertion of CLC-K by V33L Barttin Results in Loss of Hearing, but Leaves Kidney Function Intact

Hua Tan, Stefanie Bungert-Plümke, Christoph Fahlke\* and Gabriel Stölting\*

Institute of Complex Systems - Zelluläre Biophysik (ICS-4), Forschungszentrum Jülich, Jülich, Germany

## OPEN ACCESS

### Edited by:

Francisco Javier Alvarez-Leefmans,  
Wright State University, USA

### Reviewed by:

Xavier Gasull,  
University of Barcelona, Spain  
Jorge Arreola,  
Universidad Autónoma de San Luis  
Potosí, Mexico

### \*Correspondence:

Christoph Fahlke  
c.fahlke@fz-juelich.de  
Gabriel Stölting  
g.stoelting@fz-juelich.de

### Specialty section:

This article was submitted to  
Membrane Physiology and Membrane  
Biophysics,  
a section of the journal  
Frontiers in Physiology

**Received:** 21 February 2017

**Accepted:** 12 April 2017

**Published:** 15 May 2017

### Citation:

Tan H, Bungert-Plümke S, Fahlke Ch  
and Stölting G (2017) Reduced  
Membrane Insertion of CLC-K by  
V33L Barttin Results in Loss of  
Hearing, but Leaves Kidney Function  
Intact. *Front. Physiol.* 8:269.  
doi: 10.3389/fphys.2017.00269

In the mammalian ear, transduction of sound stimuli is initiated by  $K^+$  entry through mechano-sensitive channels into inner hair cells.  $K^+$  entry is driven by a positive endocochlear potential that is maintained by the marginal cell layer of the stria vascularis. This process requires basolateral  $K^+$  import by  $NKCC1 Na^+ - 2Cl^- - K^+$  co-transporters as well as  $Cl^-$  efflux through  $ClC-Ka/barttin$  or  $ClC-Kb/barttin$  channels. Multiple mutations in the gene encoding the obligatory CLC-K subunit barttin, *BSND*, have been identified in patients with Bartter syndrome type IV. These mutations reduce the endocochlear potential and cause deafness. As CLC-K/barttin channels are also expressed in the kidney, patients with Bartter syndrome IV typically also suffer from salt-wasting hyperuria and electrolyte imbalances. However, there was a single report on a *BSND* mutation that resulted only in deafness, but not kidney disease. We herein studied the functional consequences of another recently discovered *BSND* mutation that predicts exchange of valine at position 33 by leucine. We combined whole-cell patch clamp, confocal microscopy and protein biochemistry to analyze how V33L affects distinct functions of barttin. We found that V33L reduced membrane insertion of CLC-K/barttin complexes without altering unitary CLC-K channel function. Our findings support the hypothesis of a common pathophysiology for the selective loss of hearing due to an attenuation of the total chloride conductance in the stria vascularis while providing enough residual function to maintain normal kidney function.

**Keywords:** CLC channel, barttin, Bartter syndrome, hearing loss, patch clamp

## INTRODUCTION

Barttin constitutes the obligatory  $\beta$ -subunit of two epithelial CLC-type chloride channels,  $ClC-Ka$  (also known as  $ClC-K1$  in rodents) and  $ClC-Kb$  ( $ClC-K2$  in rodents). It is required for proper membrane targeting, stabilization and activation of these channels (Fahlke and Fischer, 2010; Stölting et al., 2014a). In the kidney,  $ClC-Ka$  is the main chloride conduction pathway in the thin ascending limb of Henle's loop (Uchida et al., 1995; Vandewalle et al., 1997) whereas  $ClC-Kb$  is expressed in the thick ascending limb of Henle's loop, the distal connecting tubules and in a- and b-intercalated cells of the collecting duct (Vandewalle et al., 1997). Loss-of-function of either channel leads to disturbed kidney function as described in knock-out mouse models for the

homologous channels CLC-K1 and CLC-K2 (Matsumura et al., 1999; Grill et al., 2016; Hennings et al., 2016) but also in disease-causing mutations for the human CLC-Kb channel (Simon et al., 1997; Konrad et al., 2000). Both channels are thought to be co-expressed in the stria vascularis of the inner ear so that only the combined loss-of-function results in sensorineural deafness in addition to the renal symptoms (Schlingmann et al., 2004).

Naturally occurring mutations in the gene encoding barttin, *BSND*, cause Bartter syndrome IV that is characterized by impaired urinary concentration and deafness (Bartter et al., 1962; Birkenhäger et al., 2001). Barttin and CLC-K co-localize in the kidney and in the inner ear (Estévez et al., 2001), and most disease-causing mutations of barttin result in a loss of channel function leading to both, renal disease and deafness (Janssen et al., 2009). However, one mutant, I12T barttin, was found to cause deafness, but leave renal function unaffected (Riazuddin et al., 2009). This mutation reduces surface membrane insertion of CLC-K channels so that the total chloride transport capacity of affected epithelia is attenuated, but not abolished. Based on these findings, it was hypothesized that the inner ear is more sensitive to a reduced chloride conductance than the loop of Henle (Riazuddin et al., 2009; Fahlke and Fischer, 2010). Recently, another mutation in barttin, V33L, was associated with deafness without impaired kidney function in a Pakistani family (Shafique et al., 2014) but not studied on a molecular level so far.

We applied a combination of whole-cell patch clamp, surface biotinylation and confocal microscopy to study the effect of the V33L barttin mutation on the function and trafficking of CLC-Ka and CLC-Kb in order to further elucidate the mechanism behind barttin mutations selectively impairing hearing but not kidney function.

## METHODS

### Construction of Expression Plasmids, Mutagenesis, and Heterologous Expression

Coding regions of barttin, CLC-Ka or CLC-Kb were cloned into pcDNA3.1, pcDNA5/FRT/TO or pRc/CMV vectors (Life Technologies), with eGFP or mVenus linked to the amino-terminus of the channels and mCherry to the carboxy-terminus of barttin. Previous publications showed no effects of this procedure on expression or function of the channel or its accessory subunit (Scholl et al., 2006; Janssen et al., 2009; Fischer et al., 2010). The V33L mutation was introduced into barttin by overlapping extension PCR.

We heterologously expressed WT and mutant CLC-K/barttin channels in two different cell lines, MDCK II and HEK293T cells. MDCK II cells are known to show epithelial properties, such as cell polarization and proper sorting and trafficking (Cereijido et al., 1978), and we therefore employed confluent MDCK II cells for studies of channel localization and trafficking. However, MDCK II cells exhibit significant background currents in addition to loss of polarization upon cell dispersion which is required for whole-cell patch clamping. We performed the electrophysiological characterization of CLC-K/barttin in HEK293T cells. These cells do not resemble polarized epithelia as

well as MDCK II cells, but are well suited for electrophysiological experiments because of negligible background currents and robust expression of heterologous proteins.

HEK293T cells were co-transfected with 1 µg of pcDNA3.1 eGFP- or mVenus-CLC-Ka/-Kb and 3 µg of pcDNA3.1 barttin-mCherry (or barttin-V33L-mCherry) using the calcium phosphate technique (Fahlke et al., 2001) in a 5-cm petri dish with 3 mL growth medium. The cells were split 20 h after transfection and used for patch clamp recording the next day after splitting. For co-immunoprecipitation experiments, cells were washed with PBS supplemented with 0.05% (w/v) EDTA 20 h after transfection and harvested immediately afterwards.

MDCK II cells were transfected using Lipofectamine 2000 (Life Technologies) according to the supplied protocol, with 1.5 µg pcDNA3.1 eGFP- or mVenus-CLC-Ka/-Kb and/or 1.5 µg pcDNA3.1 barttin-mCherry (or barttin-V33L-mCherry) in a 3.5-cm ibiTreat µ-dish for the confocal imaging, or with 4 µg pcDNA3.1 eGFP- or mVenus-CLC-Ka/-Kb and/or 4 µg pcDNA3.1 barttin-mCherry (or barttin-V33L-mCherry) in a 10-cm petri dish for biotinylation. After transfection cells were grown for 1 to 2 days to reach a polarized, confluent state for confocal scanning.

### Whole-Cell Patch Clamp and Fluorescence-Current Correlation

Whole-cell patch clamp recordings were performed using an AxoPatch 200B amplifier controlled by pClamp software (Molecular Devices) (Hebeisen and Fahlke, 2005) or a HEKA EPC-10 (HEKA Elektronik) as previously described (Stölting et al., 2014b). Recordings were filtered using a 10 kHz lowpass Bessel filter. The external solution contained (in mM): 140 NaCl, 4 KCl, 2 CaCl<sub>2</sub>, 1 MgCl<sub>2</sub>, and 10 HEPES while the internal solution contained 115 NaCl, 2 MgCl<sub>2</sub>, 5 EGTA, and 5 HEPES. Both solutions were adjusted to pH 7.4. In experiments combining fluorescence measurements and whole-cell recordings the patch clamp mode was established as described above, and eGFP was excited using a Polychrom V monochromator (TILL Photonics) set to 488 nm and recorded using a Neo camera (Andor) (Schänzler and Fahlke, 2012). Total fluorescence intensities for manually selected cells of interest were analyzed using Fiji (<http://www.fiji.sc>).

### Noise Analysis

CLC channels are double-barreled, with two identical “protopores” that are opened and closed by individual as well as by common gating processes (Miller and White, 1984; Ludwig et al., 1996; Middleton et al., 1996; Stölting et al., 2014b). For such a channel, the whole cell current amplitude (*I*) depends on the number of channels in the surface membrane (*N*), the single channel pore amplitude (*i*) and the open probabilities of the two protopore gates (*P<sub>p</sub>*) and the common gate (*P<sub>c</sub>*) (Accardi and Pusch, 2000; Fischer et al., 2010):

$$I = 2N \cdot i \cdot P_p \cdot P_c \quad (1)$$

Random opening and closing of ion channels produce a Lorentzian type of noise ( $\sigma^2$ ) that depends on the number of channels as well as its unitary current amplitude and its open

probability. For a double-barreled channel  $\sigma^2$  can be calculated as Fischer et al. (2010), Weinberger et al. (2012) and Stölting et al. (2014a):

$$\sigma^2 = i \cdot I - \frac{I^2}{N} \left( 1 - \frac{1}{2P_c} \right) \quad (2)$$

In the case of CLC-Ka/barttin channels the common gate was found permanently open using single channel recordings and noise analysis (Fischer et al., 2010), thus simplifying (2) to

$$\sigma^2 = i \cdot I - \frac{I^2}{2N} \quad (3)$$

which is equivalent to:

$$\frac{\sigma^2}{I} = i - \frac{I}{2N} \quad (4)$$

Based on an ohmic current-voltage relationship, this relationship can be further simplified to:

$$\frac{\sigma^2}{I \cdot (V - V_{rev})} = \gamma - \frac{I}{2N \cdot (V - V_{rev})} \quad (5)$$

here with  $V$  the applied voltage,  $V_{rev}$  the reversal potential,  $N$  the number of functional channels in the surface membrane and  $\gamma$  the single channel pore conductance (Sesti and Goldstein, 1998). The voltage-independent background noise was recorded at the reversal potential, where CLC-Ka/barttin currents do not contribute, averaged and subtracted from the otherwise measured variance.

Unitary channel parameters of CLC-Kb/barttin have so far not been described on a detailed single channel level. The homologous CLC-K2 channel appears to exhibit properties that are incompatible with whole-cell recordings of CLC-Kb (Pinelli et al., 2016) and may not be used for comparison. We therefore estimated unitary properties using a modified noise analysis according to a method described in Stölting et al. (2015). For a regular CLC-type channel with two conduction pathways exhibiting protopore as well as common gating mechanisms (Fischer et al., 2010; Stölting et al., 2014b), combining Equations (1) and (2) results in

$$\frac{\sigma^2}{I} = i \cdot (1 - P_p (2P_c - 1)) \quad (6)$$

The ratio of variance to the mean macroscopic current depends on the product of single channel amplitudes and open probabilities of protopore and common gates, but is indifferent to variations in the number of channels.

## Confocal Imaging

Confocal imaging was performed on living MDCK II cells bathed in standard external solution on an inverted confocal laser scanning microscope (Leica TCS SP5, Leica) using a 63×/1.4 oil immersion objective. Imaging channels were scanned sequentially to avoid cross-contamination with the co-expressed fluorescent protein. eGFP was excited using a 488

nm laser and emission was collected between 490 and 580 nm, mVenus was excited at 514 nm and detected between 490 and 560 nm, and mCherry was excited using a 543 nm Laser and detected between 600 and 713 nm.

## Biochemical Analysis

Co-immunoprecipitation of barttin and human CLC-K channels was performed as described previously (Stölting et al., 2015). Transfected HEK293T cells were collected from petri dishes and lysed using ComplexioLyte-47a (Logopharm). Cleared lysates were incubated with 1 μg of monoclonal anti-GFP antibody (Life Technologies) or left as a control without antibody. Antibody-bound protein complexes were purified using protein G-sepharose beads (Thermo Scientific) and eluted using SDS loading buffer. Samples were run on a 10% SDS gel before scanning.

Cell surface expression of CLC-K channels was investigated using a modification of cell surface biotinylation methods described previously (Nothmann et al., 2011; Stölting et al., 2015; Wojciechowski et al., 2015). MDCK II cells were incubated with 1 mg of EZ linked NHS-Sulfo-SS-biotin (Thermo Scientific) in PBS for 30 min. After quenching of free biotin with 50 mM glycine in PBS for 30 min the cells were lysed using RIPA buffer and incubated with NeutrAvidin beads (Thermo Scientific) for 1 h. Biotinylated proteins were eluted off the column with 2 × SDS sample buffer and run on a 10% SDS gel. Cells transfected with cytosolic mVenus were used as control to test the specificity of this biotinylation protocol to label surface membrane proteins.

Gels were scanned on a fluorescence gel scanner (Typhoon FLA 9500, GE Healthcare) at 100 μm resolution. eGFP and mVenus were excited at 473 nm, and the emission recorded using a 530/20 bandpass filter. The signal of mCherry was recorded using a 532 nm laser and a longpass 575 nm filter. Gel images were quantified using the Fiji software. Gels were rotated up to 3° using bilinear interpolation and subsequently quantified using the built-in tools for gel analysis.

## Statistical Analysis

Unless noted otherwise, Student's  $t$ -test was used for statistical comparison with \* denoting  $p < 0.05$ , \*\* $p < 0.01$  and \*\*\* $p < 0.001$ . We chose a significance level of 5% prior to analysis and therefore did not reject the null hypothesis for comparisons yielding a  $p$ -value larger than 0.05 (labeled: "n.s."). All errors are given as s.e.m.

## RESULTS

### V33L Barttin Reduces Whole-Cell Current Amplitudes of CLC-K Channels

A recent publication (Shafique et al., 2014) reported a novel *BSND* mutation in deaf patients that predicts the exchange of valine to leucine at position 33 of barttin. V33 is located in the short extracellular loop close to the beginning of the second transmembrane domain of barttin (Figure 1A). To study the consequences of V33L barttin on chloride channel function we co-expressed WT and mutant barttin with CLC-Ka or CLC-Kb in HEK293T cells and measured whole-cell currents with the

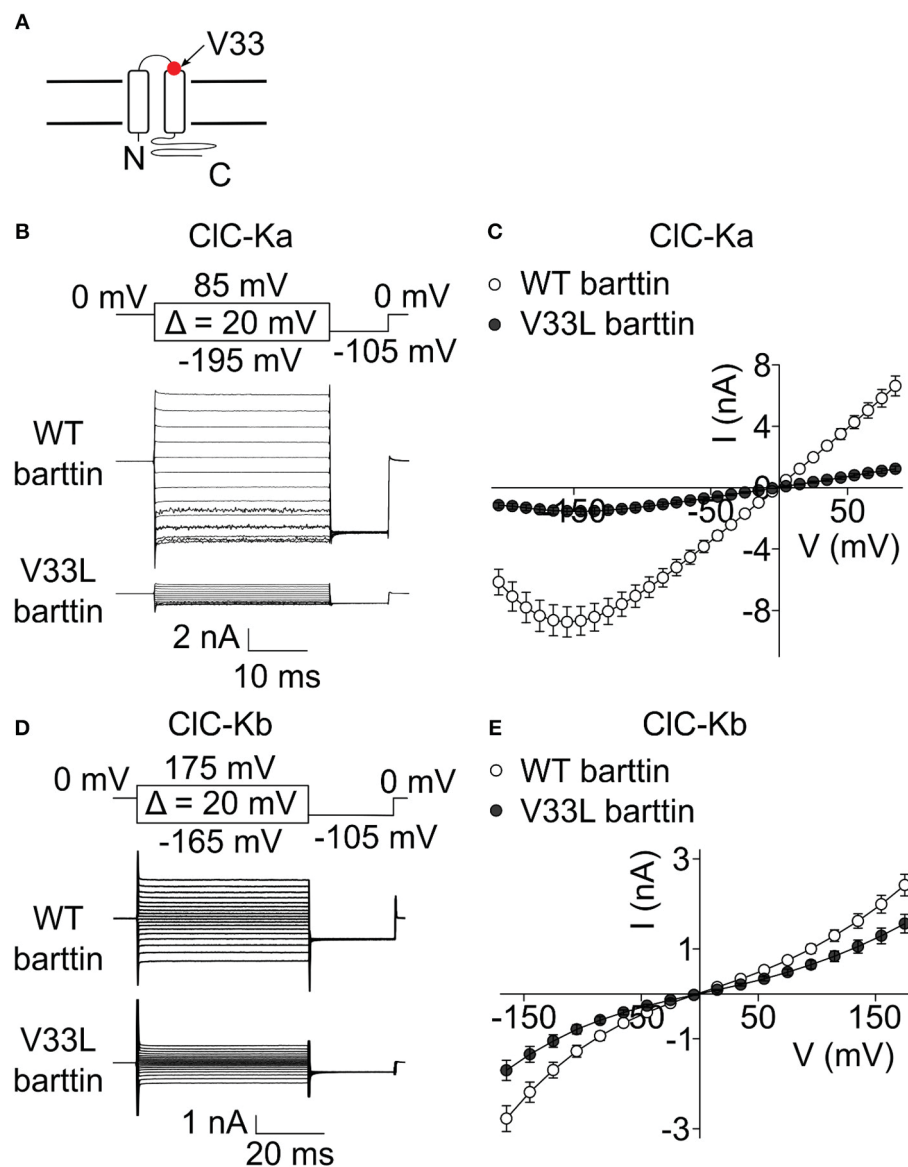


**FIGURE 1 | V33L barttin reduces macroscopic currents of CLC-K channels. (A)** Transmembrane topology of barttin with the position of V33L indicated by an arrow. **(B)** Representative current recordings from HEK293T cells co-expressing CIC-Ka with WT or V33L barttin. **(C)** Voltage-dependence of steady-state currents in cells co-expressing CIC-Ka with WT ( $n = 16$ ) or V33L barttin ( $n = 10$ ). **(D)** Representative current recordings from HEK293T cells co-expressing CIC-Kb with WT or V33L barttin. **(E)** Voltage-dependence of steady-state currents in cells co-expressing CIC-Kb with WT ( $n = 50$ ) or V33L barttin ( $n = 48$ ). All error bars indicate s.e.m.

patch clamp technique. CIC-Ka/barttin displays a linear current-voltage relationship at voltages between  $-100$  mV and  $+100$  mV. At more negative potentials, the whole-cell conductance is gradually decreasing, resulting in a “hook” at approximately  $-150$  mV (Figures 1B,C). CIC-Kb/barttin currents exhibit a characteristic bi-directional rectification (Figures 1D,E). CIC-Kb/barttin whole-cell current amplitudes are smaller than for CIC-Ka/barttin (Figures 1C,E), presumably due to smaller unitary amplitudes as reported for their rodent homologs (Fischer et al., 2010; Pinelli et al., 2016). V33L barttin left the time and voltage dependence of CIC-Ka/barttin and CIC-Kb/barttin currents unaltered (Figures 1B–E). CIC-Ka/V33L

barttin currents, however were reduced to  $<20\%$  ( $p < 0.001$  at  $-155$  mV; Figures 1B,C). The differences between CIC-Kb/WT barttin and CIC-Kb/V33L barttin currents were only slightly decreased ( $p = 0.004$  at  $-165$  mV; Figures 1D,E).

### Unitary Properties of CIC-Ka/Barttin and CIC-Kb/Barttin Are Unaffected by the V33L Mutation

The reduction in whole-cell CLC-K currents in the presence of V33L barttin might either be caused by a reduction of the open probability, diminished single channel amplitude or by a

reduced number of channels in the surface membrane. Since CLC-Ka/barttin channels exhibit a run-down in excised patches, and the gating properties of these channels make estimation of unitary channel properties difficult in the cell-attached mode (Fischer et al., 2010), we determined CLC-Ka/barttin single channel properties using a modified stationary noise analysis that has previously shown similar results to single channel recordings also for other ion channels (Sesti and Goldstein, 1998; Fischer et al., 2010; Stölting et al., 2013).

We determined steady-state current amplitudes and variances for protocols similar to the ones shown in **Figure 1** and plotted variances divided by the product of the mean current and the driving force ( $V - V_{rev}$ ) vs. the mean current divided by the driving force (Equation 5) (**Figure 2A**). A linear fit to these values yields the unitary protopore conductance as y-axis intercept, and the slope of the linear regression corresponds to the number of active protopores in the plasma membrane or the twice the number of channels ( $N$ ) according to:

$$N = \frac{-1}{2 \cdot slope} \quad (7)$$

Absolute open probabilities were calculated according to Equation 1 after obtaining protopore open probabilities by dividing current amplitudes by the protopore current amplitude  $i$  and  $N$ . We obtained unaltered unitary conductances (**Figure 2A**, inset) as well as absolute open probabilities: For both WT ( $n = 13$ ) and V33L ( $n = 8$ ), the single CLC-Ka/barttin channel pore opens in a probability range from 0.5 at  $-195$  mV to almost 1 at voltages positive to  $-105$  mV under the recording conditions. The difference in the slopes of the distributions demonstrates that V33L reduces the number of CLC-Ka channels (for WT  $1944 \pm 307$ ,  $n = 13$ ; for V33L  $444 \pm 51$ ,  $n = 8$ ).

This noise analysis is based on two assumptions, i.e., that the common gate is permanently open and that the current-voltage relationship for unitary channels is linear. These assumptions have been experimentally tested for WT CLC-Ka/barttin by single channel recordings (Fischer et al., 2010). For the homologous mouse CLC-K1/barttin channel, however, there has been an alternative interpretation in that the protopore gates are constitutively open and only common gating occurs (LHoste et al., 2013). Even in that case, the noise analysis applied to our data is still valid, although unitary current amplitudes would then correspond to openings and closures of both protopores simultaneously. Furthermore, the time and voltage dependence of macroscopic CLC-Ka/barttin currents is not affected by the V33L mutation, indicating that the mutation does not affect the current-voltage relationship. A change in slow gating would result in the occurrence of channels with two subconductance states (Miller and White, 1984). Noise analysis on currents generated by such channels produce apparent unitary current amplitudes intermediate to the single protopore and the full dimeric double protopore conductance levels (Weinberger et al., 2012; Stölting et al., 2014a). Such a change in apparent unitary current amplitude was not observed in our experiments.

Whereas the effect of V33L on unitary channel properties of CLC-Ka/barttin could be determined with noise analysis, we

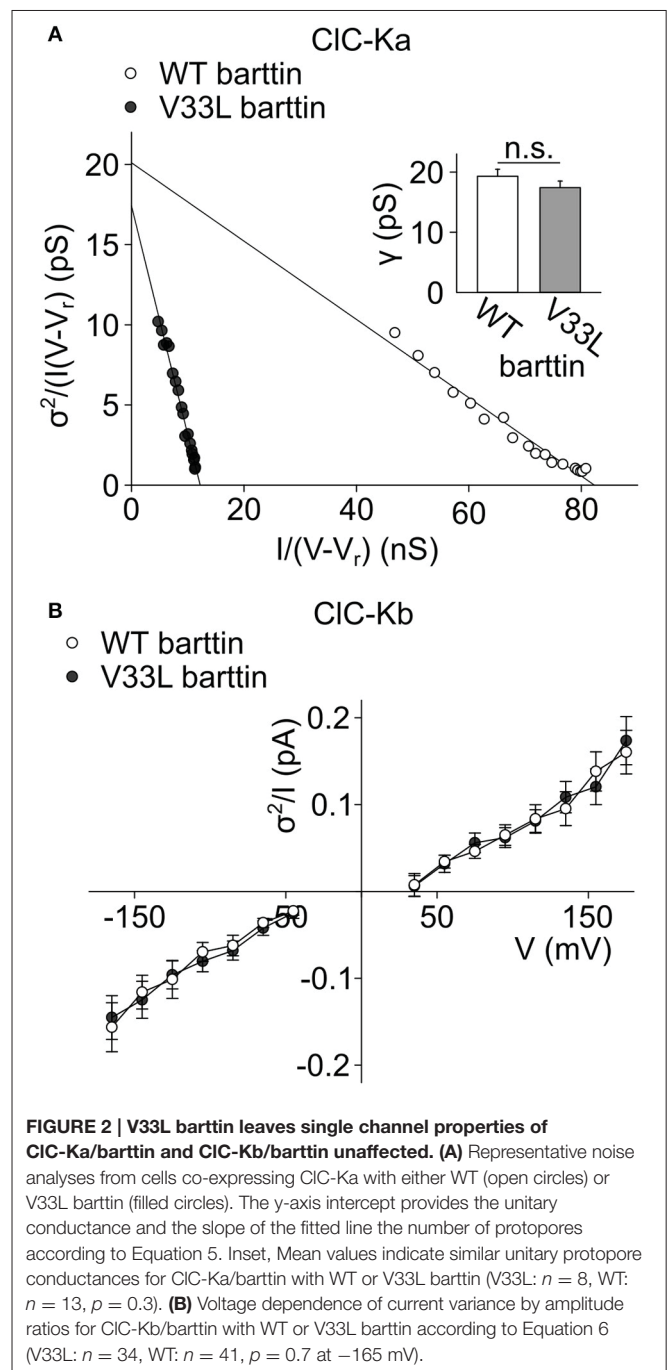


**FIGURE 2 | V33L barttin leaves single channel properties of CLC-Ka/barttin and CLC-Kb/barttin unaffected. (A)** Representative noise analyses from cells co-expressing CLC-Ka with either WT (open circles) or V33L barttin (filled circles). The y-axis intercept provides the unitary conductance and the slope of the fitted line the number of protopores according to Equation 5. Inset, Mean values indicate similar unitary protopore conductances for CLC-Ka/barttin with WT or V33L barttin (V33L:  $n = 8$ , WT:  $n = 13$ ,  $p = 0.3$ ). **(B)** Voltage dependence of current variance by amplitude ratios for CLC-Kb/barttin with WT or V33L barttin according to Equation 6 (V33L:  $n = 34$ , WT:  $n = 41$ ,  $p = 0.7$  at  $-165$  mV).

could not obtain unitary current amplitudes and absolute open probabilities of CLC-Kb/barttin channels. These channels display only small voltage-dependent changes of the open probability within the tested range. Moreover, absolute values for protopore or common gate open probability are not known, precluding the use of noise analysis for determining unitary current properties of CLC-Kb/barttin. We compared ratios of CLC-Kb/barttin current variances by current amplitudes as described previously (Stölting et al., 2015). This ratio (Equation 6) depends on the open probabilities of the protopore as well as the common gate and the

single channel amplitude. This value was found to be unchanged in recordings with WT and V33L barttin, strongly supporting the notion that single channel properties are unchanged by V33L barttin also for CLC-Kb/barttin (Figure 2B). We conclude that V33L reduces the number of CLC-Ka/barttin and CLC-Kb/barttin channels in the surface membrane of HEK293T cells.

### V33L Does Not Impair Association of Barttin with CLC-K

The observed reduction in the number of membrane-inserted CLC-K/barttin channels by V33L barttin may arise from impaired CLC-K/barttin-interaction and reduced stability of the CLC-K/barttin complex. We performed co-immunoprecipitation experiments to test whether V33L decreases the affinity of barttin binding to CLC-K. HEK293T cells were co-transfected with either eGFP tagged CLC-Ka or CLC-Kb and WT or V33L barttin-mCherry. After lysis and solubilization of membrane proteins anti-GFP antibodies were used to link eGFP-tagged CLC-K channels to protein G agarose beads. WT and V33L barttin bound to CLC-K could be co-eluted from the beads and identified using fluorescence scans of SDS-PAGE gels (Figures 3A,B).

As previously described, barttin co-expression leads to significant complex glycosylation of CLC-K channels (Waldegger et al., 2002; Janssen et al., 2009). The intensity ratios of the respective barttin bands over the summed intensities of the channel bands at all glycosylation-states were similar for WT and V33L barttin and both CLC-K channels, respectively (Figures 3C,D). These results indicate that V33L does not reduce the number of CLC-K/barttin channels in the surface membrane by impairing barttin-CLC-K interactions.

### V33L Barttin Impairs Trafficking of CLC-Ka and CLC-Kb

Reduced whole-cell current amplitudes together with unchanged unitary channel parameters and unchanged CLC-K-barttin binding strongly indicate that V33L impairs surface membrane insertion of CLC-K/barttin channels. To quantify these changes mediated by V33L barttin in HEK293T cells, we combined whole-cell patch clamp with fluorometry (Schänzler and Fahlke, 2012; Ronstedt et al., 2015).

The total number of CLC-K subunits—in intracellular organelles as well as in the surface membrane—can be determined by measuring whole-cell eGFP fluorescence. The fluorescence intensity for a single cell ( $F$ ) expressing a GFP-tagged channel can be calculated according to:

$$F = 2N \cdot f \tag{8}$$

with  $N$  being the total number of CLC-K channels in the cell and  $f$  being the mean fluorescence intensity of a single GFP-CLC-K protein. The mean steady-state macroscopic current ( $I$ ) is determined as:

$$I = 2N \cdot R_m \cdot R_{bar} \cdot i \cdot P_o \tag{9}$$

with  $R_m$  being the percentage of channels in the surface membrane;  $R_{bar}$  the percentage of channels bound to barttin;  $i$  the

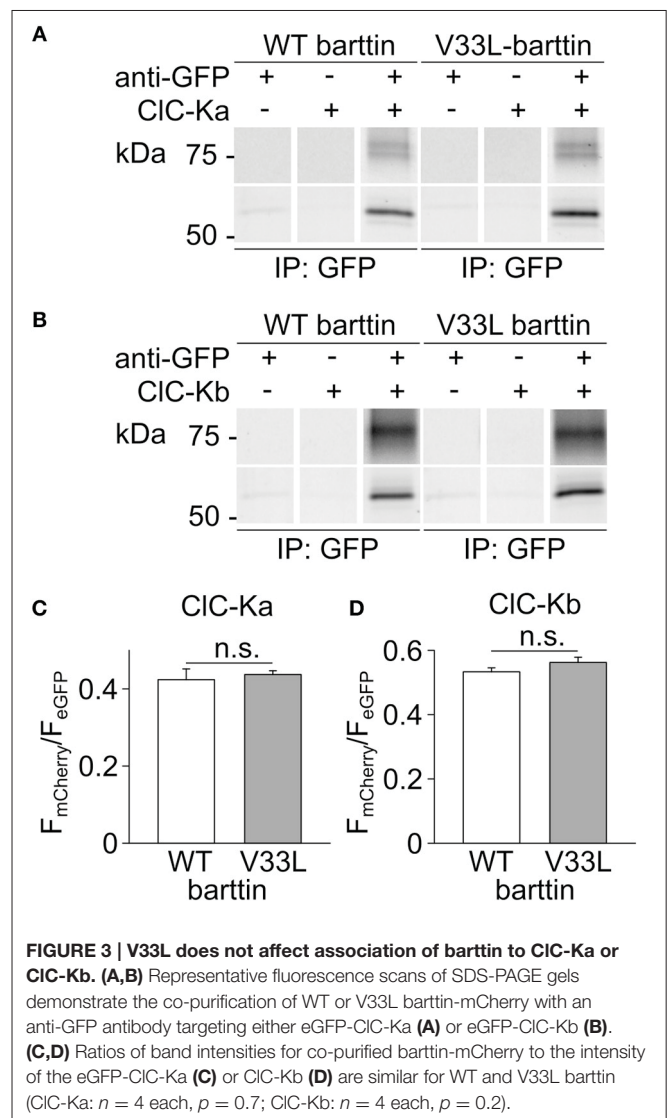


**FIGURE 3 | V33L does not affect association of barttin to CLC-Ka or CLC-Kb.** (A,B) Representative fluorescence scans of SDS-PAGE gels demonstrate the co-purification of WT or V33L barttin-mCherry with an anti-GFP antibody targeting either eGFP-CLC-Ka (A) or eGFP-CLC-Kb (B). (C,D) Ratios of band intensities for co-purified barttin-mCherry to the intensity of the eGFP-CLC-Ka (C) or CLC-Kb (D) are similar for WT and V33L barttin (CLC-Ka:  $n = 4$  each,  $p = 0.7$ ; CLC-Kb:  $n = 4$  each,  $p = 0.2$ ).

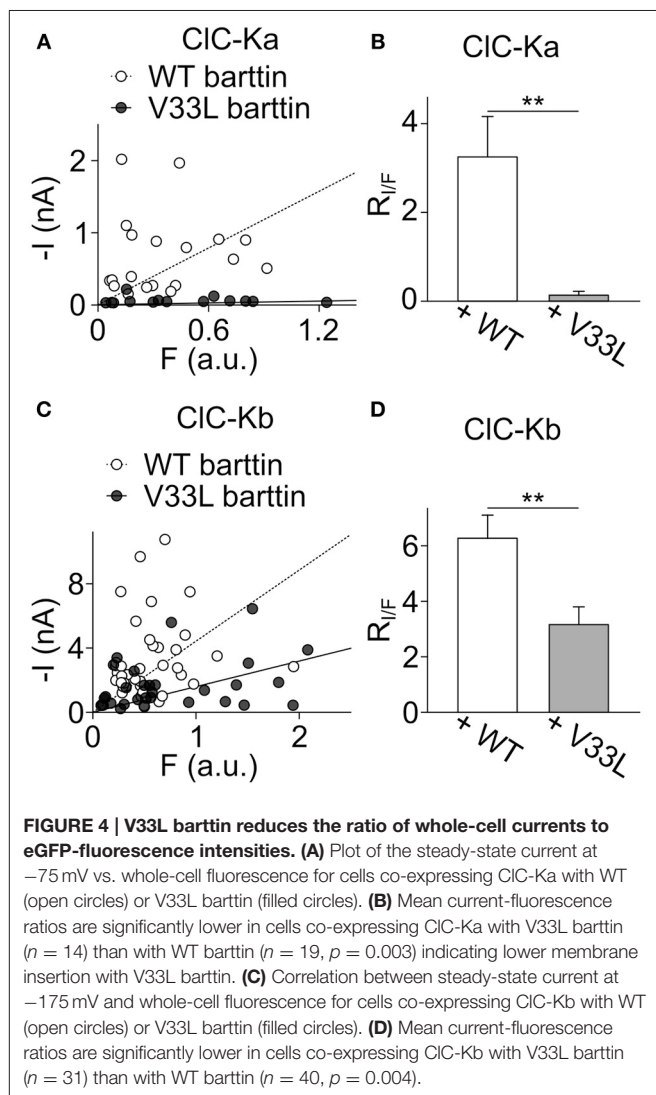
single channel amplitude and  $P_o$  the open probability of a single channel.

Dividing mean macroscopic current amplitudes by the fluorescence intensity results in

$$\frac{I}{F} = \frac{R_m \cdot R_{bar} \cdot i \cdot P_o}{f} \tag{10}$$

Single channel current amplitudes  $i$  and open probabilities  $P_o$  were shown to be identical for WT and mutant barttin, and the fluorescence of a single GFP-CLC-K protein is expected not to be changed by V33L barttin. Co-immunoprecipitation results suggested a similar affinity so that  $R_{bar}$  can be treated as constant. Ratios of whole-cell current amplitudes and fluorescence for CLC-K with either WT or V33L barttin thus provide the relative membrane insertion probabilities.

Plotting  $I$  against  $F$  yielded an overlapping distribution of values (Figures 4A,C), however, fitting linear functions provided mean current/fluorescence ratios that were significantly smaller



for CIC-Ka and CIC-Kb in the presence of V33L barttin than with WT barttin (Figures 4B,D). We conclude that V33L reduces surface membrane insertion as the underlying cause of the experimentally observed attenuation of CLC-K/barttin currents.

### V33L Barttin Impairs Plasma Membrane Insertion of CIC-Ka and CIC-Kb

HEK293T cells differ from epithelial cells in their inability to form polarized epithelia. However, trafficking and sorting of transmembrane proteins into either apical or basolateral plasma membranes is a hallmark of epithelia and crucial for directed transport of solutes across the epithelial layer. Since MDCK II cells represent an established model for studies of epithelial proteins in general and CLC-K/barttin complexes in particular, we determined the localization of CLC-K and barttin fusion proteins in transfected MDCK II cells.

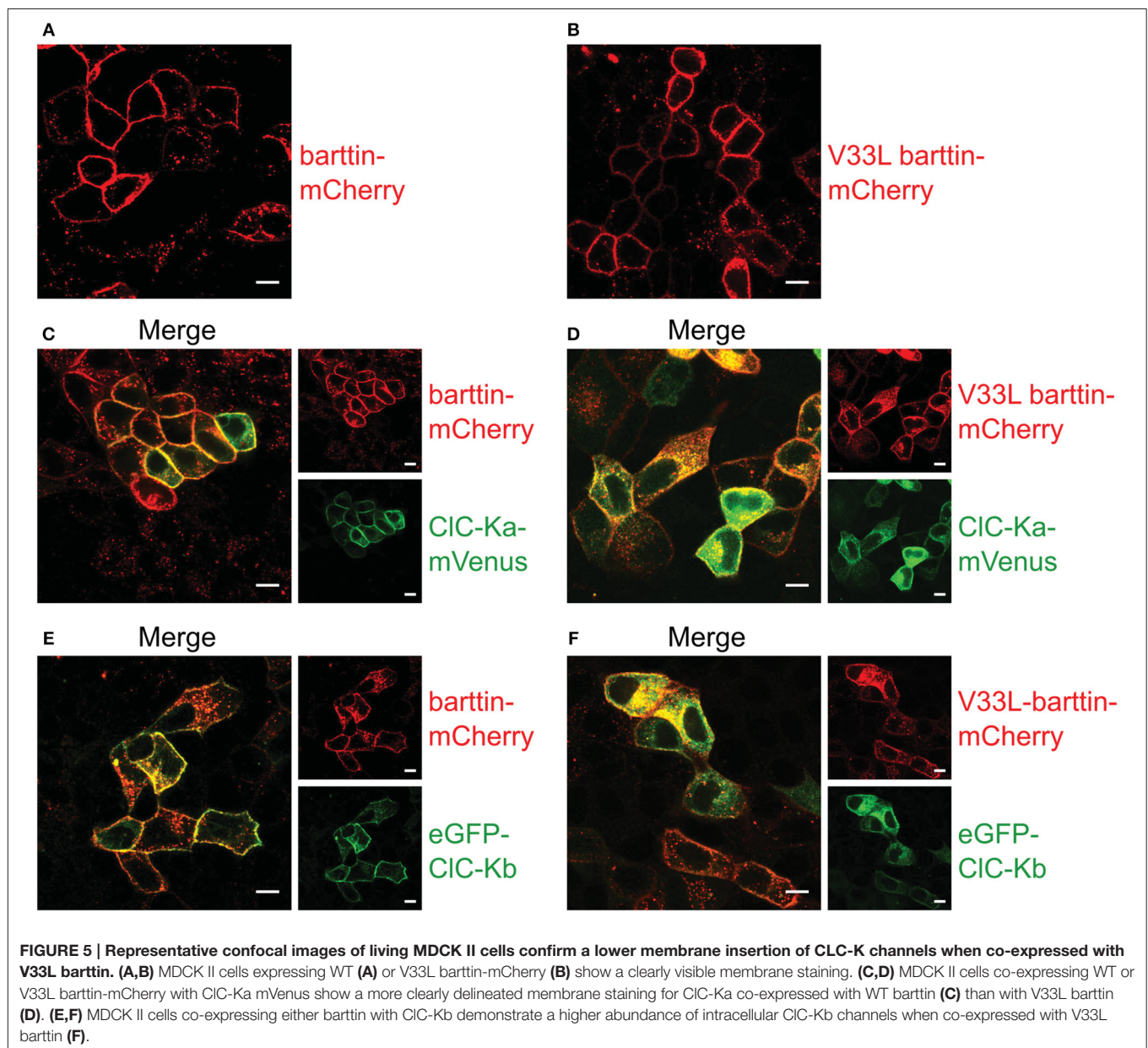
When expressed alone, WT and V33L barttin, were predominantly inserted into the surface membrane (Figures 5A,B). Without barttin, CIC-Ka and CIC-Kb are

retained in the endoplasmic reticulum (Scholl et al., 2006) while co-expression of their accessory subunit significantly increases the number of channels in the plasma membrane. The V33L mutation attenuated surface membrane insertion of CIC-Ka and CIC-Kb. When expressed together with WT barttin, most of CIC-Ka was inserted into the plasma membrane (Figure 5C). Co-expression with V33L barttin, however, resulted in a stronger perinuclear staining of eGFP-CIC-Ka in good agreement with a retention of channels in the endoplasmic reticulum (Figure 5D). Whereas WT barttin effectively brought CIC-Kb into the surface membrane, there was more intracellular staining of cells co-expression CIC-Kb with V33L barttin (Figures 5E,F). The finding that co-expression of V33L barttin with CLC-K channels also results in a more dominant intracellular staining of barttin itself suggests that mutant barttin is retained intracellularly in a complex with CLC-K channels.

We next performed surface biotinylation on transiently transfected MDCK II cells to quantify those changes in surface membrane expression. Proteins in the plasma membrane were labeled and purified, and the subsequent quantification of protein in the surface membrane and total protein provides a quantitative measure of surface membrane insertion probability. Figure 6 depicts representative fluorescence scans of SDS-PAGE gels from the biotinylated fraction (Figure 6A) and the whole cell lysate fraction (Figure 6B). Ratios of biotinylated protein by full lysates were smaller for V33L than for WT barttin (Figure 6C), for CIC-Ka as well as for CIC-Kb (Figures 6D,E), further supporting the notion that V33L reduces surface membrane insertion of CIC-Ka and CIC-Kb. Whereas the difference in whole cell current amplitudes was not as pronounced for CIC-Kb as for CIC-Ka, the change in membrane insertion as determined by surface biotinylation was comparable for the two pore-forming subunits (Figures 6D,E). This difference between expression systems suggests that cell-type specific differences in CLC-K/barttin trafficking between HEK293T and MDCK II cells. One might speculate that the two channels utilize different trafficking pathways at least in HEK293T cells and that trafficking of CLC-K channels also depends on factors other than barttin.

## DISCUSSION

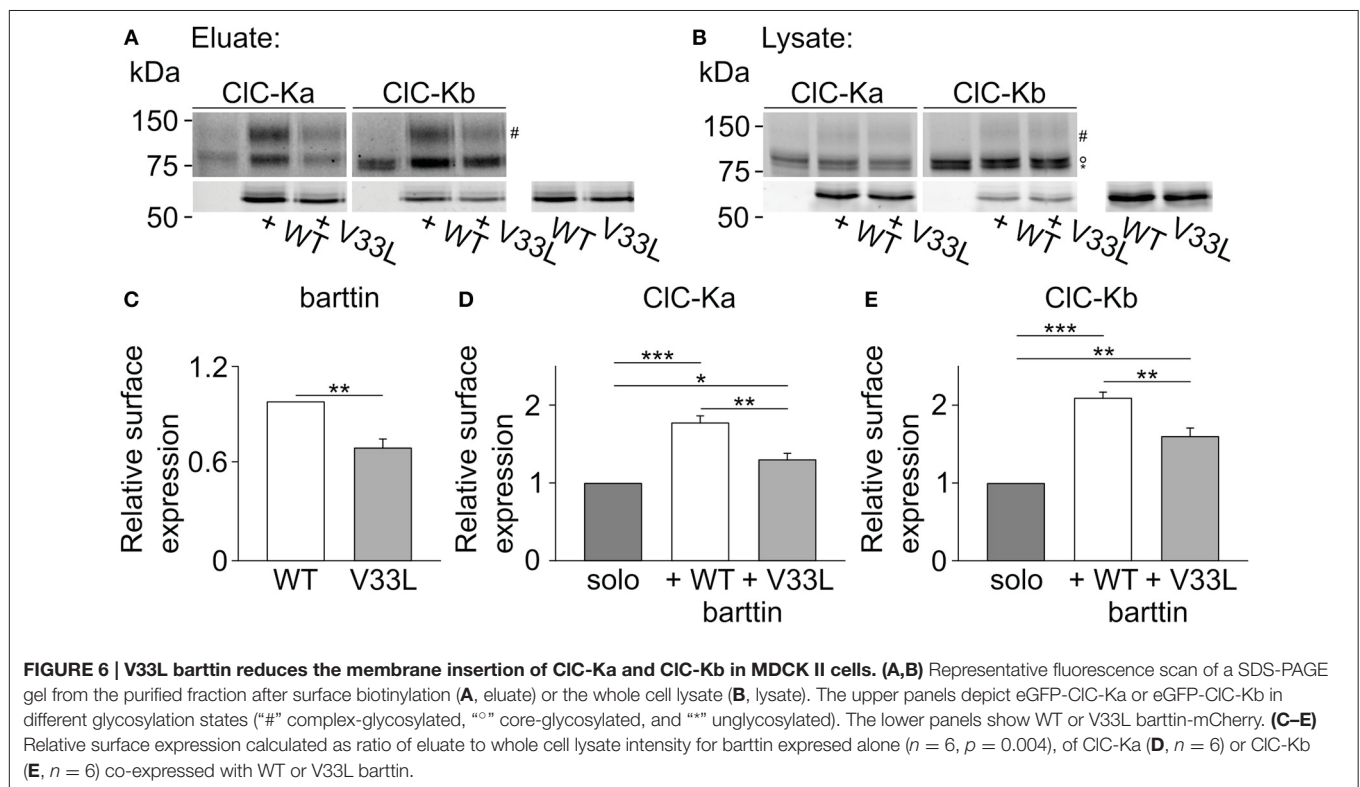
Naturally occurring *BSND* mutations can result in sensorineural deafness and salt-losing polyuria (Birkenhäger et al., 2001). Many of these disease-associated mutations are either nonsense or missense mutations which typically abolish channel activation resulting in loss-of-chloride channel function (Janssen et al., 2009). There is, however, an earlier report about the missense mutation I12T barttin that only causes deafness leaving kidney function unaffected (Riazuddin et al., 2009). In heterologous expression systems I12T only mildly affects trafficking of CLC-K/barttin channels, indicative of a decreased, but still persisting chloride conductance in affected epithelia. As the affected mutation carriers only suffered from deafness, but not impaired kidney function it was proposed that either the remaining epithelial CLC-K/barttin conductance is sufficient to prevent salt-losing polyuria or that other mechanisms might compensate for the loss of CLC-K/barttin in renal epithelia. We herein studied



the functional consequences of another naturally occurring *BSND* mutation that was reported to selectively cause deafness without renal symptoms, V33L barttin (Shafique et al., 2014). We demonstrate that V33L impairs surface membrane insertion of both CLC-Ka and CLC-Kb, (Figures 4, 6), but leaves unitary currents and absolute open probabilities of CLC-Ka/barttin and CLC-Kb/barttin unaltered (Figure 2). These changes will result in a significant reduction of epithelial chloride conductance, but not in a complete loss-of-function.

A recent computational analysis of inner ear function predicts a significant drop of the endocochlear potential upon reduction in the baso-lateral chloride conductance in marginal cells of the stria vascularis (Nin et al., 2012). The reason for this drop in endocochlear potential is that - in the absence of functional CLC-K channels - chloride accumulates, preventing

further uptake of potassium into marginal cells by NKCC1 (Nin et al., 2008; Rickheit et al., 2008). There exists only a small gradient of the chloride concentration across the baso-lateral membrane in marginal cells with slightly higher concentrations inside marginal cells than in the interstitial space (Ikeda and Morizono, 1989; Nin et al., 2012). Similarly, the membrane potential across the baso-lateral membrane of marginal cells is close to 0 mV (Salt et al., 1987) suggesting only a small constitutive outward transport of chloride ions out of the marginal cells into the intrastrial space via CLC-K/barttin facilitating the recirculation of chloride across the baso-lateral membrane. Within this assumed physiologically relevant voltage range, our electrophysiological characterization of CLC-K/barttin channels suggests a higher conductance of CLC-Ka over CLC-Kb due to the bidirectional rectification of



the latter (Figure 1). CLC-Ka might thus be more significant for the maintenance of the endocochlear potential than CLC-Kb. However, CLC-Kb must be able to compensate for a loss of CLC-Ka as the sole loss of CLC-Ka does not lead to deafness as indicated by a large cohort (Cappola et al., 2011). Additionally, both reported deafness causing mutations in barttin, I12T and V33L show a higher impact on currents through CLC-Ka than CLC-Kb (Figure 1) warranting further investigations into the significance of either isoform in mammalian hearing.

Our results predict a reduction of the total chloride current by 50% up to 80% as based on the reduction in surface expression in MDCK II cells or our current recordings from HEK293T cells. However, in the computational model a 50-fold reduction in conductance is required to cause a significant drop in the endocochlear potential. There might be additional factors that were not incorporated in the computational model (Nin et al., 2012), or V33L might exert more pronounced effects in native cells than in mammalian cells overexpressing CLC-K/barttin.

Even though animal models with a loss of *Clcnk1* (Matsumura et al., 1999) or *Clcnk2* (Grill et al., 2016; Hennings et al., 2016) have been generated, none of these animals was thoroughly tested for hearing impairment. However, one of the *Clcnk2*<sup>-/-</sup> mice was reported not to display obvious signs of deafness (Grill et al., 2016). It will be an important task for the future to test and to compare the impact of the loss of either CLC-K1 or -K2 on hearing and the generation of the endo-cochlear potential.

Our analysis of functional consequences of the V33L mutation, which selectively affects hearing thresholds,

strengthens the idea that inner ear function is more sensitive to the surface expression of CLC-K/barttin than previously believed. Given that the stria vascularis is not protected from systemic circulation by the blood-cochlear-barrier (Jahnke, 1975) this implies that great care has to be taken when considering CLC-K blockers as potential diuretic drugs in the treatment of hypertension (Imbrici et al., 2014; Liantonio et al., 2016). On the other hand, this peculiarity makes the systemic application of activators of CLC-K/barttin (Zifarelli et al., 2010) or drugs enhancing folding and trafficking of barttin (Nomura et al., 2013) for treating sensorineural deafness possible.

Our data together with earlier results support a good correlation between barttin dysfunction and severity of the clinical phenotype in *BSND*-associated diseases (Fahlke and Fischer, 2010). Whereas mutations that abolish barttin expression result in a severe clinical course with early end-stage renal failure, no renal failure occurred in patients carrying barttin mutations that do not completely prevent channel insertion into the surface membrane. Mutations that preserve CLC-K/barttin function cause deafness, but do not affect renal salt extrusion.

## AUTHOR CONTRIBUTIONS

CF and GS conceived and designed the study. All authors contributed to the design of the individual experiments. HT and SB performed experiments. HT, SB, and GS were responsible for data analysis. CF and GS drafted the article, and it was critically revised and finally approved by all authors.

## REFERENCES

- Accardi, A., and Pusch, M. (2000). Fast and slow gating relaxations in the muscle chloride channel CLC-1. *J. Gen. Physiol.* 116, 433–444. doi: 10.1085/jgp.116.3.433
- Bartter, F. C., Pronove, P., Gill, J. R. Jr., and MacCardle, R. C. (1962). Hyperplasia of the juxtaglomerular complex with hyperaldosteronism and hypokalemic alkalosis: a new syndrome. *Am. J. Med.* 33, 811–828. doi: 10.1016/0002-9343(62)90214-0
- Birkenhäger, R., Otto, E., Schürmann, M. J., Vollmer, M., Ruf, E. M., Maier-Lutz, I., et al. (2001). Mutation of *BSND* causes Bartter syndrome with sensorineural deafness and kidney failure. *Nat. Genet.* 29, 310–314. doi: 10.1038/ng752
- Cappola, T. P., Matkovich, S. J., Wang, W., Van Booven, D., Li, M., Wang, X., et al. (2011). Loss-of-function DNA sequence variant in the *CLCNKA* chloride channel implicates the cardio-renal axis in interindividual heart failure risk variation. *Proc. Natl. Acad. Sci. U.S.A.* 108, 2456–2461. doi: 10.1073/pnas.1017494108
- Cerejido, M., Robbins, E. S., Dolan, W. J., Rotunno, C. A., and Sabatini, D. D. (1978). Polarized monolayers formed by epithelial cells on a permeable and translucent support. *J. Cell Biol.* 77, 853–880. doi: 10.1083/jcb.77.3.853
- Estévez, R., Boettger, T., Stein, V., Birkenhäger, R., Otto, E., Hildebrandt, F., et al. (2001). Barttin is a Cl<sup>-</sup> channel beta-subunit crucial for renal Cl<sup>-</sup> reabsorption and inner ear K<sup>+</sup> secretion. *Nature* 414, 558–561. doi: 10.1038/35107099
- Fahlke, Ch., Desai, R. R., Gillani, N., and George, A. L. (2001). Residues lining the inner pore vestibule of human muscle chloride channels. *J. Biol. Chem.* 276, 1759–1765. doi: 10.1074/jbc.M007649200
- Fahlke, Ch., and Fischer, M. (2010). Physiology and pathophysiology of CLC-K/Barttin channels. *Front. Physiol.* 1:155. doi: 10.3389/fphys.2010.00155
- Fischer, M., Janssen, A. G., and Fahlke, Ch. (2010). Barttin activates CLC-K channel function by modulating gating. *J. Am. Soc. Nephrol.* 21, 1281–1289. doi: 10.1681/ASN.2009121274
- Grill, A., Schießl, I. M., Gess, B., Fremter, K., Hammer, A., and Castrop, H. (2016). Salt-losing nephropathy in mice with a null mutation of the *Clnk2* gene. *Acta Physiol.* 218, 198–211. doi: 10.1111/apha.12755
- Hebeisen, S., and Fahlke, Ch. (2005). Carboxy-terminal truncations modify the outer pore vestibule of muscle chloride channels. *Biophys. J.* 89, 1710–1720. doi: 10.1529/biophysj.104.056093
- Hennings, J. C., Andriani, O., Picard, N., Paulais, M., Huebner, A. K., Cayuqueo, I. K. L., et al. (2016). The CLC-K2 chloride channel is critical for salt handling in the distal nephron. *J. Am. Soc. Nephrol.* 28:2016010085. doi: 10.1681/ASN.2016010085
- Ikeda, K., and Morizono, T. (1989). Electrochemical profiles for monovalent ions in the stria vascularis: cellular model of ion transport mechanisms. *Hear. Res.* 39, 279–286. doi: 10.1016/0378-5955(89)90047-6
- Imbrici, P., Liantonio, A., Gradogna, A., Pusch, M., and Camerino, D. C. (2014). Targeting kidney CLC-K channels: pharmacological profile in a human cell line versus *Xenopus* oocytes. *Biochim. Biophys. Acta* 1838, 2484–2491. doi: 10.1016/j.bbame.2014.05.017
- Jahnke, K. (1975). The fine structure of freeze-fractured intercellular junctions in the guinea pig inner ear. *Acta Otolaryngol.* 80, 5–40. doi: 10.3109/00016487509125512
- Janssen, A. G., Scholl, U., Domeyer, C., Nothmann, D., Leinenweber, A., and Fahlke, Ch. (2009). Disease-causing dysfunctions of barttin in bartter syndrome Type IV. *J. Am. Soc. Nephrol.* 20, 145–153. doi: 10.1681/ASN.2008.010102
- Konrad, M., Vollmer, M., Lemmink, H. H., van den Heuvel, L. P., Jeck, N., Vargas-Poussou, R., et al. (2000). Mutations in the chloride channel gene *CLCNKB* as a cause of classic bartter syndrome. *J. Am. Soc. Nephrol.* 11, 1449–1459.
- L'Hoste, S., Diakov, A., Andriani, O., Genete, M., Pinelli, L., Grand, T., et al. (2013). Characterization of the mouse CLC-K1/Barttin chloride channel. *Biochim. Biophys. Acta* 1828, 2399–2409. doi: 10.1016/j.bbame.2013.06.012
- Liantonio, A., Imbrici, P., Camerino, G. M., Fracchiolla, G., Carbonara, G., Giannico, D., et al. (2016). Kidney CLC-K chloride channels inhibitors: structure-based studies and efficacy in hypertension and associated CLC-K polymorphisms. *J. Hypertens.* 34, 981–992. doi: 10.1097/HJH.0000000000000876
- Ludewig, U., Pusch, M., and Jentsch, T. J. (1996). Two physically distinct pores in the dimeric CLC-0 chloride channel. *Nature* 383, 340–343. doi: 10.1038/383340a0
- Matsumura, Y., Uchida, S., Kondo, Y., Miyazaki, H., Ko, S. B. H., Hayama, A., et al. (1999). Overt nephrogenic diabetes insipidus in mice lacking the CLC-K1 chloride channel. *Nat. Genet.* 21, 95–98. doi: 10.1038/5036
- Middleton, R. E., Pheasant, D. J., and Miller, C. (1996). Homodimeric architecture of a CLC-type chloride ion channel. *Nature* 383, 337–340. doi: 10.1038/383337a0
- Miller, C., and White, M. M. (1984). Dimeric structure of single chloride channels from Torpedo electroplax. *Proc. Natl. Acad. Sci. U.S.A.* 81, 2772–2775. doi: 10.1073/pnas.81.9.2772
- Nin, F., Hibino, H., Doi, K., Suzuki, T., Hisa, Y., and Kurachi, Y. (2008). The endocochlear potential depends on two K<sup>+</sup> diffusion potentials and an electrical barrier in the stria vascularis of the inner ear. *Proc. Natl. Acad. Sci. U.S.A.* 105, 1751–1756. doi: 10.1073/pnas.0711463105
- Nin, F., Hibino, H., Murakami, S., Suzuki, T., Hisa, Y., and Kurachi, Y. (2012). Computational model of a circulation current that controls electrochemical symptoms in the mammalian cochlea. *Proc. Natl. Acad. Sci. U.S.A.* 109, 9191–9196. doi: 10.1073/pnas.1120067109
- Nomura, N., Kamiya, K., Ikeda, K., Yui, N., Chiga, M., Sohara, E., et al. (2013). Treatment with 17-allylamino-17-demethoxygeldanamycin ameliorated symptoms of Bartter syndrome type IV caused by mutated *Bsnd* in mice. *Biochem. Biophys. Res. Commun.* 441, 544–549. doi: 10.1016/j.bbrc.2013.10.129
- Nothmann, D., Leinenweber, A., Torres-Salazar, D., Kovermann, P., Hotzy, J., Gameiro, A., et al. (2011). Hetero-oligomerization of neuronal glutamate transporters. *J. Biol. Chem.* 286, 3935–3943. doi: 10.1074/jbc.M110.187492
- Pinelli, L., Nissant, A., Edwards, A., Lourdel, S., Teulon, J., and Paulais, M. (2016). Dual regulation of the native CLC-K2 chloride channel in the distal nephron by voltage and pH. *J. Gen. Physiol.* 148, 213–226. doi: 10.1085/jgp.201611623
- Riazuddin, S., Anwar, S., Fischer, M., Ahmed, Z. M., Khan, S. Y., Janssen, A. G. H., et al. (2009). Molecular Basis of DFNB73: mutations of *BSND* can cause nonsyndromic deafness or bartter syndrome. *Am. J. Hum. Genet.* 85, 273–280. doi: 10.1016/j.ajhg.2009.07.003
- Rickheit, G., Maier, H., Strenzke, N., Andreescu, C. E., Zeeuw, C. I., Muenschler, A., et al. (2008). Endocochlear potential depends on Cl<sup>-</sup> channels: mechanism underlying deafness in Bartter syndrome IV. *EMBO J.* 27, 2907–2917. doi: 10.1038/emboj.2008.203
- Ronstedt, K., Sternberg, D., Detro-Dassen, S., Gramkow, T., Begemann, B., Becher, T., et al. (2015). Impaired surface membrane insertion of homo- and heterodimeric human muscle chloride channels carrying amino-terminal myotonia-causing mutations. *Sci. Rep.* 5:15382. doi: 10.1038/srep15382
- Salt, A. N., Mlechar, I., and Thalmann, R. (1987). Mechanisms of endocochlear potential generation by stria vascularis. *Laryngoscope* 97, 984–991. doi: 10.1288/00005537-198708000-00020
- Schänzler, M., and Fahlke, Ch. (2012). Anion transport by the cochlear motor protein prestin. *J. Physiol.* 590, 259–272. doi: 10.1113/jphysiol.2011.209577
- Schlingmann, K. P., Konrad, M., Jeck, N., Waldegger, P., Reinalter, S. C., Holder, M., et al. (2004). Salt wasting and deafness resulting from mutations in two chloride channels. *N. Engl. J. Med.* 350, 1314–1319. doi: 10.1056/NEJMoa032843
- Scholl, U., Hebeisen, S., Janssen, A. G. H., Müller-Newen, G., Alekov, A., and Fahlke, Ch. (2006). Barttin modulates trafficking and function of CLC-K channels. *Proc. Natl. Acad. Sci. U.S.A.* 103, 11411–11416. doi: 10.1073/pnas.0601631103
- Sesti, F., and Goldstein, S. A. (1998). Single-channel characteristics of wild-type IKs channels and channels formed with two minK mutants that cause long QT syndrome. *J. Gen. Physiol.* 112, 651–663. doi: 10.1085/jgp.112.6.651
- Shafique, S., Siddiqi, S., Schraders, M., Oostrik, J., Ayub, H., Bilal, A., et al. (2014). Genetic spectrum of autosomal recessive non-syndromic hearing loss in pakistani families. *PLoS ONE* 9:e100146. doi: 10.1371/journal.pone.0100146
- Simon, D. B., Bindra, R. S., Mansfield, T. A., Nelson-Williams, C., Mendonca, E., Stone, R., et al. (1997). Mutations in the chloride channel gene, *CLCNKB*, cause Bartter's syndrome type III. *Nat. Genet.* 17, 171–178. doi: 10.1038/ng1097-171
- Stölting, G., Bungert-Plümke, S., Franzen, A., and Fahlke, Ch. (2015). Carboxyl-terminal truncations of CLC-Kb abolish channel activation by barttin via modified common gating and trafficking. *J. Biol. Chem.* 290, 30406–30416. doi: 10.1074/jbc.M115.675827

- Stölting, G., Fischer, M., and Fahlke, Ch. (2014a). CLC channel function and dysfunction in health and disease. *Front. Physiol.* 5:378. doi: 10.3389/fphys.2014.00378
- Stölting, G., Fischer, M., and Fahlke, Ch. (2014b). CLC-1 and CLC-2 form hetero-dimeric channels with novel protopore functions. *Pflugers Arch.* 466, 2191–2204. doi: 10.1007/s00424-014-1490-6
- Stölting, G., Teodorescu, G., Begemann, B., Schubert, J., Nabbout, R., Toliat, M. R., et al. (2013). Regulation of CLC-2 gating by intracellular ATP. *Pflugers Arch.* 465, 1423–1437. doi: 10.1007/s00424-013-1286-0
- Uchida, S., Sasaki, S., Nitta, K., Uchida, K., Horita, S., Nihei, H., et al. (1995). Localization and functional characterization of rat kidney-specific chloride channel, CLC-K1. *J. Clin. Invest.* 95, 104–113. doi: 10.1172/JCI117626
- Vandewalle, A., Cluzeaud, F., Bens, M., Kieferle, S., Steinmeyer, K., and Jentsch, T. J. (1997). Localization and induction by dehydration of CLC-K chloride channels in the rat kidney. *Am. J. Physiol.* 272, F678–F688.
- Waldegger, S., Jeck, N., Barth, P., Peters, M., Vitzthum, H., Wolf, K., et al. (2002). Barttin increases surface expression and changes current properties of CLC-K channels. *Pflug. Arch.* 444, 411–418. doi: 10.1007/s00424-002-0819-8
- Weinberger, S., Wojciechowski, D., Sternberg, D., Lehmann-Horn, F., Jurkat-Rott, K., Becher, T., et al. (2012). Disease-causing mutations C277R and C277Y modify gating of human CLC-1 chloride channels in myotonia congenita. *J. Physiol.* 590, 3449–3464. doi: 10.1113/jphysiol.2012.232785
- Wojciechowski, D., Fischer, M., and Fahlke, Ch. (2015). Tryptophan scanning mutagenesis identifies the molecular determinants of distinct barttin functions. *J. Biol. Chem.* 290, 18732–18743. doi: 10.1074/jbc.M114.625376
- Zifarelli, G., Liantonio, A., Gradogna, A., Picollo, A., Gramegna, G., De Bellis, M., et al. (2010). Identification of sites responsible for the potentiating effect of niflumic acid on CLC-Ka kidney chloride channels. *Br. J. Pharmacol.* 160, 1652–1661. doi: 10.1111/j.1476-5381.2010.00822.x

**Conflict of Interest Statement:** The authors declare that the research was conducted in the absence of any commercial or financial relationships that could be construed as a potential conflict of interest.

Copyright © 2017 Tan, Bungert-Plümke, Fahlke and Stölting. This is an open-access article distributed under the terms of the Creative Commons Attribution License (CC BY). The use, distribution or reproduction in other forums is permitted, provided the original author(s) or licensor are credited and that the original publication in this journal is cited, in accordance with accepted academic practice. No use, distribution or reproduction is permitted which does not comply with these terms.

1 ***CLCN2* Chloride Channel Mutations in Familial Hyperaldosteronism Type II**

2

3 Ute I. Scholl<sup>1,2\*</sup>, Gabriel Stölting<sup>3#</sup>, Julia Schewe<sup>1#</sup>, Anne Thiel<sup>1</sup>, Hua Tan<sup>3</sup>, Carol  
4 Nelson-Williams<sup>4,5</sup>, Alfred A. Vichot<sup>4,5</sup>, Sheng Chih Jin<sup>4</sup>, Erin Loring<sup>4,5,6</sup>, Verena Untiet<sup>3</sup>,  
5 Taekyeong Yoo<sup>7</sup>, Jungmin Choi<sup>4,5</sup>, Shengxin Xu<sup>8</sup>, Aihua Wu<sup>8</sup>, Marieluise Kirchner<sup>9</sup>,  
6 Philipp Mertins<sup>9</sup>, Lars C. Rump<sup>1</sup>, Ali Mirza Onder<sup>10</sup>, Cory Gamble<sup>11</sup>, Daniel McKenney<sup>12</sup>,  
7 Robert W. Lash<sup>13</sup>, Deborah P. Jones<sup>14</sup>, Gary Chune<sup>15</sup>, Priscila Gagliardi<sup>16</sup>, Murim Choi<sup>7</sup>,  
8 Richard Gordon<sup>8</sup>, Michael Stowasser<sup>8</sup>, Christoph Fahlke<sup>3</sup>, and Richard P. Lifton<sup>4,5,6,17</sup>

9

10 <sup>1</sup>Department of Nephrology, Medical School, Heinrich Heine University Düsseldorf,  
11 40225 Düsseldorf, Germany.

12 <sup>2</sup>Department of Nephrology and Medical Intensive Care, Charité Universitätsmedizin  
13 Berlin, Berlin Institute of Health, 10117 Berlin, Germany.

14 <sup>3</sup>Institute of Complex Systems, Zelluläre Biophysik (ICS-4), Forschungszentrum  
15 Jülich, 52425 Jülich, Germany.

16 <sup>4</sup>Department of Genetics, Yale University School of Medicine, New Haven, CT 06510,  
17 USA.

18 <sup>5</sup>Howard Hughes Medical Institute, Yale University School of Medicine, New Haven,  
19 CT 06510, USA.

20 <sup>6</sup>Yale Center for Mendelian Genomics, New Haven, CT 06510, USA.

21 <sup>7</sup>Department of Biomedical Sciences, Seoul National University College of Medicine,  
22 Seoul 03080, Republic of Korea.

23 <sup>8</sup>Endocrine Hypertension Research Center, University of Queensland Diamantina  
24 Institute, Greenslopes and Princess Alexandra Hospitals, Brisbane, Australia.

25 <sup>9</sup>Proteomics Platform, Max Delbrück Center for Molecular Medicine in the Helmholtz  
26 Society and Core Unit Proteomics, Berlin Institute of Health, 13125 Berlin, Germany.

27 <sup>10</sup>Le Bonheur Children's Hospital, Memphis, TN 38105, USA.

28 <sup>12</sup>Cooper Clinic, PA, Fort Smith, AR 72903, USA.

29 <sup>12</sup>Peyton Manning Children's Hospital at St. Vincent, Indianapolis, IN 46260, USA.

30 <sup>13</sup>Division of Metabolism, Endocrinology, and Diabetes, University of Michigan  
31 Medical School, Ann Arbor, MI 48109, USA.

32 <sup>14</sup>Division of Nephrology and Hypertension, Department of Pediatrics, Vanderbilt  
33 University School of Medicine, Nashville, TN 37232, USA.

34 <sup>15</sup>Olin Teague Veterans Administration Hospital, Temple, TX 76504, USA.

35 <sup>16</sup>Division of Endocrinology, Nemours Children's Specialty Care, Jacksonville, FL  
36 32207, USA.

37 <sup>17</sup>Laboratory of Human Genetics and Genomics, The Rockefeller University, New  
38 York, NY 10065, USA.

39

40 #These authors contributed equally.

41

42 \*Correspondence and material requests should be addressed to: Ute I. Scholl, M.D., BIH  
43 Johanna Quandt Professorship for Hypertension and Molecular Biology of Endocrine  
44 Tumors, Department of Nephrology and Medical Intensive Care, Charité –  
45 Universitätsmedizin Berlin and Berlin Institute of Health, Charitéplatz 1, 10117

46 Berlin, Germany. Telephone: +49-30-450-543080, Fax +49-211-81-015-04086,

47 Email: [ute.scholl@charite.de](mailto:ute.scholl@charite.de)

48

49 4 figures, 1 Table; Supplementary Information

50 Primary aldosteronism, a common cause of severe hypertension<sup>1</sup>, features  
51 constitutive production of the adrenal steroid aldosterone. We analyzed a multiplex  
52 family with familial hyperaldosteronism type II (FH-II)<sup>2</sup> and 80 additional probands  
53 with unsolved early-onset primary aldosteronism. Eight probands had novel  
54 heterozygous variants in *CLCN2*, including two *de novo* mutations and four  
55 independent occurrences of the identical p.Arg172Gln mutation; all relatives with  
56 early-onset primary aldosteronism carried the *CLCN2* variant found in probands.  
57 *CLCN2* encodes a voltage-gated chloride channel expressed in adrenal glomerulosa  
58 that opens at hyperpolarized membrane potentials. Channel opening depolarizes  
59 glomerulosa cells and induces expression of aldosterone synthase, the rate-limiting  
60 enzyme for aldosterone biosynthesis. Mutant channels cause gain of function, with  
61 higher open probabilities at the glomerulosa resting potential. These findings for the  
62 first time demonstrate a role of anion channels in glomerulosa membrane potential  
63 determination, aldosterone production and hypertension. They establish the cause  
64 of a substantial fraction of early-onset primary aldosteronism.

65

66 More than 1.1 billion people worldwide have hypertension<sup>3</sup>, the single largest cause of  
67 premature mortality<sup>4</sup>. About 6% of hypertensive patients in primary care have primary  
68 aldosteronism<sup>1</sup>, with higher frequencies among patients with severe hypertension. The  
69 plasma aldosterone level in primary aldosteronism is constitutively elevated despite low  
70 levels of the normal upstream regulator renin; hypokalemia is variable. Aldosterone-  
71 producing adrenal adenomas (APAs) and idiopathic hyperaldosteronism<sup>5</sup> are common  
72 causes of primary aldosteronism. Somatic mutations in *KCNJ5*, *CACNAID*, *ATP1A1*, or  
73 *ATP2B3* that cause increased glomerulosa cell Ca<sup>2+</sup> are sufficient for producing APAs<sup>6-10</sup>;  
74 germline mutations alter *CYP11B2*<sup>11</sup> in glucocorticoid-remediable aldosteronism (GRA,  
75 FH-I), *KCNJ5*<sup>6,12</sup> in FH-III, *CACNAIH*<sup>13</sup> in FH-IV, and *CACNAID*<sup>7</sup> in PASNA  
76 syndrome<sup>14</sup>. These mutations define a common pathway for induction of aldosterone  
77 biosynthesis – glomerulosa cell membrane depolarization activates voltage-gated Ca<sup>2+</sup>  
78 channels, which induces the rate-limiting enzyme for aldosterone biosynthesis,  
79 aldosterone synthase (*CYP11B2*), along with other enzymes in the biosynthetic pathway;  
80 increased mitochondrial Ca<sup>2+</sup> may also contribute<sup>15</sup>.

81 In 1992, Stowasser et al. described a multiplex kindred featuring autosomal  
82 dominant primary aldosteronism that was clinically distinct from GRA, the only  
83 dominant syndrome then known, and hence called it FH-II<sup>2</sup>. The responsible gene in this  
84 kindred has not been identified. We recruited an additional affected individual of this  
85 kindred<sup>2,16</sup> (family 3, Fig. 1, Table 1, Supplementary Note) and performed exome  
86 sequencing<sup>13</sup> of three affected subjects, revealing two shared novel protein-changing  
87 heterozygous variants in *CLCN2* (p.Arg172Gln, NP\_004357) and *LINGO1* (p.His591Gln,  
88 NP\_116197) (Supplementary Table 1). *CLCN2* was considered the more likely candidate

89 gene based on conservation (Fig. 1), expression levels in human adrenal cortex (8.14 for  
90 *CLCN2*, 5.91 for *LINGO1*, log<sub>2</sub> scale, mean expression of all genes 7.20<sup>6</sup>), and  
91 segregation analysis in the pedigree (Supplementary Table 2, Fig. 1).

92 We next searched for rare (allele frequency <10<sup>-5</sup> in public databases) damaging<sup>17</sup>  
93 variants in *CLCN2* and *LINGO1* among the exomes of 35 unrelated individuals diagnosed  
94 with unsolved primary aldosteronism by age 10 years – an extreme phenotype<sup>13</sup>. Only  
95 *CLCN2* showed such variants. All four were heterozygous and absent in public databases  
96 (Supplementary Table 1). Remarkably, one proband had the identical p.Arg172Gln  
97 variant found in family 3. In three additional subjects, p.Met22Lys and p.Tyr26Asn  
98 occurred at positions conserved through invertebrates, and one variant produced a new  
99 splice donor site resulting in an in-frame deletion (p.Lys362del) (Fig. 1, see below).

100 Analysis of *CLCN2* in 45 additional unrelated subjects diagnosed with primary  
101 aldosteronism by age 20 years (Supplementary Table 3) revealed two additional  
102 occurrences of p.Arg172Gln (Fig. 1). Additionally, p.Ser865Arg occurred at a moderately  
103 conserved position (Fig. 1). Sanger sequencing confirmed all variants (Supplementary  
104 Fig. 1). Sequencing of Arg172 in 1587 additional subjects referred for potential  
105 Mendelian hypertension, including 375 with primary aldosteronism diagnosed after age  
106 30, identified no p.Arg172Gln variants, supporting enrichment in early-onset primary  
107 aldosteronism.

108 Among the four kindreds with p.Arg172Gln, one mutation (in kindred 318)  
109 occurred *de novo* (absent in proband's biological parents; Fig. 1, Supplementary Table 4).  
110 Among the other three kindreds, the maximum lengths of shared mutation-linked  
111 haplotypes between pairs of individuals ranged from 4,894 bp to 357,885 bp

112 (Supplementary Table 5), with the putative last shared ancestor occurring ~651 (95% CI,  
113 203–2615) to ~50,000 generations ago (95% CI, 10,000–infinity)<sup>18</sup>. While extremely  
114 remote common ancestry is a possibility, independent occurrence is overwhelmingly  
115 likely. After finding this mutation in the first family, the probability of finding, by chance,  
116 three additional independent instances of p.Arg172Gln (one *de novo*), among 80  
117 probands is  $6.5 \times 10^{-12}$  (Online Methods). The probability of any pair of these variants  
118 being identical by descent from a remote common ancestor is even lower. Lastly, the  
119 burden of rare protein-altering *CLCN2* variants in primary aldosteronism kindreds is  
120 significantly higher than in controls (8/81 vs. 6/3578,  $p=1.3 \times 10^{-10}$ , relative risk 58.9,  
121 Supplementary Table 6).

122 Sanger sequencing identified eight carriers of the p.Arg172Gln variant in family 3  
123 (Fig. 1, Supplementary Fig. 1, Table 1, Supplementary Note). Seven carriers had elevated  
124 aldosterone/renin ratios (ARRs, a screening test for primary aldosteronism); those tested  
125 had positive confirmatory fludrocortisone suppression tests (FSTs) and non-lateralizing  
126 aldosterone production. One subject had repeatedly normal ARR, suggesting incomplete  
127 penetrance. Subject 3-1, diagnosed with hypertension in her 30s and with primary  
128 aldosteronism at age 66 years, was *CLCN2* wildtype (Supplementary Table 2). In  
129 addition to later onset, she was distinct in having increased aldosterone with upright  
130 posture, typical of sporadic idiopathic hyperaldosteronism<sup>5</sup>. In kindred 1786, the  
131 proband's affected mother and brother carried the p.Arg172Gln variant. The brother had  
132 borderline ARR with suppressed renin and prehypertension at age 13 years. Subject  
133 1492-1 was diagnosed with hypertension and primary aldosteronism in infancy, but  
134 became normotensive by age 2, suggesting variable expressivity with age. Among other

135 probands, the p.Met22Lys variant was *de novo* (Supplementary Table 4). Thus in two of  
136 the four kindreds with parental data, rare *CLCN2* mutations were *de novo*.

137 *In silico* splice site analysis<sup>19</sup> of the variant in kindred 1492 predicted the creation  
138 of a new splice donor at the end of exon 10, three base pairs upstream of the normal  
139 splice donor. In a splicing assay in HEK cells (Supplementary Note), the wildtype exon  
140 was normally spliced, but the mutation resulted exclusively in splicing at the predicted  
141 upstream site, producing an in-frame deletion of codon 362 (Supplementary Fig. 1).

142 ClC-2, the chloride channel encoded by *CLCN2*, is found in many tissues,  
143 including brain, kidney, lung, and intestine<sup>20</sup>. Additionally, *CLCN2* RNA is found in the  
144 adrenal gland (see above). Immunohistochemistry with an antibody specific for ClC-2  
145 revealed intense staining of human adrenal zona glomerulosa (Fig. 2, Supplementary Fig.  
146 2), consistent with a role in regulating aldosterone production.

147 Chloride channels can conduct excitatory (membrane depolarizing) chloride  
148 efflux or inhibitory influx, depending on the ratio of chloride concentration on either side  
149 of the cell membrane. We determined the intracellular chloride concentration ( $[Cl^-]_{int}$ ) in  
150 mouse adrenal gland slices (Fig. 3a,b, Supplementary Fig. 2) using fluorescence lifetime  
151 imaging microscopy; the method is based on the concentration-dependent fluorescence  
152 quenching of a chloride-sensitive dye<sup>21</sup>. The median value of  $[Cl^-]_{int}$  was 74.7 mM. The  
153 distribution of intracellular glomerulosa chloride concentrations is rather broad, as  
154 expected for a dynamic equilibrium in cells with oscillating membrane potentials<sup>22</sup>. With  
155 a normal plasma  $Cl^-$  concentration of 100 mM, the calculated chloride reversal potential  
156 at 37°C is -8 mV, predicting that opening of ClC-2 in glomerulosa cells will result in  
157 chloride efflux and depolarization from the resting potential of about -80 mV<sup>22</sup>. This

158 depolarization is predicted to activate voltage-gated  $\text{Ca}^{2+}$  channels, inducing aldosterone  
159 biosynthesis.

160 A facultative subunit of ClC-2 in glia, GlialCAM/HEPACAM<sup>23</sup>, is not expressed  
161 in human adrenal gland (GTEX portal, see URLs). We therefore expressed wildtype (ClC-  
162 2<sup>WT</sup>) and each of the mutant ClC-2s (ClC-2<sup>MUT</sup>) alone in HEK293T cells and performed  
163 whole-cell patch clamp electrophysiology at  $[\text{Cl}^-]_{\text{int}}=75$  mM. ClC-2<sup>WT</sup> channels are closed  
164 at depolarized voltages and activate slowly at voltages negative to the chloride reversal  
165 potential<sup>20,24,25</sup>. All mutants shifted the activation curve to more positive voltages (Fig. 3,  
166 Supplementary Fig. 3, Supplementary Table 8). ClC channels are homodimers, with  
167 each subunit forming a separate conduction pathway. Each protopore can be individually  
168 opened and closed by a fast protopore gate, and a common slow gating mechanism acts  
169 on both pores<sup>24,26</sup>. Whereas p.Ser865Arg altered protopore open probability and  
170 deactivation time constants (Fig. 3), all other mutations modified common gating by  
171 increasing the minimum open probability and accelerating activation and deactivation  
172 time constants (Fig. 3, Supplementary Fig. 3). Mass spectrometry demonstrated that  
173 p.Ser865 was phosphorylated, suggesting a regulatory mechanism (Supplementary Fig. 4).  
174 The observed gating alterations with ClC-2<sup>MUT</sup> predict significantly larger chloride efflux  
175 versus ClC-2<sup>WT</sup> in glomerulosa cells at physiological membrane potentials.

176 To characterize the impact of ClC-2<sup>WT</sup> and ClC-2<sup>MUT</sup> in human adrenal  
177 glomerulosa cells, we expressed channels in human H295R adrenocortical cancer cells,  
178 an established model of aldosterone production<sup>27</sup>. Confocal microscopy revealed partial  
179 colocalization of YFP-tagged ClC-2<sup>WT</sup> and ClC-2<sup>MUT</sup> with a surface membrane marker;  
180 p.Met22Lys showed less colocalization than ClC-2<sup>WT</sup> (Supplementary Fig. 4). RNA-Seq

181 (Fig. 4a, Supplementary Table 9) demonstrated that transfection of untagged WT and  
182 p.Arg172Gln *CLCN2* both significantly increased expression of *CYP11B2* and its  
183 upstream regulator *NR4A2* (*NURRI*)<sup>28</sup>; *RGS4*, which provides feedback inhibition of Ang  
184 II-triggered signaling<sup>29</sup>, was also upregulated. Quantitative real-time PCR of *CYP11B2*  
185 revealed that transfection of *CLCN2*<sup>MUT</sup> produced significantly greater increases in  
186 *CYP11B2* expression than *CLCN2*<sup>WT</sup> (Fig. 4b). In contrast, transfection of loss-of-  
187 function *CLCN2* mutations<sup>30</sup> did not change *CYP11B2* expression (Supplementary Fig. 5).  
188 H295R cells and their subclone HAC15 have negative membrane potentials<sup>31</sup>. Current-  
189 clamp recordings demonstrated significant depolarization of HAC15 upon WT *CLCN2*  
190 expression; p.Arg172Gln amplified this effect (Fig. 4c).

191         The finding of four independent occurrences of p.Arg172Gln (one *de novo*), along  
192 with four additional novel variants (one *de novo*) among 81 probands with early-onset  
193 primary aldosteronism provides strong evidence implicating these variants in disease  
194 pathogenesis. The localization of ClC-2 in adrenal zona glomerulosa is consistent with  
195 this observation. The electrophysiologic impact of mutant channels and their effect on  
196 aldosterone synthase expression demonstrate that these mutations cause gain of function,  
197 producing membrane depolarization and increasing *CYP11B2* expression (Fig. 4d).  
198 Because the syndrome in kindred 3 was named “FH-II”<sup>2</sup>, we suggest to use this term for  
199 patients with germline *CLCN2* variants.

200         Retrospectively, efforts to map the disease gene in family 3<sup>32</sup> were challenged by  
201 a phenocopy (sporadic idiopathic hyperaldosteronism) in subject 3-1, incomplete  
202 penetrance and phenotypic uncertainty. Rare *CLCN2* variants explained primary  
203 aldosteronism in ~10% of the early-onset cohort studied, suggesting there are likely

204 additional genes yet undiscovered. Genetic testing for germline mutations in *CLCN2* and  
205 other early primary aldosteronism genes can be useful for establishing diagnosis, defining  
206 treatment options and assessing risk to future offspring.

207 Probands with FH-II showed early-onset primary aldosteronism and hypertension,  
208 often with hypokalemia. Hypertension was controlled with mineralocorticoid receptor  
209 antagonists or other antihypertensives (Supplementary Note). This phenotype appears  
210 indistinguishable from patients with *CACNAIH* mutations<sup>13</sup>. Hybrid steroid production  
211 and/or response to glucocorticoids, historically used to diagnose GRA<sup>11</sup>, were absent, as  
212 were massive adrenal hyperplasia (present in many subjects with *KCNJ5* variants<sup>6,12</sup>) and  
213 neurodevelopmental abnormalities (characteristic of *CACNAID* mutation<sup>7</sup>). Despite  
214 widespread *CLCN2* expression, subjects with gain-of-function *CLCN2* variants shared no  
215 apparent pathology other than primary aldosteronism, whereas loss-of-function *CLCN2*  
216 variants cause leukoencephalopathy with ataxia<sup>33</sup>, with a similar phenotype in mice<sup>34</sup>.  
217 Incomplete penetrance or phenotypic amelioration with age, as sometimes occurs with  
218 germline mutations in *CYP11B2*, *KCNJ5*, *CACNAID* and *CACNAIH*<sup>7,12,13,35</sup>, occurred in  
219 some subjects with *CLCN2* mutations.

220 Our findings for the first time implicate activity of an anion channel in the  
221 regulation of aldosterone biosynthesis, primary aldosteronism and hypertension. Whether  
222 previously described slowly activating tiny chloride currents at strongly negative voltages  
223 in rat glomerulosa cells<sup>15</sup> or Ras-dependent chloride currents<sup>36</sup> represent ClC-2 is unclear.  
224 *In vivo*, ClC-2 may contribute to hyperpolarization-induced depolarization of adrenal  
225 glomerulosa cells, cyclic membrane potential oscillations, and aldosterone production<sup>22</sup>.

226 Variants in primary aldosteronism would likely amplify these effects. Mouse models may  
227 prove useful to study such effects.

228

#### 229 **URLs**

230 ClinVar, <https://www.ncbi.nlm.nih.gov/clinvar/>; github,  
231 [https://github.com/murim76/gene\\_burden\\_test/blob/master/Compare\\_VCF\\_for\\_Scholl.pl](https://github.com/murim76/gene_burden_test/blob/master/Compare_VCF_for_Scholl.pl);  
232 GEO series accession, <https://www.ncbi.nlm.nih.gov/geo/query/acc.cgi?acc=GSE107030>;  
233 The Human Protein Atlas, <http://www.proteinatlas.org/ENSG00000165478->  
234 HEPACAM/cell/HEK+293, retrieved on 06/27/2017; FastQC,  
235 <https://www.bioinformatics.babraham.ac.uk/projects/fastqc/>; GTEx Portal,  
236 <http://www.gtexportal.org/home/gene/HEPACAM>.

237

#### 238 **Acknowledgments**

239 We thank our patients and their families for their invaluable contributions, the Yale  
240 Center for Genome Analysis for next-generation sequencing, the Center for Advanced  
241 Imaging (CAi) at Heinrich Heine University for providing a confocal microscope,  
242 Stefanie Weidtkamp-Peters and Sebastian Hänsch for technical assistance, Junhui Zhang  
243 for helpful discussions, Eric Seidel, Nadine Erlenhardt and Nicolai Klöcker for providing  
244 immunoprecipitation protocols and helpful discussions, Celso Gomez-Sanchez (The  
245 University of Mississippi) for providing plasmids, William Rainey (University of  
246 Michigan) for providing HAC15 cells and Matthias Haase (Heinrich Heine University  
247 Düsseldorf) for providing H295R cells. Computational support and infrastructure were in  
248 part provided by the Centre for Information and Media Technology (Düsseldorf).

249 Supported in part by the Ministerium für Kultur und Wissenschaft des Landes Nordrhein-  
250 Westfalen (Rückkehrprogramm and Junges Kolleg), the Deutsche  
251 Forschungsgemeinschaft (SCHO 1386/2-1) (all UIS), the NIH Center for Mendelian  
252 Genomics (5U54HG006504), NIH P01DK17433, and the Howard Hughes Medical  
253 Institute (all RPL).

254

### 255 **Author Contributions**

256 UIS, GS, ChF, and RPL designed the study. MS and RG recruited and characterized  
257 Family 3. AMO, CG, DM, RWL, DPJ, GC, PG, EL, CNW, and RPL ascertained and  
258 recruited probands with early-onset primary aldosteronism. AAV, EL, and UIS recruited  
259 additional members of selected families. CNW, SX, and AW prepared DNA samples;  
260 UIS, AAV, SCJ, TY, MC, and RPL analyzed exome sequencing results; UIS identified  
261 the disease gene; CNW, AT, and AAV performed and analyzed targeted DNA  
262 sequencing; JS performed immunohistochemistry, immunoprecipitation and real-time  
263 PCR; JS and AT made constructs and generated stable cell lines; JS and JC prepared  
264 samples for and analyzed RNA sequencing; JS and UIS performed and analyzed splicing  
265 assay and confocal microscopy; GS, HT, VU and ChF performed and analyzed FLIM and  
266 electrophysiology; MK and PM performed and analyzed mass spectrometry; LCR read  
267 and revised the manuscript; UIS wrote the initial draft of the manuscript, with  
268 contributions and/or revisions from all authors.

269

### 270 **Competing financial interests**

271 The authors declare no competing financial or non-financial interests.

273 **References**

- 274 1. Monticone, S. *et al.* Prevalence and Clinical Manifestations of Primary  
275 Aldosteronism Encountered in Primary Care Practice. *J Am Coll Cardiol* **69**,  
276 1811-1820 (2017).
- 277 2. Stowasser, M. *et al.* Familial hyperaldosteronism type II: five families with a  
278 new variety of primary aldosteronism. *Clin Exp Pharmacol Physiol* **19**, 319-22  
279 (1992).
- 280 3. Collaboration, N.C.D.R.F. Worldwide trends in blood pressure from 1975 to  
281 2015: a pooled analysis of 1479 population-based measurement studies with  
282 19.1 million participants. *Lancet* (2016).
- 283 4. Lim, S.S. *et al.* A comparative risk assessment of burden of disease and injury  
284 attributable to 67 risk factors and risk factor clusters in 21 regions, 1990-  
285 2010: a systematic analysis for the Global Burden of Disease Study 2010.  
286 *Lancet* **380**, 2224-60 (2012).
- 287 5. Funder, J.W. *et al.* The Management of Primary Aldosteronism: Case  
288 Detection, Diagnosis, and Treatment: An Endocrine Society Clinical Practice  
289 Guideline. *J Clin Endocrinol Metab* **101**, 1889-916 (2016).
- 290 6. Choi, M. *et al.* K<sup>+</sup> channel mutations in adrenal aldosterone-producing  
291 adenomas and hereditary hypertension. *Science* **331**, 768-72 (2011).
- 292 7. Scholl, U.I. *et al.* Somatic and germline CACNA1D calcium channel mutations  
293 in aldosterone-producing adenomas and primary aldosteronism. *Nat Genet*  
294 **45**, 1050-4 (2013).
- 295 8. Azizan, E.A. *et al.* Somatic mutations in ATP1A1 and CACNA1D underlie a  
296 common subtype of adrenal hypertension. *Nat Genet* **45**, 1055-60 (2013).
- 297 9. Beuschlein, F. *et al.* Somatic mutations in ATP1A1 and ATP2B3 lead to  
298 aldosterone-producing adenomas and secondary hypertension. *Nat Genet* **45**,  
299 440-4 (2013).
- 300 10. Fernandes-Rosa, F.L. *et al.* Genetic spectrum and clinical correlates of somatic  
301 mutations in aldosterone-producing adenoma. *Hypertension* **64**, 354-61  
302 (2014).
- 303 11. Lifton, R.P. *et al.* A chimaeric 11 beta-hydroxylase/aldosterone synthase gene  
304 causes glucocorticoid-remediable aldosteronism and human hypertension.  
305 *Nature* **355**, 262-5 (1992).
- 306 12. Scholl, U.I. *et al.* Hypertension with or without adrenal hyperplasia due to  
307 different inherited mutations in the potassium channel KCNJ5. *Proc Natl Acad*  
308 *Sci U S A* **109**, 2533-8 (2012).
- 309 13. Scholl, U.I. *et al.* Recurrent gain of function mutation in calcium channel  
310 CACNA1H causes early-onset hypertension with primary aldosteronism. *Elife*  
311 **4**(2015).
- 312 14. Korah, H.E. & Scholl, U.I. An Update on Familial Hyperaldosteronism. *Horm*  
313 *Metab Res* **47**, 941-6 (2015).
- 314 15. Spat, A. & Hunyady, L. Control of aldosterone secretion: a model for  
315 convergence in cellular signaling pathways. *Physiol Rev* **84**, 489-539 (2004).

- 316 16. Carss, K.J., Stowasser, M., Gordon, R.D. & O'Shaughnessy, K.M. Further study  
317 of chromosome 7p22 to identify the molecular basis of familial  
318 hyperaldosteronism type II. *J Hum Hypertens* **25**, 560-4 (2011).
- 319 17. Dong, C. *et al.* Comparison and integration of deleteriousness prediction  
320 methods for nonsynonymous SNVs in whole exome sequencing studies. *Hum*  
321 *Mol Genet* **24**, 2125-37 (2015).
- 322 18. Genin, E., Tullio-Pelet, A., Begeot, F., Lyonnet, S. & Abel, L. Estimating the age  
323 of rare disease mutations: the example of Triple-A syndrome. *J Med Genet* **41**,  
324 445-9 (2004).
- 325 19. Dogan, R.I., Getoor, L., Wilbur, W.J. & Mount, S.M. SplicePort--an interactive  
326 splice-site analysis tool. *Nucleic Acids Res* **35**, W285-91 (2007).
- 327 20. Thiemann, A., Grunder, S., Pusch, M. & Jentsch, T.J. A chloride channel widely  
328 expressed in epithelial and non-epithelial cells. *Nature* **356**, 57-60 (1992).
- 329 21. Untiet, V. *et al.* Glutamate transporter-associated anion channels adjust  
330 intracellular chloride concentrations during glial maturation. *Glia* **65**, 388-  
331 400 (2017).
- 332 22. Hu, C., Rusin, C.G., Tan, Z., Guagliardo, N.A. & Barrett, P.Q. Zona glomerulosa  
333 cells of the mouse adrenal cortex are intrinsic electrical oscillators. *J Clin*  
334 *Invest* **122**, 2046-53 (2012).
- 335 23. Jeworutzki, E. *et al.* GlialCAM, a protein defective in a leukodystrophy, serves  
336 as a ClC-2 Cl(-) channel auxiliary subunit. *Neuron* **73**, 951-61 (2012).
- 337 24. Stolting, G. *et al.* Regulation of ClC-2 gating by intracellular ATP. *Pflugers Arch*  
338 **465**, 1423-37 (2013).
- 339 25. Niemeyer, M.I., Cid, L.P., Zuniga, L., Catalan, M. & Sepulveda, F.V. A conserved  
340 pore-lining glutamate as a voltage- and chloride-dependent gate in the ClC-2  
341 chloride channel. *J Physiol* **553**, 873-9 (2003).
- 342 26. Jentsch, T.J. Discovery of CLC transport proteins: cloning, structure, function  
343 and pathophysiology. *J Physiol* **593**, 4091-109 (2015).
- 344 27. Rainey, W.E., Bird, I.M. & Mason, J.I. The NCI-H295 cell line: a pluripotent  
345 model for human adrenocortical studies. *Mol Cell Endocrinol* **100**, 45-50  
346 (1994).
- 347 28. Bassett, M.H., Suzuki, T., Sasano, H., White, P.C. & Rainey, W.E. The orphan  
348 nuclear receptors NURR1 and NGFIB regulate adrenal aldosterone  
349 production. *Mol Endocrinol* **18**, 279-90 (2004).
- 350 29. Romero, D.G. *et al.* Regulators of G-protein signaling 4 in adrenal gland:  
351 localization, regulation, and role in aldosterone secretion. *J Endocrinol* **194**,  
352 429-40 (2007).
- 353 30. Garcia-Olivares, J. *et al.* Gating of human ClC-2 chloride channels and  
354 regulation by carboxy-terminal domains. *J Physiol* **586**, 5325-36 (2008).
- 355 31. Tauber, P. *et al.* Cellular Pathophysiology of an Adrenal Adenoma-Associated  
356 Mutant of the Plasma Membrane Ca(2+)-ATPase ATP2B3. *Endocrinology* **157**,  
357 2489-99 (2016).
- 358 32. Lafferty, A.R. *et al.* A novel genetic locus for low renin hypertension: familial  
359 hyperaldosteronism type II maps to chromosome 7 (7p22). *J Med Genet* **37**,  
360 831-5 (2000).

361 33. Depienne, C. *et al.* Brain white matter oedema due to ClC-2 chloride channel  
362 deficiency: an observational analytical study. *Lancet Neurol* **12**, 659-68  
363 (2013).  
364 34. Blanz, J. *et al.* Leukoencephalopathy upon disruption of the chloride channel  
365 ClC-2. *J Neurosci* **27**, 6581-9 (2007).  
366 35. Stowasser, M. *et al.* Clinical, biochemical and genetic approaches to the  
367 detection of familial hyperaldosteronism type I. *J Hypertens* **13**, 1610-3  
368 (1995).  
369 36. Chorvatova, A., Gendron, L., Bilodeau, L., Gallo-Payet, N. & Payet, M.D. A Ras-  
370 dependent chloride current activated by adrenocorticotropin in rat adrenal  
371 zona glomerulosa cells. *Endocrinology* **141**, 684-92 (2000).  
372  
373  
374  
375  
376  
377  
378  
379  
380  
381  
382  
383  
384  
385  
386  
387

388 **Figure Legends**

389 **Figure 1.**

390 **Kindreds with Hypertension and Primary Aldosteronism with *CLCN2* Mutations.**

391 (a) Pedigrees of eight kindreds with primary aldosteronism and hypertension, with  
392 indicated novel *CLCN2* variants. Filled black symbols denote subjects with primary  
393 aldosteronism, and filled grey symbols denote subjects with early-onset hypertension or  
394 borderline elevated ARRs. Genotypes are shown beneath each symbol, M/+ denotes the  
395 indicated novel *CLCN2* variant in the heterozygous state, and +/+ denotes homozygous  
396 wildtype sequence. (b) Position of the indicated variants in the N-terminus, D helix, K  
397 helix and C-terminus of the ClC-2 chloride channel encoded by *CLCN2*. Red ellipses  
398 represent C-terminal CBS domains. (c) Conservation of the respective amino acid  
399 positions among orthologous species (*H. sapiens*, human; *M. musculus*, mouse; *G. gallus*,  
400 chicken; *X. tropicalis*, western clawed frog; *D. rerio*, zebrafish; *C. intestinalis*, vase  
401 tunicate; *D. mojavensis*, fruit fly; *C. elegans*, roundworm).

402

403 **Figure 2.**

404 **Expression of CIC-2 in Human Adrenal Gland.**

405 (a) Section of human adrenal cortex (C, capsule; G, glomerulosa; F, fasciculata; R,  
406 reticularis) stained by immunohistochemistry and counterstained with hematoxylin. One  
407 of two technical replicates is shown. Left, anti-CIC-2; middle, control preincubation of  
408 the anti-CIC-2 antibody with the antigenic peptide; right, anti-Dab2 as marker of the  
409 adrenal zona glomerulosa. The comparison of the three panels demonstrates specific  
410 expression of CIC-2, predominantly in the zona glomerulosa. Scale bars represent 200  
411  $\mu\text{m}$ . (b) Higher magnifications of the zona glomerulosa, scale bars represent 100  $\mu\text{m}$ .

412

413 **Figure 3.**

414 ***CLCN2* Mutations Increase Excitatory Anion Efflux by Modifying the Voltage**  
415 **Dependence of Channel Opening.**

416 (a) Representative mouse adrenal gland section loaded with MQAE at 37°C. Short  
417 lifetimes (red, 1 ns) indicate high, long lifetimes (blue, 4 ns) low intracellular chloride  
418 concentrations. Scale bar, 10  $\mu\text{m}$ . (b) Insert, calibration curve of MQAE fluorescence  
419 lifetimes in cells with preset intracellular chloride concentrations. A kernel density  
420 estimation of intracellular chloride concentrations for glomerulosa cells was obtained  
421 (Gaussian kernel, bandwidth=8.0 as determined by Scott's rule). Median intracellular  
422 chloride concentration was 74.7 mM (300 cells, 12 slices, five animals). Box,  
423 interquartile range; whiskers, 1.5x interquartile range; line, median. (c) Whole-cell patch  
424 clamp recordings of representative  $\text{ClC-2}^{\text{WT}}$  and  $\text{ClC-2}^{\text{MUT}}$  and voltage protocol (150 mM  
425  $[\text{Cl}^-]_{\text{out}}$ , 75 mM  $[\text{Cl}^-]_{\text{int}}$ , see Online Methods for solutions) are shown. (d) Time constants  
426 for representative  $\text{ClC-2}^{\text{WT}}$  and  $\text{ClC-2}^{\text{MUT}}$  with mean values  $\pm$  95% confidence intervals  
427 are shown (Supplementary Table 8). (e) and (f) Mean relative open probabilities (e) and  
428 common gate open probabilities (f) were fit with a Boltzmann function (bold lines,  
429 Supplementary Table 8) with 95% confidence intervals as calculated from a bootstrap  
430 resampling (translucent areas). Open probabilities of mutant channels are significantly  
431 higher at the glomerulosa resting potential of  $\sim$ -80 mV (WT,  $0.22 \pm 0.02$  (n=11);  
432 p.Arg172Gln,  $0.45 \pm 0.02$  (n=13;  $p < 0.001$  vs. WT); p.Ser865Arg,  $0.33 \pm 0.02$  (n=12;  
433  $p < 0.001$  vs. WT); all mean  $\pm$  SEM, one-way ANOVA;  $F=36.307$ ; d.f.=5). The insert in (e)  
434 demonstrates the shift in voltage activation as assessed by the point of half maximal  
435 activation (Supplemental Table 8). \*\*,  $p < 0.01$ .

436

437 **Figure 4.**

438 **CIC-2 Increases Aldosterone Synthase Expression in H295R cells.**

439 (a) RNA sequencing of H295R cells transfected with *CLCN2* (WT or p.Arg172Gln), and  
440 vector control (heatmap). FPKM, fragments per kilobase of transcript per million  
441 fragments mapped. *CLCN2* and *CYP11B2* show the largest increase in expression versus  
442 control. Genes involved in adrenal function or calcium pathway are highlighted. (b)  
443 Relative expression levels of *CYP11B2* (box, interquartile range; whiskers, 1.5x  
444 interquartile range; line, median) in the H295R cell line after transfection with empty  
445 vector (control), *CLCN2*<sup>WT</sup> (blue), and *CLCN2*<sup>MUT</sup> (yellow). Parallel transfections and  
446 real-time PCRs were performed in each group. *CYP11B2* expression significantly  
447 increases after transfection of *CLCN2*<sup>MUT</sup> (see Supplementary Table 8 for statistical  
448 analysis). (c) Resting membrane potential (plots as above) of HAC15 cells stably  
449 expressing *CLCN2* (WT or p.Arg172Gln) and untransfected controls. WT and  
450 p.Arg172Gln cause significant depolarization versus control, and p.Arg172Gln causes  
451 significant depolarization versus WT (see Supplementary Table 8 for statistical analysis).  
452 (d) Model of CIC-2 function in human adrenal glomerulosa. Resting cells are  
453 hyperpolarized. Angiotensin II (AngII) and hyperkalemia cause depolarization, activation  
454 of voltage-dependent calcium channels, calcium influx, and increased *CYP11B2*  
455 expression via the transcription factor *NR4A2* (*NURR1*). CIC-2<sup>MUT</sup> causes increased  
456 *CYP11B2* expression by membrane depolarization via increased Cl<sup>-</sup> efflux. \*\*, p<0.01;  
457 \*\*\*, p<0.001; \*\*\*\*, p<0.0001.

458

459 **Table 1. Clinical Characteristics of Subjects with *CLCN2* Variants**

Family ID	Subject ID	<i>CLCN2</i> variant	Gender	Age dx / blood draw	BP (mmHg)	BP %ile	K <sup>+</sup> (mM)	Aldo (ng/dl)	PRA (ng/ml/h)	ARR (ng/dl: ng/ml/h)
Normal range						<95 <sup>th</sup> in adults <140/90 in adults	<95 <sup>th</sup> in children	3.5-5.5		< 20
3	2	p.Arg172Gln	F	24	120/80 on 3 meds	NA	3.0	40.2	0.3	134.0
3	4	p.Arg172Gln	M	36	98/70 (age 24)	NA	4.2	24.5	1.2	20.4
3	5	p.Arg172Gln	F	19	150/100 on 1 med	NA	3.3	27.4	0.1	274.0
3	7	p.Arg172Gln	F	20	140/100	NA	3.8	26.5	0.1	265.0
3	9	p.Arg172Gln	M	18	120/80 (age 19)	NA	4.0	24.7	1.5	16.5
3	10	p.Arg172Gln	M	17	130/85	90-95th	4.0	26.2	0.1	262.0
3	11	p.Arg172Gln	F	14	94/62	≤ 50th	4.0	21.2	0.1	212.0
3	35	p.Arg172Gln	F	16	170/110	>99th	3.4	25.5	≤0.2	≥127.5
1786	1	p.Arg172Gln	F	15	150/100	>99th	2.9	47.9	<1.0	>47.9
1786	2	p.Arg172Gln	F	32	118/68 on 2 meds	NA	3.0	46.3	<1.0	>46.3
1786	3	p.Arg172Gln	M	13	121/75 (24 h)	>75th	4.4	12.0	<0.6	>20.0
537	1	p.Arg172Gln	F	11	160/120	>99th	3.0	26.0	0.3	86.7
318	1	p.Arg172Gln	M	7	170/140	>99th	2.6	9.5	0.21	45.2
1281	1	p.Met22Lys	F	1	117/71	>99th	4.1	17.0	<0.5	>34.0
531	1	p.Tyr26Asn	F	6	280/188 at age 20	NA	NA	100.0	<3.0	>33.3
840	1	p.Ser865Arg	M	15	130/100	90-95 <sup>th</sup> / <sup>&gt;</sup> 99 <sup>th</sup>	3.2	37.0	0.2	185.0
1492	1	p.Lys362del	M	0.2	150/90	>99th	4.0	63.8	<0.15	>425.3

460 Age dx, age at diagnosis; BP, blood pressure (office unless otherwise indicated); BP %ile,  
461 blood pressure percentile for subjects under age 18 years; K<sup>+</sup>, serum potassium level;  
462 Aldo, serum aldosterone level; PRA, plasma renin activity; ARR, aldosterone/renin ratio.  
463 F, female; M, male; NA, not available or not applicable; med(s), antihypertensive  
464 medication(s). Reference values are given below each parameter.  
465

466 **Online Methods**

467 **Subjects.** Study subjects included the Australian kindred<sup>2,32,37</sup>, 35 unrelated primary  
468 aldosteronism subjects without known disease-causing mutations, diagnosed by age 10  
469 years (clinical characteristics published<sup>13</sup>), and 45 subjects diagnosed with primary  
470 aldosteronism by age 20 years (Supplementary Table 3). Selected families had additional  
471 members recruited. Controls were 3,578 unaffected parents of autistic offspring<sup>38</sup>.  
472 Research protocols were approved by local institutional review boards at Yale University  
473 and University of Queensland, and all probands and family members provided informed  
474 consent. Primary aldosteronism was diagnosed based on elevated aldosterone/renin ratio  
475 (ARR, >20 ng/dl:ng/ml/h or equivalent values)<sup>5</sup>, with aldosterone >15 ng/dl, or  
476 marginally elevated values in the presence of hypokalemia. Confirmatory testing was  
477 performed according to the referring centers' guidelines<sup>5</sup>. Venous blood or saliva samples  
478 were obtained from subjects and family members and subjected to exome and/or Sanger  
479 sequencing<sup>13</sup>.

480

481 **DNA preparation and exome sequencing.** DNA was prepared from venous blood or  
482 saliva samples using standard procedures. Exome capture was performed using the 2.1M  
483 NimbleGen Exome reagent (Roche NimbleGen, Madison, WI), and 75 base paired end  
484 sequencing on the Illumina (San Diego, CA) platform and analysis were performed as  
485 described<sup>13</sup>.

486

487 **Sanger sequencing of genomic DNA and genotyping of parent-offspring trios.** Direct  
488 bidirectional Sanger sequencing of candidate variants from genomic DNA of indicated

489 subjects was performed at Beckman Coulter Genomics (UK) or the Keck DNA  
490 sequencing facility at Yale University following PCR amplification. Rare variants  
491 identified in index cases through exome sequencing were genotyped by targeted PCR and  
492 Sanger sequencing in both parents to confirm paternity / maternity.

493

494 **Immunohistochemistry and immunofluorescence.** Formalin-fixed, paraffin-embedded  
495 5  $\mu$ m human adrenal gland sections were obtained from US Biomax (Rockville, MD,  
496 USA) and Pantomics (Richmond, CA, USA). Immunohistochemistry was performed as  
497 described<sup>7</sup>, with the exception that 10% donkey serum was used for blocking. The  
498 concentration of the antigenic peptide was 0.4 mg/ml, and 1  $\mu$ g peptide per  $\mu$ g antibody  
499 was used. Images were recorded on a Zeiss (Oberkochen, Germany) Axioplan 2 Imaging  
500 microscope (10x and 40x objectives) with a Zeiss AxioCam Mrc5 camera. Image  
501 cropping was performed in Adobe Illustrator CS4. Primary antibody against CIC-2 was  
502 HPA014545 (Sigma-Aldrich Prestige Antibodies, St. Louis, MO, USA; 1:100, incubation  
503 overnight at 4°C), and antibody against Dab2 was #sc-13982 (Santa Cruz, Santa Cruz,  
504 CA, USA; 1:100 dilution). Secondary antibody was donkey  $\alpha$ -rabbit (#035-152, 1:200,  
505 Jackson, Bar Harbor, ME, USA, 2 h at room temperature) for human samples. To confirm  
506 the selection of the zona glomerulosa in mouse adrenal slices for fluorescence lifetime  
507 imaging (FLIM), slices were stained with the Dab2 antibody (1:100 dilution, incubation  
508 overnight at 4°C). Secondary antibody was donkey  $\alpha$ -rabbit conjugated to Alexa Fluor  
509 647 (A-31573, ThermoFisher Scientific; 1:1000, 2h at room temperature).  
510 Immunofluorescent images were recorded on a Leica TCS SP5 laser scanning confocal  
511 microscope (Leica Microsystems, Heidelberg, Germany).

512

513 **Molecular cloning.** Site directed mutagenesis (QuikChange, Agilent Technologies, Santa  
514 Clara, CA) was performed to introduce mutations into pcDNA5/FRT/TO *CLC-2*<sup>24</sup>  
515 according to the manufacturer's instructions. Primer sequences (M22K\_F/\_R,  
516 Y26N\_F/\_R, R172Q\_F/\_R, K362 del new\_F/\_R) are given in Supplementary Table 10.  
517 Each construct was validated by sequencing of the entire coding region. Mutant cDNAs  
518 were subcloned in frame into the pRcCMV vector containing the YFP cDNA using *NotI*  
519 and *PmlI* for use in confocal microscopy only. Two independent clones were assessed in  
520 all experiments (Supplementary Fig. 3).

521

522 **Generation of stable cell lines.** Stable HEK293 cell lines were generated using the Flp-  
523 In T-REx system (Invitrogen, Life Technologies, Carlsbad, CA, USA) according to the  
524 manufacturer's instructions. HEK293 cells do not express HEPACAM (Human Protein  
525 Atlas, see URLs). Flp-In T-REx 293 cells (authenticated, Eurofins Genomics) were  
526 cultured in high glucose DMEM (Biochrom GmbH, Berlin, Germany) with 10% FBS  
527 (Biochrom), 1% Penicillin/Streptomycin, 100 µg/mL Zeocin and 15µg/mL Blasticidin  
528 (all Invitrogen) at 37°C and 5% CO<sub>2</sub> humidified atmosphere. Cells were transfected with  
529 2.4 µg pcDNA5/FRT/TO + insert (*CLCN2* mutants: p.Met22Lys, p.Tyr26Asn,  
530 p.Arg172Gln, p.Lys362del, p.Ser865Arg; two clones each) and 21.6 µg pOG44 using  
531 Lipofectamine 2000 (Invitrogen) and OPTIMEM (Gibco by Life Technologies, Carlsbad,  
532 CA, USA). The following day, the medium was changed to high glucose DMEM + 10%  
533 Tet-free FBS (Gibco) and 1% Penicillin/Streptomycin. 48 h after transfection, cells were  
534 split onto 15 cm dishes and selected with 15 µg/mL Blasticidin and 150 µg/mL

535 Hygromycin (Invitrogen). Single colonies were selected. Variants were confirmed by  
536 Sanger sequencing of DNA extracted from stable cell lines, and inducible expression was  
537 verified by western blot (CIC-2 antibody #ACL-002, Alomone labs, Jerusalem, Israel).  
538 The HAC15 cell line was kindly provided by Dr. William Rainey (University of  
539 Michigan), authenticated by short tandem repeat (STR) analysis (ATCC Cell Line  
540 Authentication Service) and cultured in DMEM/F12 (GlutaMAX; Gibco) + 5% HyClone  
541 Cosmic Calf Serum (CCS; GE Healthcare Life Sciences, Buckinghamshire, UK) +1%  
542 Penicillin-Streptomycin (Gibco) + 1% Insulin-Transferrin-Selenium (ITS; Gibco) +1%  
543 MEM Non-Essential Amino Acids Solution (Gibco) + 0.1% CD Lipid Concentrate  
544 (Gibco) at 37°C and 5% CO<sub>2</sub> in humidified atmosphere. Stable cell lines were prepared  
545 using the Piggybac transposon system (System Biosciences, Palo Alto, CA, USA).  
546 cDNAs of *CLCN2* (WT and Arg172Gln) were subcloned into pENTR-2B-Dual using  
547 NotI and XhoI. Gateway LR recombination (Invitrogen) was performed with pPiggybac-  
548 EF1 Neo + pTF rLTA (a kind gift of Dr. Celso Gomez-Sanchez, The University of  
549 Mississippi). Inserts were verified by Sanger sequencing. HAC15 cells were transfected  
550 using an Amaxa Nucleofector I (Lonza, Cologne, Germany; 2 million cells, 2 µg plasmid  
551 DNA, 0.8 µg Super Piggybac transposase; program X-005). After 48h, selection was  
552 initiated by addition of 5 µg/mL Blasticidin (Gibco) to the growth medium. Inducible  
553 expression was verified by western blot (CIC-2 antibody #ACL-002) after incubation  
554 with 1 µg/mL Doxycycline (Sigma Aldrich) for 24h.

555

556 **Preparation of acute adrenal slices.** After anesthetizing animals with isoflurane and  
557 decapitation, both adrenal glands were rapidly removed and placed in ice-cold

558 Bicarbonate Buffered Saline (BBS) (125 mM NaCl, 2 mM KCl, 26 mM NaHCO<sub>3</sub>, 0.1  
559 mM CaCl<sub>2</sub>, 5 mM MgCl<sub>2</sub>, 10 mM glucose, constantly oxygenated with 5% CO<sub>2</sub> in O<sub>2</sub>) for  
560 the removal of surrounding fat. The adrenal glands were embedded in 4% agarose in BBS,  
561 mounted, cut at 4°C (150-200 µm thick) with a Microm HM 650V (Thermo Scientific,  
562 Walldorf, Germany; frequency 60 Hz, amplitude 1 mm, drive 10) and held at 35°C for 30  
563 min in BBS. Slices were subsequently stored in BBS at 37°C for further experiments.  
564 During each experiment, slices were constantly perfused with solution at 37°C, and all  
565 measurements were completed within 8 h of organ removal.

566

567 **Fluorescence lifetime imaging microscopy (FLIM).** Prior to chloride imaging  
568 experiments, adrenal slices were incubated in BBS containing 10 mM 1-  
569 (ethoxycarbonylmethyl)-6-methoxyquinolinium bromide (MQAE; Sigma-Aldrich,  
570 Munich, Germany<sup>39</sup>) for 45-60 min at room temperature. Slices were transferred to an  
571 imaging chamber, perfused with BBS solution containing 2 mM instead of 0.1 mM Ca<sup>2+</sup>,  
572 and FLIM was performed as described<sup>21</sup>. The solution was perfused through a heating  
573 coil resulting in a temperature of 37°C in the perfusion chamber. Fluorescence was  
574 stimulated by two-photon excitation ( $\lambda_{\text{exc}} = 750 \text{ nm}$ ), MQAE fluorescence was filtered  
575 (short pass filter, 500 nm,  $\lambda_{\text{obs}} < 510 \text{ nm}$ ; Omega Optical, Brattleboro, VT), and mean  
576 fluorescence lifetimes were measured using multidimensional time-correlated single  
577 photon counting (TCSPC). TCSPC electronics (SPC-152; Becker & Hickl) and  
578 acquisition software were used for FLIM as described<sup>40</sup>. We recorded data of 12 slices  
579 from 5 different C57BL/6 mice (2 male, 3 female) of age 3 months or older.

580 For chloride concentration calibration, MQAE fluorescence lifetimes of preset  $[Cl^-]$  were  
581 measured. Adrenal slices were incubated in HEPES-buffered solution (140 mM  $K^+$ , 10  
582 mM  $Na^+$ , 10 mM HEPES, 10–80 mM  $Cl^-$ , 70–140 mM gluconate, adjusted to 310  
583 mOsmol/L with K–gluconate and to pH 7.4 with KOH, 37°C) containing 10  $\mu$ M nigericin  
584 (sodium salt; Sigma-Aldrich, Munich, Germany) and 10  $\mu$ M tributyltin (chloride salt;  
585 Sigma-Aldrich)<sup>21,40-42</sup>. The inverse fluorescence lifetime ( $1/\tau$ ) was plotted, and the  
586 calibration curve was fitted as described before<sup>21</sup>. The Stern-Volmer constant ( $K_{SV} = 3.96$ )  
587 was determined as the product of  $\tau_0$  and the slope of the calibration curve. Since the  
588 fluorescence lifetime of MQAE is reduced by chloride via collisional quenching, MQAE  
589 fluorescence lifetimes and  $[Cl^-]$  show a linear relationship:

$$\frac{\tau_0}{\tau} = 1 + K_{SV}[Cl^-]$$

590 Zona glomerulosa  $[Cl^-]_{int}$  could then be calculated according to this relationship.  
591 The three outermost cell layers were assumed to form the zona glomerulosa based on  
592 their characteristic nucleus to cytoplasm ratio and the corresponding staining with anti-  
593 DAB2 (#sc-13982, Santa Cruz) performed separately. Each cell was defined as a region  
594 of interest (ROI) with the exclusion of the nucleus, and fluorescence lifetimes were  
595 determined as mean values of the average fluorescence lifetimes of all pixels in a given  
596 ROI. Fluorescence lifetimes were calculated using SPCImage 5.6 (Becker&Hickl, Berlin,  
597 Germany) and exported for further extraction in Fiji. Statistics were performed using  
598 SigmaPlot 12 (Systat) and Python 3.5.2 + numpy 1.12.1 + scipy 0.18.1 + pandas 0.19.2 +  
599 seaborn 0.7.1 using built-in functions. The FLIM datasets generated during or analyzed

600 during the current study are available on request. Python scripts for analysis are based on  
601 built-in functions of the above mentioned packages but are available on request.

602

603 **Electrophysiological recordings.** Flp-In T-REx stable cell lines were used for  
604 electrophysiological recordings. For each construct, at least two clones using at least two  
605 separate preparations were included in the analysis. To avoid chloride depletion at large  
606 current amplitudes<sup>24</sup>, Flp-In T-REx cells were used without induction. Whole-cell patch  
607 clamp currents were recorded on an EPC10 amplifier using PatchMaster software (both  
608 HEKA, Lambrecht/Pfalz, Germany). Borosilicate glass pipettes with open resistances  
609 between 0.9 and 2.5 MΩ were used. The extracellular solution for whole-cell recordings  
610 contained (in mM): NaCl (140), KCl (4), CaCl<sub>2</sub> (2), MgCl<sub>2</sub> (1) and HEPES (10) at pH 7.4.  
611 The intracellular solution contained (in mM): NaCl (73), MgCl<sub>2</sub> (1), NaGluconate (42),  
612 EGTA (5), HEPES (10) and MgATP (1) at pH 7.4. The liquid junction potential was  
613 calculated to be 1.9 mV and corrected for *a priori*. Cells were held at the calculated  
614 chloride reversal potential of -17.5 mV at rest.

615 Instantaneous current amplitudes at the fixed tail step to +60 mV were normalized and  
616 plotted against the preceding voltage step to reveal relative open probability curves. The  
617 durations of the voltage steps were 5 s for ClC-2<sup>WT</sup> and ClC-2<sup>Ser865Arg</sup> and 1 s for all other  
618 mutations so that steady-state open probabilities were determined. Open probabilities  
619 ( $P_{open}$ ) were fitted using a modified Boltzmann equation:

$$P_{open}(V) = \frac{1}{1 + e^{\frac{-(V-V_{1/2})}{k}}}$$

620 to allow for a comparison of the half-maximal activation( $V_{1/2}$ ).

621 Fitting of the activation and deactivation current traces with the sum of two exponential  
622 functions revealed fast ( $\tau_1$ ) and slow ( $\tau_2$ ) time constants, respectively:

$$I(t) = A_0 + A_1 \cdot e^{-\frac{t}{\tau_1}} + A_2 \cdot e^{-\frac{-t}{\tau_2}}$$

623 CLC chloride channels are double-barreled channels with two conduction pathways.  
624 Protopores can be individually opened and closed by a fast gating process, but also jointly  
625 by slow common gating. Under the assumption that protopore and common gating  
626 processes are independent, the overall open probability equals the product of the  
627 respective individual open probabilities<sup>43</sup>:

$$P_{open} = P_{fast} \cdot P_{slow}$$

628 By inserting a 15 ms pulse to -220 mV between the variable test pulse and the tail pulse,  
629 the CLC-2 fast gate is maximally opened ( $P_{fast} = 1$ )<sup>44</sup>, and the common gate open  
630 probability can be determined. Fast protopore gate open probabilities were calculated by  
631 dividing the overall open probability by the common gate open probability.

632 Resting potentials in untransfected or in induced (1  $\mu$ g tetracycline/ml medium for 24h)  
633 stably transfected HAC15 cells were measured using the perforated patch technique<sup>45</sup> in  
634 the current clamp mode. The extracellular solution contained (in mM): 140 NaCl, 10  
635 HEPES, 4 KCl, 2 CaCl<sub>2</sub>, 1 MgCl<sub>2</sub> adjusted to a pH of 7.4. The pipette solution contained  
636 (in mM): 130 KCl, 10 HEPES, 5 NaCl with the pH adjusted to 7.4. To maintain the  
637 native intracellular [Cl<sup>-</sup>], we included the pore-forming, monovalent cation selective  
638 antibiotic gramicidin D (Sigma-Aldrich) in the pipette solution to obtain access to the  
639 inside of the cell<sup>45</sup>. Gramicidin stock solution (50 mg/ml in DMSO) was prepared daily,  
640 and the diluted solution (final concentration: 100  $\mu$ g/ml) was prepared every 2 h. The tip  
641 of the pipette (open resistance 1.5-3 M $\Omega$ ) was filled with solution lacking gramicidin to

642 facilitate gigaseal formation. Break-in was typically observed after 15-45 minutes.  
643 Resting potentials were determined using a HEKA EPC-10 patch clamp amplifier and the  
644 PatchMaster software (HEKA Elektronik) from the mean of 10-60 s long voltage  
645 recording segments with the current clamped to 0 pA. Only cells that exhibited CLC-2 like  
646 currents (visible slow activation upon hyperpolarization and a current larger than 40 pA  
647 at -160 mV in subsequent voltage-clamp experiments) were used for analysis.

648 Analysis of all electrophysiological experiments was performed using FitMaster software  
649 (HEKA Elektronik), SigmaPlot 12 (Systat) and Python 3.5.2 + numpy 1.12.1 + scipy  
650 0.18.1 + pandas 0.19.2 using built-in functions. The electrophysiology datasets generated  
651 during or analyzed during the current study are available on request. Python scripts for  
652 analysis are based on built-in functions of the above mentioned packages but are  
653 available on request. Normality was assessed by Shapiro-Wilk test.

654

655 **Culture of H295R cells.** H295R human adrenocortical cells (a kind gift of Dr. Matthias  
656 Haase, Düsseldorf) were authenticated by short tandem repeat (STR) analysis (ATCC  
657 Cell Line Authentication Service) and cultured in DMEM/F12 + HEPES (Gibco) + 2.5 %  
658 Ultrosor G (Pall, Port Washington, NY, USA) + 1% Insulin-Transferrin-Selenium+ (ITS+;  
659 Corning, Corning, NY, USA) + 1 % Penicillin/Streptomycin (Gibco) at 37°C and 5%  
660 CO<sub>2</sub> in humidified atmosphere.

661

662 **Quantitative real-time PCR.** Three million H295R cells were resuspended in 100 µl  
663 Nucleofector solution R (Lonza) plus 3 µg plasmid DNA (pcDNA/FRT/TO empty vector,  
664 WT or mutant *CLCN2*) and electroporated with program P-20 using an Amaxa

665 Nucleofector I (Lonza). After recovering of the cells in RPMI 1640 medium (Gibco) for  
666 15 min at 37°C, they were plated on 12-well plates. 24h after transfection, H295R cells  
667 were starved in DMEM/F12 + HEPES + 0.1 % Ultrosor G + 1 % Penicillin/Streptomycin  
668 for additional 24h. Total RNA was isolated using the RNeasy® Mini Kit (Qiagen GmbH,  
669 Hilden, Germany) and quantified with a Nanodrop 2000 (Thermo Scientific, Wilmington,  
670 DE, USA). After reverse transcription of RNA using Quantitect RT Kit (Qiagen),  
671 Taqman gene expression assays (Applied Biosystems, Foster City, CA, USA) for  
672 *GAPDH* (HS02758991\_g1) as housekeeping gene and *CYP11B2* (Hs01597732\_m1) as  
673 gene of interest were performed using the Taqman Gene Expression Master Mix. Each  
674 variant was assessed in parallel with wildtype and empty vector control. Gene expression  
675 was evaluated relative to the housekeeping gene and expressed as  $2^{\Delta\Delta Ct}$ . Normality was  
676 assessed by Shapiro-Wilk test. Statistical differences were assessed by ratio-paired two-  
677 tailed t tests (for normally distributed individual data), one-way ANOVA (for normally  
678 distributed multiple comparisons; adjusted p value reported) or Friedman test (multiple  
679 comparisons, no normal distribution; adjusted p value reported) in Graphpad Prism 7.

680

681 **Whole-transcriptome sequencing, read alignment and differential gene expression**  
682 **analysis.** H295R cells were transfected in two independent reactions as above, RNA was  
683 isolated using Trizol (Thermo Fisher Scientific), followed by DNase digest and column  
684 purification (RNeasy, Qiagen). Libraries were prepared after Poly A selection. Samples  
685 were sequenced on the Illumina HiSeq2500 at the Yale Center for Genome Analysis,  
686 producing a mean of 47.9 million 75-bp single-end reads. The quality of the raw  
687 sequencing reads was evaluated using FastQC version 0.10.4 (see URLs), and the base of

688 lower quality (base quality score < 20) in the last position was trimmed. Tophat v2.1.1<sup>46</sup>  
689 was used to align the high quality sequencing reads to the reference human genome  
690 sequence build hg19. Differentially expressed genes were identified by Cuffdiff v2.2.1<sup>47</sup>.  
691 An FDR adjusted p value (q value)  $\leq 0.05$  and  $|\log_2(\text{Fold Change})| \geq 1$  were set as the  
692 cutoffs for significantly differential expression.

693

694 **Estimation of the probability of observing one *de novo* and two transmitted**  
695 **p.Arg172Gln variants in *CLCN2*.** From the identification of the novel p.Arg172Gln  
696 variant in family 3, we calculated the probability of finding an identical *de novo* mutation  
697 and two independent instances of the same transmitted variant by chance among 80  
698 probands. Using the genome-wide mutation rate of  $1.67 \times 10^{-8}$  per base per generation  
699 from a recent study<sup>48</sup>, we estimated that the probability of seeing any specific *de novo*  
700 mutation in one individual is  $3.34 \times 10^{-8}$ . For transmitted events, we applied the  
701 UnseenEst<sup>49</sup> algorithm to estimate the probability of finding an unseen missense mutation  
702 in human populations. A total of 33,778 healthy individuals were selected from the ExAC  
703 database<sup>50</sup> to match the population distribution of the 2,010 U.S. Census. The U.S.  
704 Census-matched dataset was trained in the UnseenEst<sup>49</sup> algorithm to estimate the  
705 frequency distribution of distinct unseen missense mutations for the US population. The  
706 predicted frequency distribution was used to extrapolate the probability of observing one  
707 unseen transmitted event (probability =  $2.81 \times 10^{-5}$ ). Taken together, the probability of  
708 observing one *de novo* and two transmitted p.Arg172Gln mutations among 80  
709 independent samples is estimated to be

710  $\binom{80}{2} \times (2.81 \times 10^{-5})^2 \times (1 - 2.81 \times 10^{-5})^{78} \times \binom{78}{1} \times (3.34 \times 10^{-8})^1 \times (1 -$   
711  $3.34 \times 10^{-8})^{77}$   
712  $= 6.49 \times 10^{-12}.$

713

714 **Shared haplotypes and estimation of the mutation age of p.Arg172Gln in *CLCN2*.**

715 Genotypes of SNPs flanking the *CLCN2*<sup>Arg172Gln</sup> mutation were extracted from exome  
716 data. To estimate the mutation age of the *CLCN2* p.Arg172Gln mutation testing the  
717 assumption that the mutation is identical by descent among each possible pair of kindreds  
718 with the variant (except the documented *de novo* mutation), we used the ESTIAGE  
719 algorithm to estimate the pairwise time of coalescence for the three pairs of kindreds as  
720 previously described<sup>13,18</sup>. ESTIAGE uses a maximum-likelihood approach to estimate the  
721 mutation age, which takes into account the frequencies of the shared allele at each marker  
722 and the recombination fractions between the mutation of interest and polymorphic  
723 markers located within or at the boundaries of the shared haplotype. Seventeen  
724 polymorphic markers spanning the shared haplotype were used for input (Supplementary  
725 Table 5). The marker allele frequencies were estimated from the Finnish and Non-Finnish  
726 European populations in the ExAC database<sup>50</sup>, and the mutation rate was set to  $2 \times 10^{-8}$ .

727

728 **Statistics.** The statistical analyses used throughout the manuscript are described in the  
729 corresponding results and Online Methods paragraphs, Figure legends or Supplementary  
730 Tables.

731

732 **Data availability.** *CLCN2* variants are deposited in ClinVar (accession numbers  
733 SCV000606833-7), RNAseq data are at GEO (accession number GSE107030, see URLs).

734

735 **Code availability.** Code for gene burden analysis is available at github (see URLs).

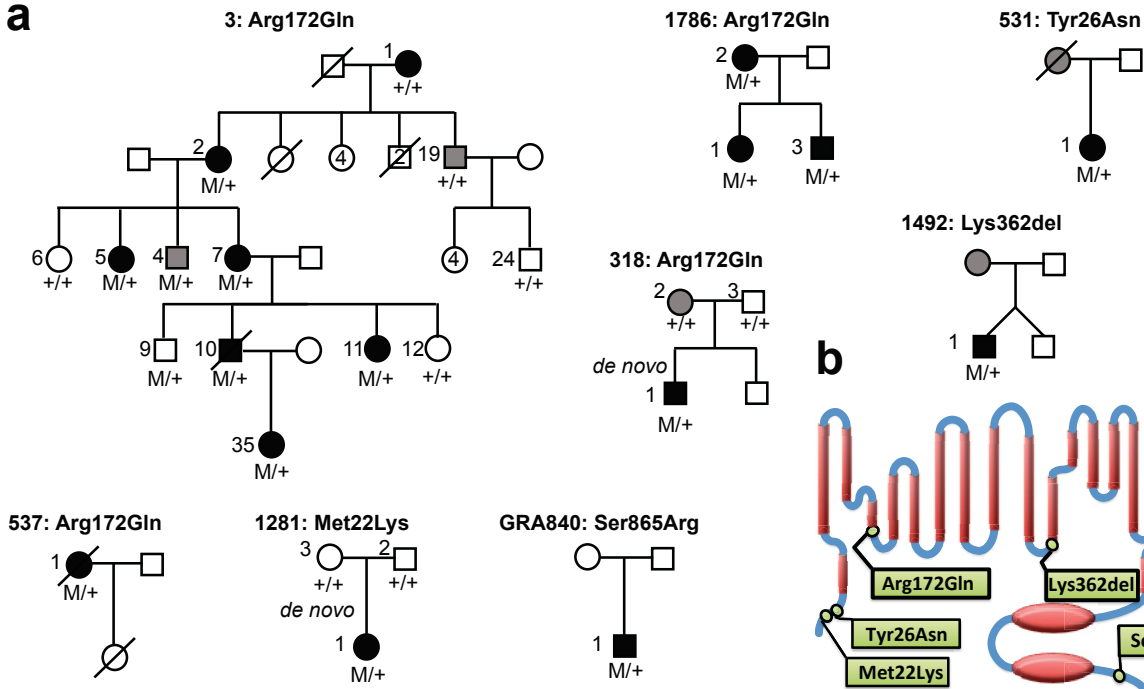
736

### 737 **Methods-only References**

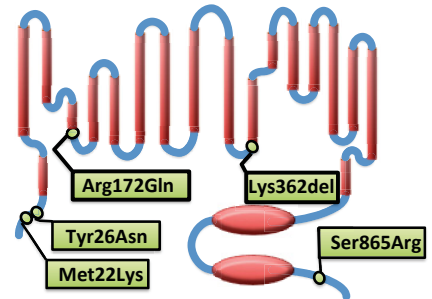
- 738 37. Torpy, D.J. *et al.* Familial hyperaldosteronism type II: description of a large  
739 kindred and exclusion of the aldosterone synthase (CYP11B2) gene. *J Clin*  
740 *Endocrinol Metab* **83**, 3214-8 (1998).
- 741 38. Krumm, N. *et al.* Excess of rare, inherited truncating mutations in autism. *Nat*  
742 *Genet* **47**, 582-8 (2015).
- 743 39. Verkman, A.S. Development and biological applications of chloride-sensitive  
744 fluorescent indicators. *Am J Physiol* **259**, C375-88 (1990).
- 745 40. Kaneko, H., Putzier, I., Frings, S., Kaupp, U.B. & Gensch, T. Chloride  
746 accumulation in mammalian olfactory sensory neurons. *J Neurosci* **24**, 7931-8  
747 (2004).
- 748 41. Bevensee, M.O., Apkon, M. & Boron, W.F. Intracellular pH regulation in  
749 cultured astrocytes from rat hippocampus. II. Electrogenic Na/HCO<sub>3</sub>  
750 cotransport. *J Gen Physiol* **110**, 467-83 (1997).
- 751 42. Chao, A.C., Dix, J.A., Sellers, M.C. & Verkman, A.S. Fluorescence measurement  
752 of chloride transport in monolayer cultured cells. Mechanisms of chloride  
753 transport in fibroblasts. *Biophys J* **56**, 1071-81 (1989).
- 754 43. Accardi, A. & Pusch, M. Fast and slow gating relaxations in the muscle  
755 chloride channel CLC-1. *J Gen Physiol* **116**, 433-44 (2000).
- 756 44. de Santiago, J.A., Nehrke, K. & Arreola, J. Quantitative analysis of the voltage-  
757 dependent gating of mouse parotid CLC-2 chloride channel. *J Gen Physiol* **126**,  
758 591-603 (2005).
- 759 45. Rhee, J.S., Ebihara, S. & Akaike, N. Gramicidin perforated patch-clamp  
760 technique reveals glycine-gated outward chloride current in dissociated  
761 nucleus solitarii neurons of the rat. *J Neurophysiol* **72**, 1103-8 (1994).
- 762 46. Kim, D. *et al.* TopHat2: accurate alignment of transcriptomes in the presence  
763 of insertions, deletions and gene fusions. *Genome Biol* **14**, R36 (2013).
- 764 47. Trapnell, C. *et al.* Differential analysis of gene regulation at transcript  
765 resolution with RNA-seq. *Nat Biotechnol* **31**, 46-53 (2013).
- 766 48. Samocha, K.E. *et al.* A framework for the interpretation of de novo mutation  
767 in human disease. *Nat Genet* **46**, 944-50 (2014).
- 768 49. Zou, J. *et al.* Quantifying unobserved protein-coding variants in human  
769 populations provides a roadmap for large-scale sequencing projects. *Nat*  
770 *Commun* **7**, 13293 (2016).
- 771 50. Lek, M. *et al.* Analysis of protein-coding genetic variation in 60,706 humans.  
772 *Nature* **536**, 285-91 (2016).



**a**

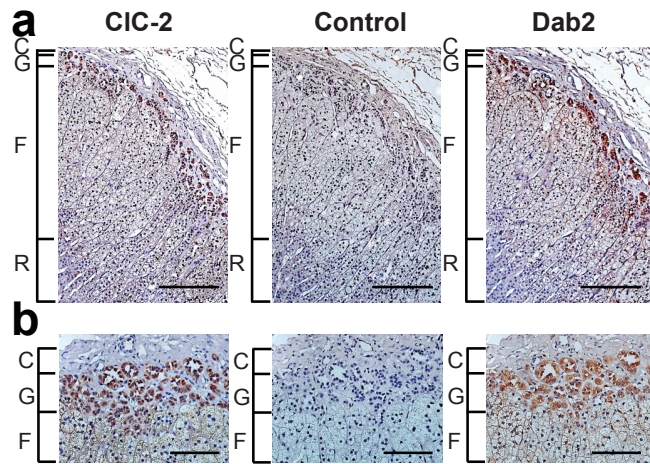


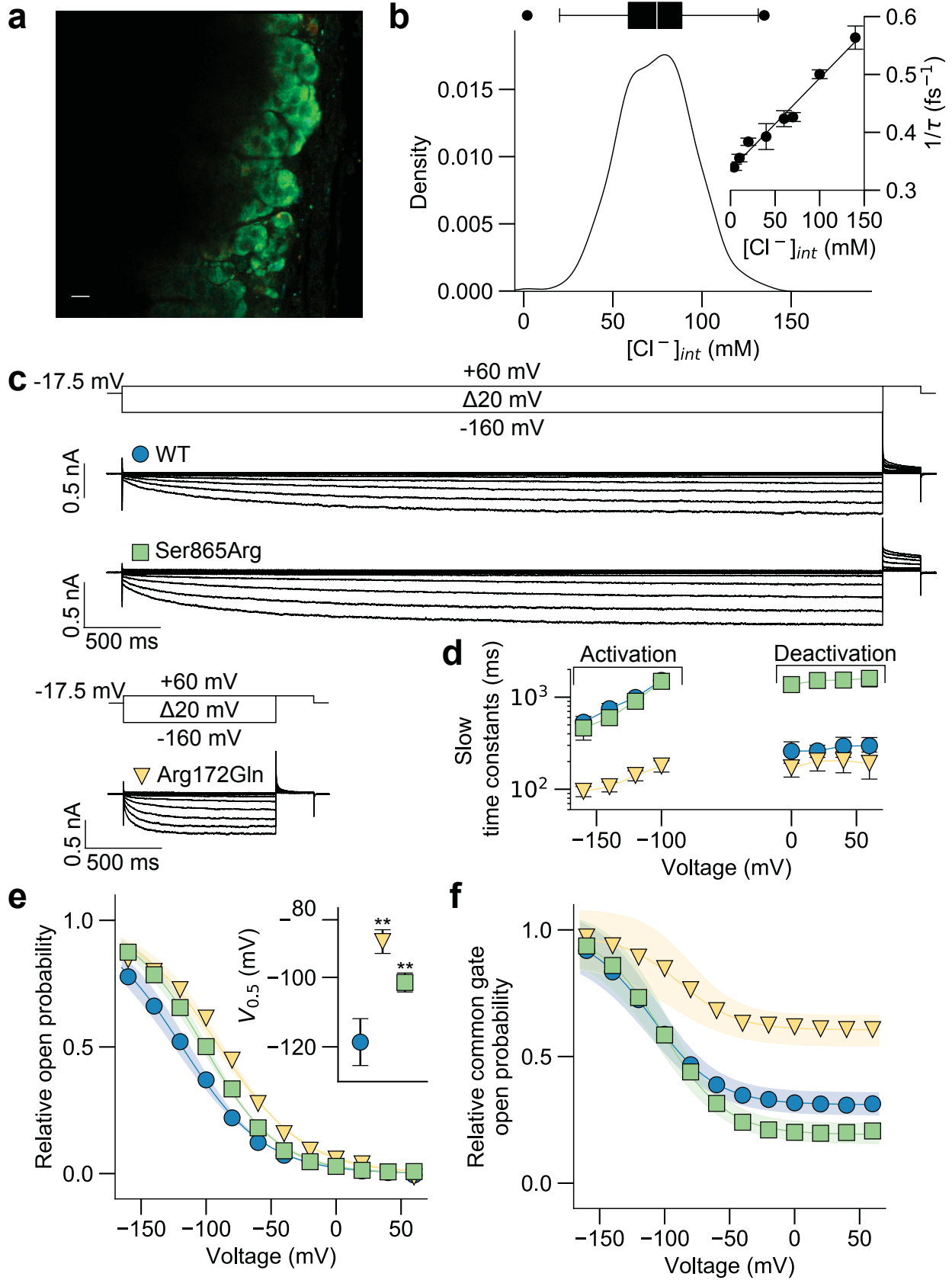
**b**



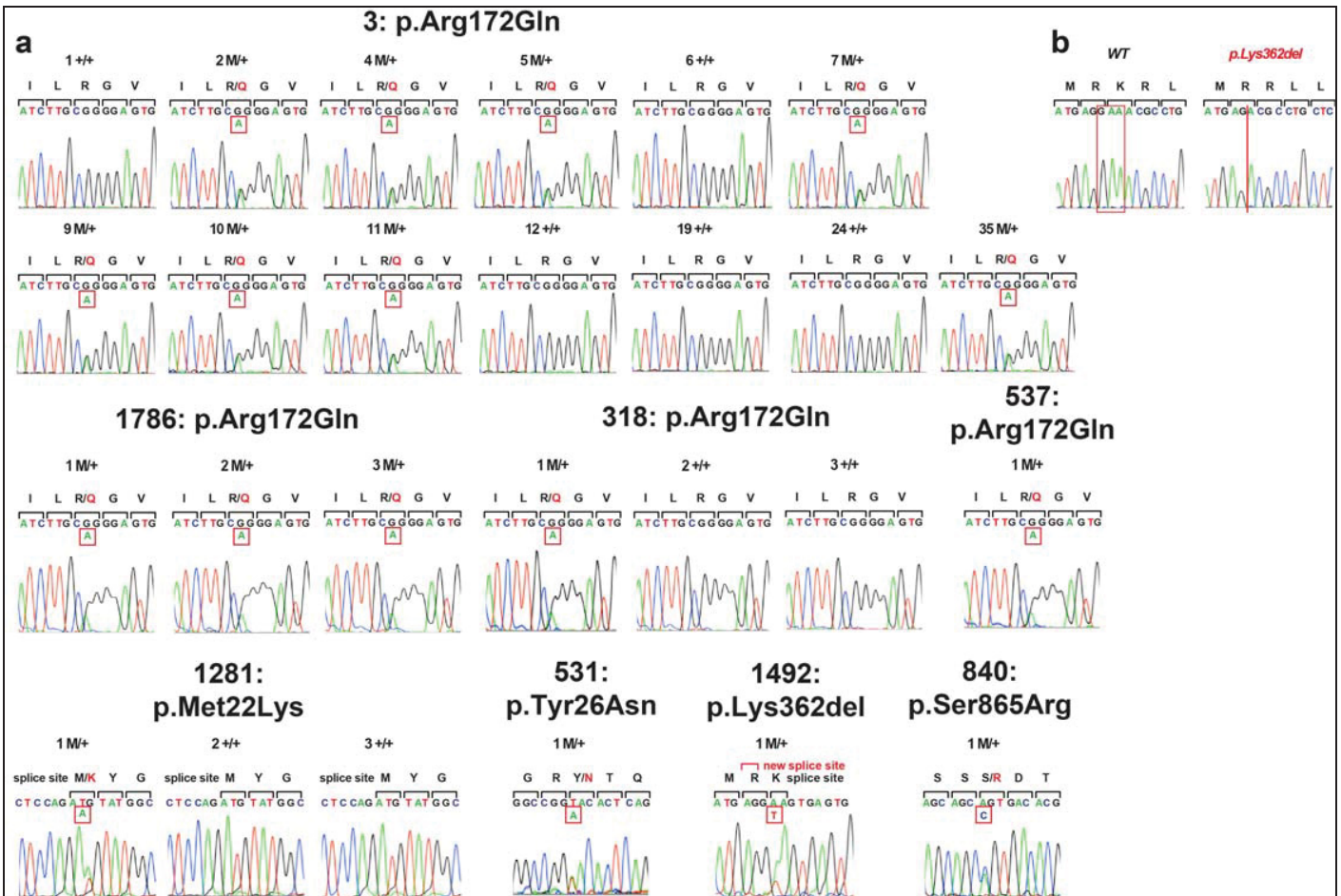
**c**

	Met22	Tyr26	Arg172	Lys362	Ser865
<i>H. sapiens</i>	Y E Q T L M Y G R Y T Q D L G	M K T I L R G V V L K	R F L M R K R L L F P	S A T S S S S D T E T T	
<i>M. musculus</i>	Y E Q T L M Y G R Y T Q E L G	M K T I L R G V V L K	R F L M R K R L L F P	S A T S S S S D T E T T	
<i>G. gallus</i>	Y E Q T L M Y G R Y T Q D L G	M K T I L R G V V L K	R F L M K K R L L F P	S S T S A G E L D T T	
<i>X. tropicalis</i>	Y E Q T L M Y G R Y T Q D L G	M K T I L R G V V L K	R F L M K K R L L F P	S V T S S S D T E T T	
<i>D. rerio</i>	Y E Q T L M Y G R Y T Q E L G	M K T I L R G V V L K	K F L M K K R L L Y P	S G T S G ... S E S E A T	
<i>C. intestinalis</i>	Y E P T L M Y G K Y S K E L S	M K T I M R G V V L H	E F L Q R N R F I Y P	R Y N H D ... N N E E S	
<i>D. mojavensis</i>	Y T H T L M Y G R Y T K D L G	M K T I L R G V A L K	K F L Q K N R F L Y P	S K P A ... G ... S D I E M E	
<i>C. elegans</i>	L Q P G S H L G V Y K T V R G	M K T I L R G V I L K	M I F Q K Y W L I Y P	E P P T ... G ... T P N R M S	





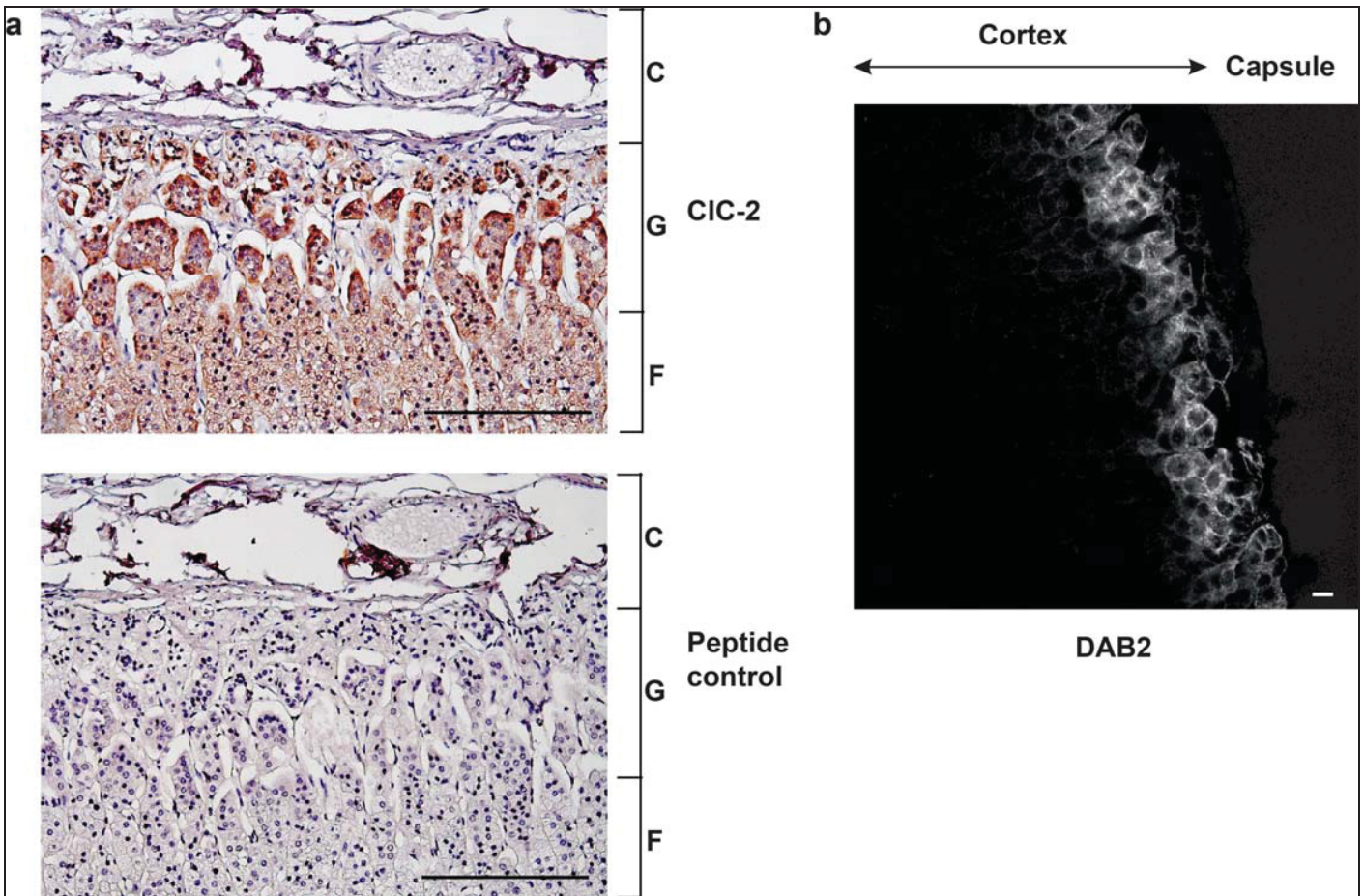




**Supplementary Figure 1**

Sanger sequences.

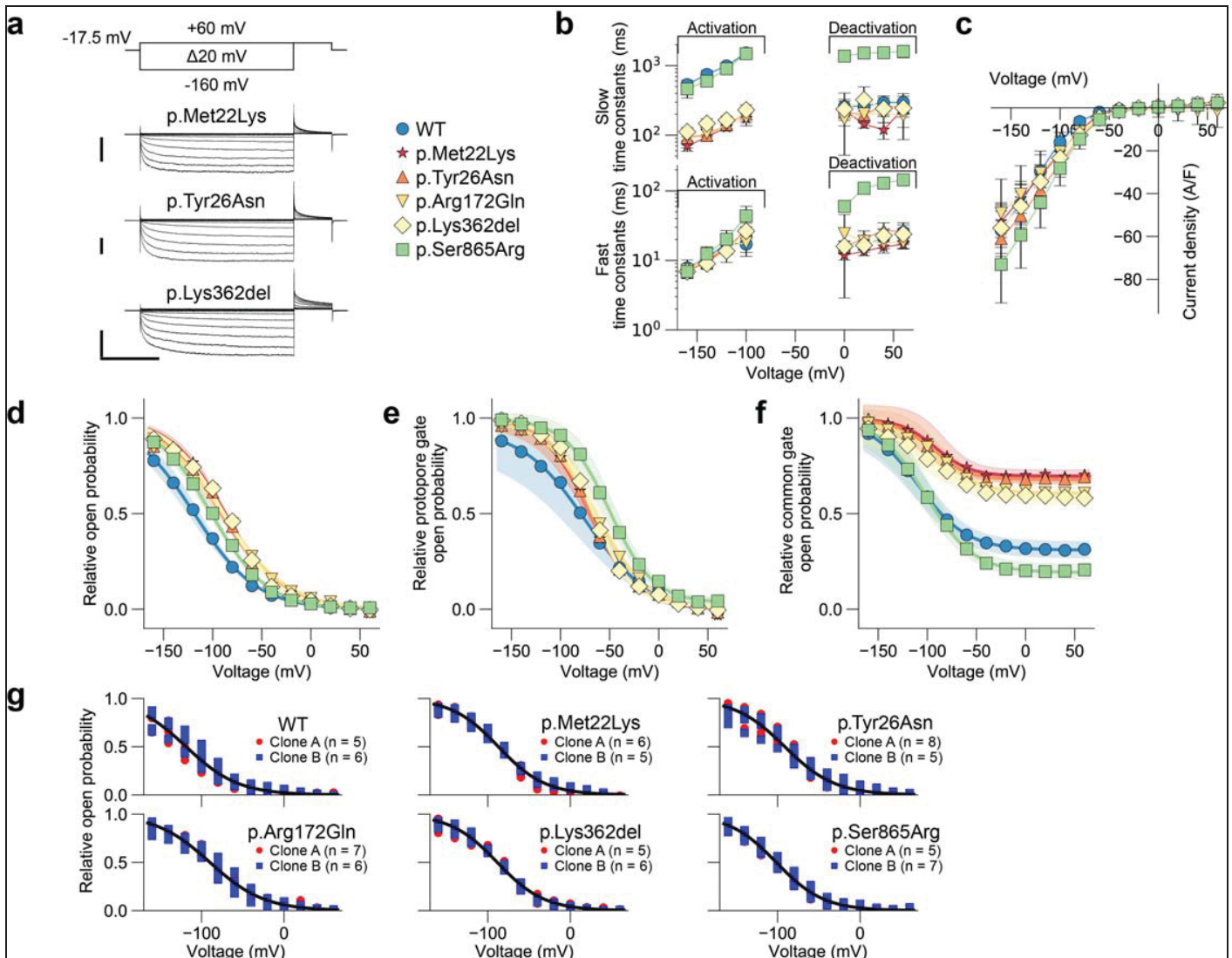
(a) Sanger sequences of kindreds with *CLCN2* variants. M/+ denotes the indicated novel *CLCN2* variant in the heterozygous state, and +/+ denotes homozygous wildtype sequence. Mutant bases are indicated by a red frame, and encoded amino acid sequences are shown above. (b) Splicing assay of p.Lys362del mutation. Exons 9-11 of *CLCN2* were cloned, and HEK293T cells were transfected with WT DNA and DNA carrying the variant found in kindred 1492. RNA was isolated and cDNA transcribed. Shown are Sanger sequences of PCRs covering the exon 10/11 splice site affected by the variant. A new donor site on exon 10 is used, resulting in the deletion of the last three base pairs of exon 10 (red rectangle in WT sequence, red line in mutant sequence). These results were consistent with *in silico* prediction.



**Supplementary Figure 2**

Immunohistochemistry.

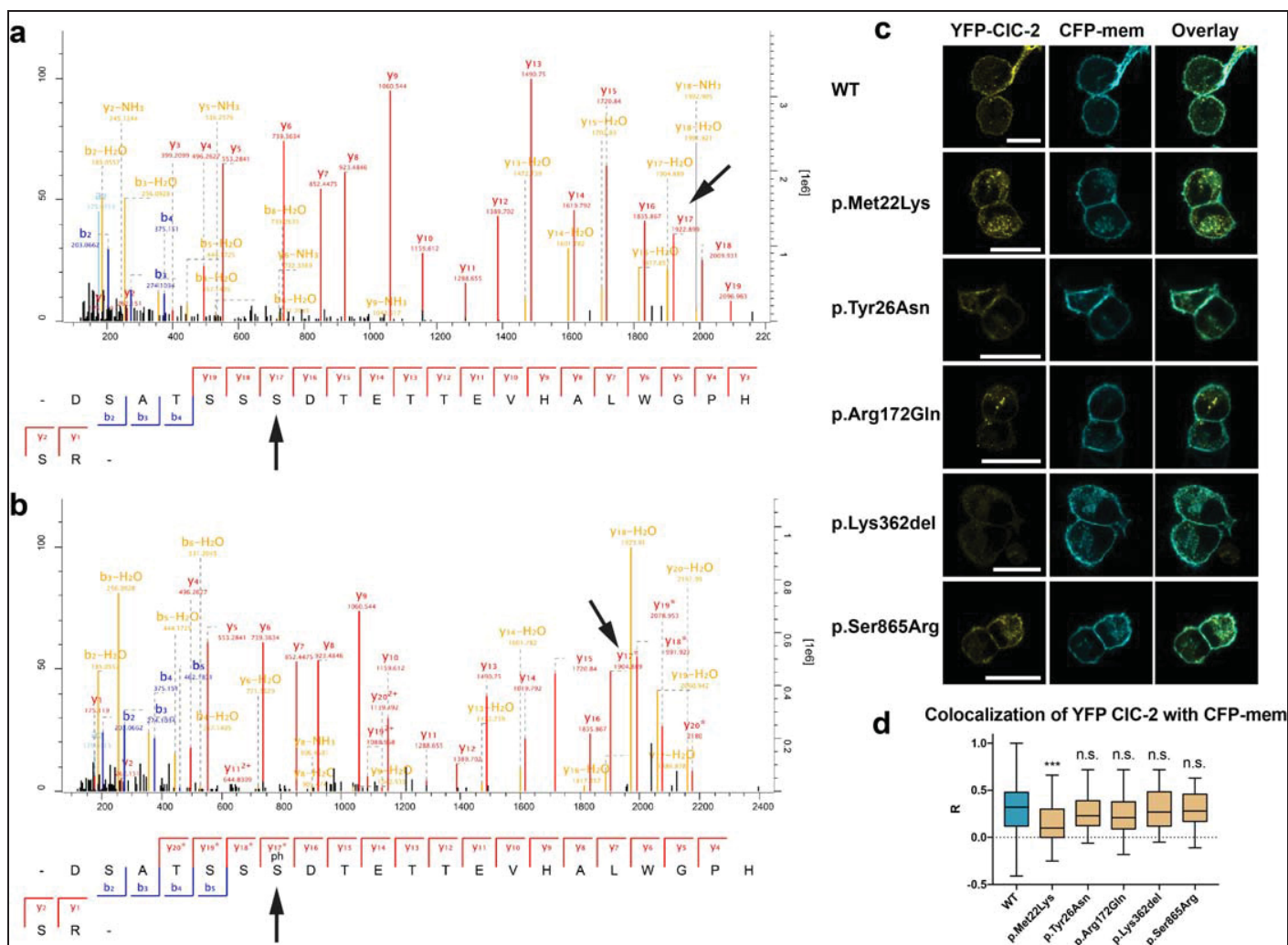
(a) Immunohistochemistry as in Fig. 2 was performed on the adrenal gland of a second human subject (one of two technical replicates shown). Peptide control, antibody was pre-incubated with immunogenic peptide. Scale bar, 100  $\mu\text{m}$ . C, capsule; G, *glomerulosa*; F, *fasciculata*. (b) Immunofluorescent staining mouse adrenal gland, with DAB2 as marker of the *zona glomerulosa*. Scale bar, 10  $\mu\text{m}$ .



### Supplementary Figure 3

Gating Analysis, Time Constants of Activation / Deactivation and Current Density-Voltage Plots of WT and Mutant CIC-2 Channels.

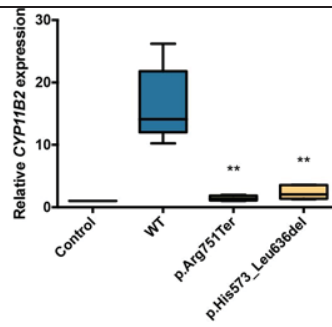
(a) Whole-cell patch clamp recordings of representative CIC-2<sup>MUT</sup> and voltage protocol (150 mM Cl<sup>-</sup> outside, 75 mM Cl<sup>-</sup> inside, see Online Methods for solutions) for the indicated mutations are shown. (b) Time constants for WT and mutant CIC-2 channels (see Online Methods for details). Mean values  $\pm$  95% confidence intervals are shown (WT, p.Arg172Gln and p.Ser865Arg are reproduced from Fig. 3; WT: n=11, p.Met22Lys: n=12, p.Tyr26Asn: n=13, p.Arg172Gln: n=13, p.Lys362del: n=12; p.Ser865Arg: n=11). (c) Plot of the steady-state current densities. Values are shown as mean  $\pm$  95% confidence interval; WT: n=11, p.Met22Lys: n=12, p.Tyr26Asn: n=13, p.Arg172Gln: n=13, p.Lys362del: n=12, p.Ser865Arg: n=11. Median values at -80 mV and results of a Kruskal-Wallis one-way ANOVA ( $H = 14.823$ , d.f.=5) followed by Dunn's method when appropriate are (A/F): WT: -5.75, p.Met22Lys: -10.28, n.s. vs. WT, p.Tyr26Asn: -13.66,  $P < 0.05$  vs. WT, p.Arg172Gln: -9.13, n.s. vs. WT, p.Lys362del: -13.69,  $P < 0.05$  vs. WT, p.Ser865Arg: -12.58,  $P < 0.05$  vs. WT. (d)-(f) Total (d), protopore (e) and common gate (f) open probabilities were determined as described (Online Methods for details; WT, p.Arg172Gln and p.Ser865Arg total and common open probabilities are reproduced from Fig. 3; WT: n=11, p.Met22Lys: n=12, p.Tyr26Asn: n=13, p.Arg172Gln: n=13, p.Lys362del: n=12, p.Ser865Arg: n=12). Data points were fit using a Boltzmann function (bold line), and 95% confidence intervals were determined using bootstrap sampling. The overall shift in activation of mutant CIC-2 channels apart from p.Ser865Arg mostly results from a higher common gate open probability, whereas the fast gate open probability of p.Ser865Arg is shifted to more positive potentials. (g) Individual data and stable cell line clones used in the analysis shown in Fig. 3 and this figure.



**Supplementary Figure 4**

Mass spectrometry and confocal microscopy.

(a),(b) LC-MS/MS based identification of phosphorylation site of CIC-2 at position Ser865. CIC-2 was identified with 43 peptides and sequence coverage of 52.8%. Shown are annotated MS/MS spectra of the unmodified (a) and phosphorylated (b) peptide DSATSSSDTETTEVHALWGPHSR corresponding to amino acids 859-881 of CIC-2. x axis shows m/z, left y axis relative abundance, and right y axis absolute signal intensity. Unmodified peptide: 16 MS/MS counts, posterior error probability (PEP):  $1.21 \times 10^{-35}$ , Score 160.47; Ser865 phosphorylated peptide: 11 MS/MS counts, PEP:  $1.61 \times 10^{-36}$ , Score 166.49. The phosphorylation site at position Ser865 was fully localized, with a localization probability of 0.813811 (mass error of 0.28027 ppm). One of two independent preparations (Online Methods) is shown; similar results were obtained for another two independent preparations using a different solvent. (c),(d) Live cell confocal microscopy of YFP-tagged WT and mutant CIC-2 and surface membrane marker CFP-mem in H295R Cells. (c) The respective variant is noted on the left. Left panel, confocal image using the YFP channel; middle panel, CFP channel; right panel, overlay. Scale bars, 20  $\mu\text{m}$ . Two independent clones of each plasmid were assessed, and representative images are shown. (d) Correlation R between YFP and CFP fluorescence for each construct. WT,  $0.29 \pm 0.03$  (n=71); p.Met22Lys,  $0.15 \pm 0.02$  (n=81;  $p=0.0001$  vs. WT); p.Tyr26Asn,  $0.25 \pm 0.03$  (n=53;  $p>0.9999$  vs. WT); p.Arg172Gln,  $0.24 \pm 0.03$  (n=56;  $p=0.5862$  vs. WT); p.Lys362del,  $0.29 \pm 0.03$  (n=65;  $p>0.9999$  vs. WT); p.Ser865Arg,  $0.30 \pm 0.02$  (n=59;  $p>0.9999$  vs. WT); all mean  $\pm$  SEM, Kruskal-Wallis test; Dunn's multiple comparisons test; Kruskal-Wallis statistic 28.47, d.f.=5. Box, interquartile range; whiskers, 1.5x interquartile range; line, median; \*\*\*,  $p<0.001$ ; n.s., not significant.



### Supplementary Figure 5

*CYP11B2* expression in H295R cells after transfection of non-functional *CLCN2*.

Relative expression levels of *CYP11B2* determined by real-time PCR in H295R cells transfected with empty vector control, wildtype *CLCN2* (blue), or two constructs with C-terminal deletions that affect ion channel function (yellow, corresponding deletions noted below the graph)<sup>30</sup>. Values were normalized to empty vector control. *CYP11B2* expression is significantly lower after transfection of non-functional channels than after transfection of the wildtype channel (mean±SEM; WT, 16.35±2.72; p.Arg751Ter, 1.46±0.18, p=0.0089 vs. WT, p.His573\_Leu636del, 2.38±0.50, p=0.0077 vs WT; \*\*, p < 0.01). N=5, one-way ANOVA for all constructs, Dunnett's multiple comparisons test, F=31.52, d.f.=4. Box, interquartile range; whiskers, 1.5x interquartile range; line, median.

## **Supplementary Note**

### **Case Reports**

**Subject 3-1**, a female, was evaluated for primary aldosteronism at age 66 years, after a 30-year history of hypertension. Aldosterone/renin ratio (ARR) was 62.0 ng/dl:ng/ml/h (normal <20; plasma aldosterone 24.8 ng/dl, plasma renin activity (PRA) 0.4 ng/ml/h), and aldosterone failed to suppress during fludrocortisone suppression test (FST) (18.8 ng/dl at 10 AM on day 5). Dexamethasone produced complete suppression of recumbent, but not upright plasma aldosterone (<1 ng/dl at 8 AM and 22.7 ng/dl at 10 AM on day 5). Plasma aldosterone rose with upright posture (from 10.4 to 28.3 ng/dl). Adrenal CT was normal. Adrenal venous sampling was consistent with bilateral aldosterone production. The patient was treated with spironolactone.

**Subject 3-2**, a female, was diagnosed with hypertension at age 24 years and developed hypokalemia at 46 years. She was then found to have an elevated ARR with positive FST. Aldosterone did not suppress during dexamethasone suppression testing and was unresponsive to upright posture. CT showed a bulky left adrenal gland, but a 75 selenium-methyl-cholesterol scan was normal. Adrenal venous sampling was consistent with bilateral disease, and hypertension and hypokalemia responded to treatment with spironolactone.

**Subject 3-4**, a male, was evaluated at ages 24 years (BP 98/70 mmHg, aldosterone 14.5 ng/dl, PRA 1.8 ng/ml/h, K<sup>+</sup> 4.0 mmol/l (normal 3.5-5.5)), at age 29 years (aldosterone 17.3 ng/dl, PRA 1.7 ng/ml/h, K<sup>+</sup> 4.8 mmol/l) and at age 36 years (borderline elevated

ARR with aldosterone 24.5 ng/dl, PRA 1.2 ng/ml/h, K<sup>+</sup> 4.2 mmol/l). At age 49 years, his BP remained normal at 116/77 mmHg.

**Subject 3-5**, a female, was diagnosed with hypertension at the age of 19 years. At age 25 years, plasma K<sup>+</sup> was 3.3 mmol/L, aldosterone 27.4 ng/dl, PRA 0.1 ng/ml/h, and ARR 274 ng/dl:ng/ml/h. Plasma aldosterone did not suppress during FST (27.1 ng/dl at 10 AM on day 5) or dexamethasone suppression test (17.3 ng/dl at 8 AM and 28.3 ng/dl at 10 AM on day 5). Adrenal CT showed a small (8 mm) nodule in the left adrenal. Plasma aldosterone fell with upright posture (from 60.6 to 27.4 ng/dl). Aldosterone/cortisol ratios were higher in both adrenal veins when compared with peripheral ratios, consistent with bilateral production of aldosterone, and the patient was treated with spironolactone with correction of hypokalemia and hypertension.

**Subject 3-7**, a female, first developed mild hypertension at age 20 years and was later shown to have elevated ARR with positive FST. Aldosterone was only partially suppressible during dexamethasone suppression test, but fell with upright posture. CT showed mild bulkiness of the left adrenal gland. Adrenal venous sampling did not show lateralization. Hypertension was controlled on spironolactone.

**Subject 3-9**, a male, had normal BP (120/80 mmHg) at age 19 years, and repeated ARRs over a course of 12 years (starting at age 18 years) were normal.

**Subject 3-10** had high-normal BP (130/85 mmHg) and was normokalemic when assessed at the age of 17 years. His ARR was elevated at 262 ng/dl:ng/ml/h (plasma aldosterone 26.2 ng/dl, PRA 0.1 ng/ml/h), but he declined further workup and deceased at age 29 years.

**Subject 3-11**, a female, had plasma aldosterone 21.2 ng/dl, PRA 0.1 ng/ml/h, and ARR 212 ng/dl:ng/ml/h at age 14 years. Her blood pressure was normal (94/62 mmHg), and CT was also normal. Aldosterone failed to suppress with fludrocortisone (11.5 ng/dl at 10 AM on day 4), consistent with primary aldosteronism, and aldosterone did not rise with upright posture (recumbent 16.8 ng/dl, upright 16.1 ng/dl).

**Subject 3-19**, a male, was assessed at age 41 years. His BP was 144/94 mmHg without medication, ARR was 38 ng/dl:ng/ml/h (plasma aldosterone 26.7 ng/dl, PRA 0.7 ng/ml/hr), and aldosterone suppressed during FST (4.6 ng/dl at 10 AM on day 5). Dexamethasone produced complete suppression of recumbent, but not upright plasma aldosterone (<1 ng/dl at 8 AM and 16.7 ng/dl at 10 AM on day 5). Plasma aldosterone rose with upright posture (from 16.3 to 28.1 ng/dl). Adrenal CT was normal.

**Subject 3-35** was diagnosed with hypertension (blood pressure 170/110 mmHg) at age 16 years. Plasma potassium was 3.4 mmol/l, plasma aldosterone 25.5 ng/dl, PRA  $\leq$ 0.2 ng/ml/h, and ARR was elevated at  $\geq$ 127.5 ng/dl:ng/ml/h. Aldosterone failed to suppress during FST (37.5 ng/dl at 10 AM on day 4), consistent with primary aldosteronism. Aldosterone did not rise with upright posture. Both adrenal glands were normal by CT, and adrenal venous sampling indicated bilateral aldosterone production. Hypertension was controlled with amiloride.

**Subject 318-1**, a male, was diagnosed with migraine headaches and hypertension at age 7 years, with BP readings up to 170/140 mmHg. Workup for decreased renal function (serum creatinine 0.9-1.0 mg/dl (normal 0.2-0.6 mg/dl), endogenous creatinine clearance 75-90 ml/min), including renal ultrasound with Doppler, captopril nuclear renal scan and renal biopsy were insignificant. Persistent hypokalemia (serum K<sup>+</sup> 2.6 mmol/l) and mild

metabolic alkalosis (serum CO<sub>2</sub> 29-30 mmol/l) were noted. He was diagnosed with primary aldosteronism (serum aldosterone 9.5 ng/dl, PRA 0.21 ng/ml/h, urinary aldosterone 15 µg/24 hours (normal 4-22 µg/24 hours)). His family history was significant for a mother who had been diagnosed with hypertension at age 18 years, a maternal grandmother who died in her 40s from cerebrovascular accident and maternal grandaunts with early-onset hypertension.

**Subject 531-1**, a female, presented with hypertension at age 6 years. Evaluation was consistent with primary aldosteronism (primary aldosteronism) (aldosterone 100 ng/dl; plasma renin activity (PRA) <3 ng/ml/h). At age 20 years, she was admitted with a diagnosis of hypertensive crisis (blood pressure (BP) 280/188 mmHg). Weight loss was attributed to anorexia nervosa, and chronic leukocytosis was found. Urine analysis was positive for blood. Her family history was significant for a mother who died at age 30 years from a cerebrovascular accident.

**Subject 537-1**, a female, presented with hypertension at age 11 years, with peak BPs of about 160/120 mmHg. Laboratory evaluation revealed persistent hypokalemia (serum K<sup>+</sup> 3.0-3.4 mmol/l), mild hypernatremia (Na<sup>+</sup> 146 mmol/l), and metabolic alkalosis (CO<sub>2</sub> 33 mmol/l). Serum aldosterone was 26 ng/dl, and PRA was suppressed at 0.3 ng/ml/h. Urinary aldosterone was elevated at 28 µg/24 h, and serum 18-hydroxycorticosterone was normal at 19 ng/dl (normal 6-85 ng/dl). Captopril suppression test was positive, and adrenal computed tomography was negative for tumors or enlargement. The patient was treated with doxazosin, KCl and amiloride, with difficulties achieving normokalemia and normotension. The family history was positive for hypertension in both parents and a paternal grandmother. The patient was lost to follow up and deceased at age 21 years.

**Subject 840-1**, a male, was diagnosed with hypertension during a routine examination at age 15 years (BP 130/100 mmHg), but treatment was not initiated. At age 17 years, sustained BP elevations to 180/120 mmHg for one- to two-hour periods were noted. Urinary catecholamines were unremarkable, as were cranial and abdominal MRI, a renal arteriogram and renal ultrasound. Adrenal CT scan was normal. After initiation of treatment with atenolol and amlodipine, hypotensive episodes were observed, with the subject being near-syncopal or BP not measurable. Serum potassium was 2.6 mmol/l during one of these episodes, and potassium supplementation was started. Further evaluation at age 20 years revealed an aldosterone of 37 ng/dl, and PRA of 0.2 ng/ml/h without medication. Treatment with 25 mg spironolactone was then initiated. The family history was positive for hypertension in the maternal grandfather.

**Subject 1281-1**, a female, presented at age 1 year with hypertension (BP 117/71 mmHg) and transient hypokalemia and was diagnosed with primary aldosteronism (aldosterone 17 ng/dl, PRA <0.5 ng/dl/h). She was treated with amlodipine.

**Subject 1492-1**, a male, was admitted to the pediatric intensive care unit after an apneic episode at age 11 weeks. Severe hypertension with BP readings up to 150/90 mmHg was noted. Evaluation revealed normokalemia (4.0 mmol/l), elevated aldosterone (63.8 ng/dl) and suppressed PRA (<0.15 ng/ml/h). His perinatal history was significant for a twin pregnancy with mild pre-eclampsia in his mother, birth at 37 weeks gestational age and transient hypokalemia as a newborn. Renal ultrasound, evaluation for congenital adrenal hyperplasia, thyroid function, cardiac echocardiogram and cranial computed tomography were normal. After the blood draw for aldosterone and PRA, treatment with captopril 5 mg three times per day was started, with partial improvement of BP levels. Hypertension

resolved by age 2 years. The family history was positive for hypertension in the mother during adolescence, which was attributed to obesity and improved with weight loss, and essential hypertension in the maternal grandmother.

**Subject 1786-1**, a female, was diagnosed with hypertension at age 15 years during a routine examination, with BP readings of 140-150/90-100 mmHg. She had been asymptomatic with the exception of shortness of breath while running. Laboratory evaluation revealed hypokalemia ( $K^+$  2.9 mmol/l), elevated aldosterone (47.9 ng/dl) and suppressed PRA (<1.0 ng/ml/h). Urinary aldosterone was 22.4  $\mu$ g/24 h.

**Subject 1786-2**, her mother, was first diagnosed with hypertension at age 32 years. Her past medical history was significant for grand mal and petit mal seizures that were diagnosed at age 18 months and temporarily treated with phenobarbital, and a seizure-free interval after discontinuation of treatment from teenage to early adult years. After a fall, she developed myoclonic seizures that were attributed to traumatic brain injury and treated with clonazepam. There was an allergic reaction to lamotrigine. Seizures did not recur after discontinuation of treatment. Past medical history further included endometriosis and a gall bladder cyst, and her family history was significant for a father, paternal grandmother and paternal grandfather with hypertension. A blood pressure increase was associated with hypokalemia, and serum aldosterone was found to be elevated at 59.4 ng/dl. Urinary 18-hydroxycortisol was normal (90.9  $\mu$ g/24h, reference range 43-295  $\mu$ g/24 h), and plasma free metanephrine and normetanephrine were also normal. Saline suppression test was positive. Computed tomography did not reveal adrenal abnormalities, and there was no lateralization on adrenal venous sampling. Repeat aldosterone was 46.3 ng/dl, and renin was <1.0 ng/ml/h, with serum potassium 3.0

mmol/l. She was treated with 10 mg amlodipine, 75 mg eplerenone and 20 mmol KCl daily, but continued to have suppressed renin levels (<0.6 ng/ml/h).

**Subject 1786-3**, her 13-year old son, had an aldosterone of 12 ng/dl, with PRA <0.6 ng/ml/h and K<sup>+</sup> 4.4 mmol/l. 24h ambulatory BP monitoring revealed average values of 121/75 mmHg, with 123/77 mmHg during the wake period and 114/64 mmHg during the sleep period, which was classified as prehypertension.

## **Additional Online Methods**

**Confocal microscopy.** H295R cells were transfected with 3  $\mu\text{g}$  plasmid DNA (2  $\mu\text{g}$  pRcCMV CLCN2 (WT or mutant) and 1  $\mu\text{g}$  pECFP-Mem (Clontech, Palo Alto, CA, USA)) as for real-time PCR (Online Methods). After recovering of the cells, they were plated in ibidi  $\mu$ -dishes (35mm, low, ibidi, Madison, WI, USA). The cells were cultured for 48 h and subsequently investigated at 37°C using the confocal microscope LSM 710 (Zeiss) at the Center for Advanced Imaging (CAi) at Heinrich Heine University Düsseldorf. Analysis was performed using ZEN (black edition, Zeiss). After determining fluorescence intensity thresholds based on cells transfected with only one construct, individual cells were manually identified as regions of interest, and Pearson's correlation coefficient was determined in ZEN. Cells with fluorescence below the threshold were excluded from the analysis.

**Immunoprecipitation.** HAC15 cells stably expressing CIC-2<sup>WT</sup> were lysed in homogenization buffer containing cOmplete Protease Inhibitor Cocktail (Roche, Basel, Switzerland), Phosphatase Inhibitor Cocktail 3, 10 mM NaF, 10 mM  $\beta$ -Glycerophosphate and 10 mM sodium pyrophosphate (all Sigma-Aldrich). After centrifugation (125,000 g, 4°C, 40 min), the cell pellet was resuspended in solubilization buffer containing 1% NP-40. The cell suspension was incubated on ice for 30 min and centrifuged as above. The protein concentration of the supernatant (membrane fraction) was determined using the Micro BCA Protein Assay Kit (Thermo Scientific). 40  $\mu\text{l}$  (run 1) or 100  $\mu\text{l}$  (run 2) Dynabeads Protein A (Novex by Life Technologies) were labeled with 2  $\mu\text{g}$  (run 1) or 10  $\mu\text{g}$  (run 2) CIC-2 antibody (HPA014545, Sigma-Aldrich) and incubated with 1 mg

membrane fraction for 2.5 h at 4°C on an orbital shaker. Beads were washed 3x in homogenization buffer and 3x in PBS (5 min each, 4°C, orbital shaker), separated on a DynaMag-2 (Novex by Life Technologies) magnet and kept at -80°C.

### **Mass spectrometry.**

After final washing in PBS, beads were resuspended in 100 µl 50 mM ammonium bicarbonate (ABC) buffer. Proteins were reduced for 30 min at room temperature in 10 mM DL-Dithiothreitol (DTT, Sigma), followed by alkylation with 55 mM chloroacetamide (Merck, Darmstadt, Germany) for 20 min in the dark at room temperature. The sample was digested with 1 µg endopeptidase LysC (Wako, Osaka, Japan) for 4 hours at 30°C, followed by an over-night digestion with 1 µg sequence-grade modified trypsin (Promega, Fitchburg, WI, USA) at 30°C. The supernatant (containing the peptides) was transferred to a fresh tube, and the beads were further incubated with 100 µl ABC buffer and 100 µl water (LC-MS grade). All fractions were pooled and acidified with formic acid (2% final concentration). Peptides were extracted and desalted using the standard StageTip protocol<sup>1</sup>. For mass spectrometric measurements, the peptide mixture was separated by reversed-phase chromatography using an EasyLC 1200 system (Thermo Fisher Scientific) on in-house-manufactured 20 cm fritless silica microcolumns (packed with ReproSil-Pur C18-AQ 3 µm resin) with an inner diameter of 75 µm. Peptides were separated using an 8–60% acetonitrile gradient (94 min length) at a nanoflow rate of 200 nl/min. Eluting peptides were directly ionized by electrospray ionization and analyzed on a Thermo Orbitrap Fusion instrument (Thermo). Mass spectrometry was performed in data-dependent positive mode with one full scan (m/z

range = 300-2000; R = 60,000; target value:  $5 \times 10^5$ ; maximum injection time = 50 ms). The ten most intense ions with a charge state between 2 and 7 were selected (R = 15,000, target value =  $5 \times 10^4$ ; isolation window = 0.7 m/z; maximum injection time = 500 ms). Dynamic exclusion for selected precursor ions was set to 30 s. Two replicates were measured. Data analysis was performed using MaxQuant software package (version 1.5.1.2). The internal Andromeda search engine was used to search MS<sup>2</sup> spectra against a decoy human UniProt database (HUMAN.2017-01) containing forward and reverse sequences. The search included variable modifications of methionine oxidation, N-terminal acetylation, deamidation (N and Q), phosphorylation (S, T and Y) and the fixed modification of carbamidomethyl cysteine. The minimal peptide length was set to seven amino acids, and a maximum of 3 missed cleavages were allowed. The FDR was set to 0.01 for peptide, protein and site identifications. To filter for confidently identified peptides, the MaxQuant score was set to a minimum of 40. Annotated MS<sup>2</sup> spectra were extracted using MaxQuant Viewer application.

**Splicing assay.** A fragment encoding exons 9 to 11 of *CLCN2* was amplified by PCR from blood DNA of an unaffected individual using primers CLCN2E9-11\_2Fs and CLCN2\_E9-11\_2R (Supplementary Table 10), cloned into the pCR2.1 TOPO vector (Invitrogen) and verified by Sanger sequencing. After subcloning into pcDNA3.1(+) using the HindIII and XhoI enzymes (NEB), the variant chr3:184074782T>A (hg19) was introduced by site-directed mutagenesis (QuikChange) using primers K362gF and K362gR (Supplementary Table 10) and again verified by Sanger sequencing. HEK293T cells (American Type Culture Collection, cultured as described<sup>13</sup> and authenticated

(Eurofins Genomics, Ebersberg, Germany)) were transfected with two independent clones of wildtype and mutant constructs of pcDNA3.1(+) *CLCN2* using Lipofectamine 2000 (Invitrogen). RNA was isolated using the RNeasy Mini Kit (Qiagen) and cDNA prepared using the QuantiTect Reverse Transcription Kit (Qiagen). After PCR amplification of the spliced region using primers C2\_E9-11SF and C2\_E9-11SR (Supplementary Table 10), the products were resolved on an agarose gel, an approximately 250 bp fragment was excised, purified and subjected to bidirectional Sanger sequencing.

### **Gene expression analysis**

Gene expression data for *HEPACAM* were obtained from the GTEx Portal on 03/27/2017 (see URLs).

**Orthologs.** Proteins encoded by orthologs of CIC-2 in vertebrate and invertebrate species were identified by a BLAST search. GenBank accessions included NP\_004357.3 (*Homo sapiens*), NP\_034030.2 (*Mus musculus*), XP\_015147031.1 (*Gallus gallus*), XP\_002935192.2 (*Xenopus tropicalis*), NP\_001303244.1 (*Danio rerio*), XP\_018667478.1 (*Ciona intestinalis*), XP\_015021958.1 (*Drosophila mojavensis*) and NP\_001300530.1 (*Caenorhabditis elegans*).

**Animal studies.** Animals were housed under standard conditions in the animal facility of the Forschungszentrum Jülich, Germany, according to institutional guidelines under a 12-h light/dark cycle. All experiments were in compliance with the German Law for

Protection of Animals and were approved by the regulatory authorities, the Forschungszentrum Jülich, and the Landesamt für Natur, Umwelt und Verbraucherschutz of Nordrhein-Westfalen, Germany.

#### **Supplementary Note Reference**

1. Rappsilber, J., Ishihama, Y. & Mann, M. Stop and go extraction tips for matrix-assisted laser desorption/ionization, nanoelectrospray, and LC/MS sample pretreatment in proteomics. *Anal Chem* **75**, 663-70 (2003).

## Supplementary Tables

### Supplementary Table 1. Novel Variants

#### Variants Shared Among Three Affected Individuals in Family 3

Chr	Position (hg19)	Gene	Ref base	Nonref base	Het / Hom var	mRNA	ExAC	gnomAD	AA change
chr15	77906476	<i>LINGO1</i>	G	C	Het	NM_032808	Novel	Novel	p.His591Gln
chr3	184075850	<i>CLCN2</i>	C	T	Het	NM_004366	Novel	Novel	p.Arg172Gln

#### *CLCN2* Variants in Primary Aldosteronism

Kindred	Chr	Position (hg19)	Ref base	Nonref base	Het / Hom var	ExAC	gnomAD	AA change
531	chr3	184076907	A	T	Het	Novel	Novel	p.Tyr26Asn
1281	chr3	184076918	A	T	Het	Novel	Novel	p.Met22Lys
3, 318, 1786, 537	chr3	184075850	C	T	Het	Novel	Novel	p.Arg172Gln
1492	chr3	184074782	T	A	Het	Novel	Novel	p.Lys362del
840	chr3	184064498	T	G	Het	Novel	Novel	p.Ser865Arg

Upper panel, novel variants shared among subjects 3-5, 3-11, and 3-35; lower panel, *CLCN2* variants in subjects with primary aldosteronism. Chr, chromosome; hg19, human genome version 19; Ref base, reference base; Nonref base, non-reference base; Het/ Hom var, heterozygous versus homozygous variant; ExAC, frequency in the ExAC database; gnomAD, frequency in the gnomAD database; AA change, amino acid change (corresponding to the proteins encoded by indicated mRNAs); *LINGO1*, leucine rich repeat and Ig domain containing 1; *CLCN2*, chloride channel, voltage-sensitive 2.

**Supplementary Table 2. Sanger Sequencing of Candidate Variants in Kindred 3**

<b>Subject ID</b>	<b>Clinical diagnosis of primary aldosteronism</b>	<b><i>CLCN2</i> p.Arg172Gln</b>	<b><i>LINGO1</i> p.His591Gln</b>
1	Yes	+/+	+/+
2	Yes	+/M	+/+
4	Possible	+/M	+/+
5	Yes	+/M	+/M
6	No	+/+	+/+
7	Yes	+/M	+/M
9	No	+/M	+/+
10	Yes	+/M	+/M
11	Yes	+/M	+/M
12	No	+/+	+/M
19	No	+/+	+/+
24	No	+/+	+/+
35	Yes	+/M	+/M

+/M, heterozygous for the indicated variant; +/+, homozygous reference sequence at the position of the indicated variant. See Supplementary Table 1 for the genomic positions of variants. *LINGO1* shows homozygous wildtype sequence at position His591 in affected individual 3-2.

**Supplementary Table 3. Clinical Features of 45 Patients with Primary Aldosteronism and Onset by Age 20 Years**

ID	Gen-der	Age at Dx	BP at Dx	K at Dx	Aldo at Dx	PRA at Dx	ARR at Dx	Age at Referral	BP at Referral	K at Referral	Aldo at Referral	PRA at Referral	ARR at Referral
195-1	F	13	NA	NA	NA	NA	NA	41	136/78	4.1	43.0	1.0	43.00
201-1	M	19	NA	NA	NA	NA	NA	24	130/78	2.6	35.0	0.2	175.00
360-1	F	12	240/90	2.9	62.0	1.5	41.33	13	128-140/88-96	3.6	98.0	0.8	122.50
370-1	F	20	185/110	NA	NA	NA	NA	45	178/110	3.1	16.0	0.35	45.71
424-1	F	15	150/100	NA	NA	NA	NA	15	150/100	2.9	19.0	0.1	190.00
463-1	M	20	NA	NA	NA	NA	NA	NA	105-157/85-112	3.4	35.0	0.4	87.50
510-1	M	16	140/90	NA	NA	NA	NA	19	142/94	4.6	18.3	0.04	45.75
526-1	F	17	NA	NA	NA	NA	NA	68	250/90	4.0	286.0	0.2	1430.00
537-1	F	11	NA	3.0	26.0	0.3	86.67	15	152/102	NA	18.0	0.4	45.00
642-1	M	19	NA	NA	NA	NA	NA	30	170/115-120	3.3	38.0	0.2	190.00
705-1	F	teens	NA	NA	24 <sup>a</sup>	0.1 <sup>a</sup>	240.00 <sup>a</sup>	41	NA	NA	NA	NA	NA
722-1	M	16	160/90	NA	NA	NA	NA	15	148/100	2.8	107.0	0.2	535.00
753-1	M	20	NA	NA	NA	NA	NA	56	160/90	4.1	58.0	0.56	103.57
840-1	M	15	130/100	NA	NA	NA	NA	20	120/70	3.2	37.0	0.2	185.00
850-1	F	12	NA	NA	NA	NA	NA	32	153/97	3.3 <sup>b</sup>	36.4 <sup>b</sup>	0.4 <sup>b</sup>	91.00 <sup>b</sup>
855-1	M	16	160/110	NA	NA	NA	NA	55	140/95	3.0	56.0	0.6	93.33
949-1	M	18	NA	NA	NA	NA	NA	51	143/73	3.7	67.0	0.5	134.00
1038-1	F	16	199/102	NA	NA	NA	NA	52	160/95	3.1	29.9	<0.15	>199.33
1074-1	M	13	NA	NA	NA	NA	NA	42	172/102	3.1	36.2	0.1	362.00
1075-1	M	12	153-163/92-99	2.6	20.9	0.19	110.00	12	105/77	NA	NA	NA	NA
1101-1	F	13	NA	3.2-3.4	16.8	<0.15	>112	55	158/106	3.3	NA	NA	NA
1117-1	M	12	NA	NA	NA	NA	NA	45	186/94	3.5	117.5	<0.15	>783.33
1163-1	F	18	220/100	NA	NA	NA	NA	36	117/68	4.9	36.7	0.7	52.43
1191-1	F	12	210/140	2.8	66	8	8.25	12	125/66	4.3	108.0	<0.1	>1080.00

ID	Gen-der	Age at Dx	BP at Dx	K at Dx	Aldo at Dx	PRA at Dx	ARR at Dx	Age at Referral	BP at Referral	K at Referral	Aldo at Referral	PRA at Referral	ARR at Referral
1255-1	M	18	178/70	NA	NA	NA	NA	75	165/68	3.6	27.0	0.1	270.00
1270-1	F	36	NA	NA	NA	NA	NA	39	175/93	2.6	11.0	0.1	110.00
1291-1	F	16	NA	NA	NA	NA	NA	48	132/78	4.8	25.6	<0.15	≥170.67
1300-1	F	19	170/80	NA	NA	NA	NA	39	140-200/80-110	3.9-5.4	23.3	<0.15	>155.33
1317-1	F	5	NA	3.8	20.0	0.1	200.00	5	NA	NA	NA	NA	NA
1328-1	F	20	NA	3.4	19.3	0.1	193.00	36	140/100	NA	NA	NA	NA
1386-1	F	18	NA	3.2	19.3	<0.1	>193	18	130/90	4.6	NA	NA	NA
1415-1	M	18	NA	NA	NA	NA	NA	53	138/82	4.6	110.0	<0.6	>183.33
1417-1	F	15	NA	NA	NA	NA	NA	46	212/110	3.5	26.0	0.6	43.33
1426-1	M	17	NA	2.8 <sup>c</sup>	22.0 <sup>c</sup>	<0.6 <sup>c</sup>	>36.67 <sup>c</sup>	47	134/90	4.5	33.0	0.6	55.00
1447-1	F	17	200/100	NA	NA	NA	NA	24	150/100	4.5	17.0	0.2	85.00
1491-1	M	20	NA	NA	NA	NA	NA	54	203/113	3.9	28.4	<0.15	>189.33
1502-1	M	20	NA	NA	NA	NA	NA	54	138/96	NA	21.0	0.04	525.00
1504-1	M	20	NA	3.4	12.4	0.1	124.00	66	144/82	4.8	22.8	0.27	84.44
1562-1	M	11	NA	NA	NA	NA	NA	65	168/88	3.5	12.0	0.19	63.16
1566-1	M	16	NA	NA	NA	NA	NA	26	160/90	3.5	15.8	0.16	98.75
1572-1	F	16	180/110	NA	22 <sup>d</sup>	<0.5 <sup>d</sup>	>44.00 <sup>d</sup>	21	155/85	3.3	13.0	0.28	46.43
1573-1	M	17	140/90	NA	NA	NA	NA	45	130/70	3.5	17.7	0.1	177.00
1590-1	F	15	NA	3.7	10.8	<0.15	>72.00	15	140/86	3.3	7.3	<0.15	>48.67
1645-1	M	34	208/104	NA	NA	NA	NA	43	138/88	2.7	16.0	0.22	72.73
1786-1	F	15	150/100	2.9	47.9	<1.0	>47.9	17	137/92	3.3	34.0	<0.6	>56.67

Subjects referred for genetic study of primary aldosteronism. ID, subject identification number; F, female; M, male; Dx, diagnosis; BP, blood pressure (mmHg); K, serum potassium (mmol/l, normal 3.5-5.5); Aldo, aldosterone (ng/dl); PRA, plasma renin activity

(ng/ml/h); ARR, aldosterone/renin ratio (ng/dl:ng/ml/h, values >20 with aldosterone >15 or borderline values in the presence of hypokalemia are considered indicative of primary aldosteronism); NA, not available. Subjects with *CLCN2* variants are shown in red.

<sup>a</sup>, at age 26 years; <sup>b</sup>, at age 27 years; <sup>c</sup>, before treatment at age 47 years; <sup>d</sup>, at age 18 years.

**Supplementary Table 4. Segregation of Very Rare Variants in Kindreds 318 and 1281 is Consistent with Paternity / Maternity**

Chr	Position (hg19)	Ref base	Nonref base	Gene	ExAC	Genotypes		
						318-1 (index case)	318-2 (mother)	318-3 (father)
chr1	36933522	C	T	<i>CSF3R</i>	Novel	<b>CT</b>	CC	CT
chr10	49968457	C	T	<i>WDFY4</i>	Novel	<b>CT</b>	CT	CC
chr11	533586	G	C	<i>HRAS</i>	8.3x10 <sup>-6</sup>	GC	CC	GC
chr12	29649201	T	G	<i>OVCH1</i>	Novel	<b>TG</b>	<b>TG</b>	TT
chr12	95694096	T	C	<i>VEZT</i>	Novel	TC	TT	TC
chr15	81633821	T	A	<i>TMC3</i>	6.5x10 <sup>-5</sup>	<b>TA</b>	<b>TA</b>	AA
chr19	2808339	A	G	<i>THOP1</i>	Novel	<b>AG</b>	AA	<b>AG</b>
chr3	195594345	T	C	<i>TNK2</i>	Novel	TC	TT	TC
chr9	139890991	G	A	<i>CLIC3</i>	4.7x10 <sup>-5</sup>	<b>GA</b>	<b>GA</b>	GG

Chr	Position (hg19)	Ref base	Nonref base	Gene	ExAC	Genotypes		
						1281-1 (index case)	1281-2 (father)	1281-3 (mother)
chr15	90333774	T	C	<i>ANPEP</i>	Novel	TC	TT	TC
chr12	1967782	C	T	<i>CACNA2D4</i>	1.7x10 <sup>-5</sup>	<b>CT</b>	CT	CC
chr17	78899186	A	G	<i>RPTOR</i>	9.2x10 <sup>-5</sup>	<b>AG</b>	<b>AG</b>	AA
chr14	94942473	C	G	<i>SERPINA9</i>	Novel	<b>CG</b>	CC	<b>CG</b>
chr1	53555521	C	T	<i>SLC1A7</i>	8.2x10 <sup>-6</sup>	<b>CT</b>	CT	CC

Chr, chromosome; hg19, human genome version 19; Ref base, reference base; Nonref base, non-reference base; Het/ Hom var, heterozygous versus homozygous variant; ExAC, frequency in the ExAC database; AA change, amino acid change.

All variants were heterozygous in the index case and were genotyped by PCR and Sanger sequencing in both parents. The nonreference allele is marked in bold. Segregation was consistent with paternity / maternity for all variants tested.

**Supplementary Table 5. Haplotypes flanking *CLCN2*<sup>Arg172Gln</sup> in three kindreds support no recent shared ancestry.**

Chr 3 Pos.	rs #	ExAC Freq	537 inferred haplotype	1786 inferred haplotype	3 inferred haplotype	537-1 Gntp	1786-1 Gntp	1786-2 Gntp	1786-3 Gntp	3-1 Gntp	3-4 Gntp	3-7 Gntp
184071017	rs41266265	0.265	G	A	A	G/G	G/A	A/A	G/A	G/A/	A/A	G/A
184071019	rs11920716	0.265	T	T	C	T/T	C/T	T/T	T/C	T/C	C/C	T/C
184071063	rs9820367	0.537	G	C	C	G/G	C/C	C/C	C/C	G/C	C/C	G/C
184075047	rs2228291	0.243	A	A	A	A/A	A/G	A/A	A/G	A/A	NA	A/A
184075850	*p.Arg172Gln*	Novel	T	T	T	C/T	C/T	C/T	C/T	C/T	C/T	C/T
184075958	rs41266271	0.285	C	T	T	C/C	C/T	T/T	T/C	C/T	T/T	C/T
184090266	rs6141	0.532	C	T	T	C/C	T/T	T/T	T/T	C/T	T/T	C/T
184099378	rs35929225	0.315	C	A	A	C/C	C/A	A/A	C/A	C/A	A/A	C/A
184101408	Novel	Novel	G	G	G	G/G	G/G	G/G	G/G	G/G	G/G	G/T
184289152	rs13069661	0.216	A	A	A	A/A	A/A	A/A	A/A	A/A	A/G	A/A
184293610	rs9823034	0.154	T	T	T/C	T/T	T/T	T/T	T/T	NA	T/C	T/C
184293769	rs7652597	0.329	T	C/T	T/C	T/T	C/T	C/T	C/T	T/C	T/C	T/C
184299068	rs9881589	0.181	G	G	G/A	G/G	G/G	G/G	G/G	G/A	G/A	G/A
184299167	rs1138510	0.316	T	T	T/C	T/T	T/T	T/T	T/T	T/C	T/C	T/C
184299414	rs2230596	0.224	C	C	C/T	C/C	C/C	C/C	C/C	NA	C/T	C/T
184428903	rs9872799	0.737	G/T	G	T	G/T	G/T	G/T	G/A	T/T	T/T	T/G

The inferred haplotypes for SNPs flanking the *CLCN2*<sup>Arg172Gln</sup> mutation in 3 kindreds (537, 1786 and Family 3) are shown. The maximum haplotype shared by kindred 537 with either of the other two kindreds is indicated in peach, and the maximum haplotype shared by kindreds 1786 and Family 3 is indicated in gray. The maximum haplotype shared among all three kindreds is enclosed by the black box. To the right of the columns showing inferred haplotypes, the genotypes (Gntp) of SNPs at each position in each family member are indicated. Chr 3 Pos., position on chromosome 3 in hg19; rs#, SNP identifier in dbSNP database (the novel mutation

shared by all kindreds is denoted \*p.Arg172Gln\*); ExAC Freq, frequency of minor allele in ExAC database; NA, insufficient data to make a genotype call.

**Supplementary Table 6. Enrichment of Rare *CLCN2* Variants with Large Effect in a Cohort of 35 Patients with PA Diagnosed by Age 10 years**

Gene	PA		Controls		OR (95% CI)	Fisher's Exact P-value
	Number of Variant Alleles	Number of Reference Alleles	Number of Variant Alleles	Number of Reference Alleles		
<i>CLCN2</i>	8	154	6	7150	61.7 (18.5, 219.4)	1.3x10 <sup>-10</sup>

Heterozygous variants were filtered for rarity (allele frequency  $\leq 10^{-5}$  across all samples in 1000 Genomes, EVS, and ExAC), and high-quality heterozygotes (pass GATK VQSR, minimum 8 total reads, GQ score  $\geq 20$ ). Only MetaSVM<sup>17</sup>-deleterious missense variants and loss-of-function (nonsense, canonical splice-site, frameshift indels) were included in the analysis. All variants were confirmed by *in silico* visualization of aligned reads. OR, odds ratio; 95% CI, 95% confidence interval. A two-tailed Fisher's exact test was conducted to compare the frequency of rare heterozygotes among index cases to 3,578 independent autism parental controls.

**Supplementary Table 7. Clinical Characteristics of Individuals from Family 3 without *CLCN2* p.Arg172Gln Variant**

Subject ID	Gender	Age dx/blood draw	BP (mmHg)	K <sup>+</sup> (mM)	Aldo (ng/dl)	PRA (ng/ml/h)	ARR (ng/dl: ng/ml/h)	FST	CT Adrenals
Normal range			<140/90	3.5-5.5			< 20	neg	normal
1	F	66	168/98**	3.7	24.8	0.4	62.0	pos	normal
6	F	49	Normal*	4.2	4.9	10.2	0.5	N/A	NA
12	F	20	110/70	4.2	10.1	2.9	3.5	N/A	NA
19	M	41	144/94**	3.9	26.7	0.7	38.1	neg	normal
24	M	35	Normal*	4.7	8.9	2.2	4.0	N/A	NA

Age dx, age at diagnosis; BP, blood pressure; K<sup>+</sup>, serum potassium level; Aldo, serum aldosterone level; PRA, plasma renin activity; ARR, aldosterone/renin ratio; FST, fludrocortisone suppression test; F, female; M, male; NA, not available; pos, positive; neg, negative; reference values are given below each parameter.

\*Self reported by patient and not on any antihypertensive medications

\*\*On no medications

**Supplementary Table 10. Primer Sequences.**

Forward		Reverse	
CLCN172F	5'-GGACCCCTGAAATGGGTGCATCG-3'	CLCN172R	5'-GTGAGTCGGGAGGGGGCCCGCCCTG-3'
CLCN865F	5'-GAGGAGTCTGACATCTGGTCCAGAC-3'	CLCN865R	5'-CATTCTGGGCTGACGGGCATGGCTAGC-3'
CLCN2_4_5_F	5'-ACAGCCTGTCGTATCAGCG-3'	CLCN2_4_5_R	5'-GCCTGGCCTCCTCTCC-3'
CLCK362SF	5'-CAGAGGACCTGAGGAGGCCTTAGTC-3'	CLCK362SR	5'-CTGCAGGAGCTGCCAGCCTTTGCTG-3'
clcm22Sf	5'-CTGGGAGAAGAGGAGTGGAGGCTC-3'	clcm22SR	5'-CAGGTCCCCTGCCCCACCCCAG-3'
M22K_F	5'-GAGCAGACCCTGAAGTATGGCCGGTAC-3'	M22K_R	5'-GTACCGCCATACTTCAGGGTCTGCTC-3'
Y26N_F	5'-GATGTATGGCCGGAACACTCAGGACC-3'	Y26N_R	5'-GGTCCTGAGTGTTCGGCCATACATC-3'
R172Q_F	5'-GAAGACCATCTTGCAGGGAGTGGTGCTG-3'	R172Q_R	5'-CAGCACCACTCCCTGCAAGATGGTCTT C-3'
K362 del new_F	5'-CTTCCTCATGAGACGCCTGCTCTTC-3'	K362 del new_R	5'-GAAGAGCAGGCGTCTCATGAGGAAG-3'
CLCN2E9-11_2Fs	5'-TCCTGTTCTGCCTGTGGTTA-3'	CLCN2E9-11_2R	5'-CCTCTGCTGTTCTTCCTTTAG-3'
K362gF	5'-CTTCCTCATGAGGTAGTGAGTGGCTCTC-3'	K362gR	5'-GAGAGCCACTCACTACCTCATGAGGAAG-3'
C2_E9-11SF	5'-CCCTCTTCAAACCCGATTC-3'	C2_E9-11SR	5'-ATGAACTGTCCAAAGCCAGG-3'

Sequences of indicated primers (see also Online Methods and Supplementary Note).



## Chapter 3

# Discussion

Out of the CLC isoforms studied in this thesis, CLC-Ka and -Kb are mainly involved in renal electrolyte reabsorption and the formation of the endocochlear potential, while CLC-2 is important in maintaining a specific intracellular chloride concentration and modulating the membrane potential in various cell types. While their specific roles may be different, their main task is similar: generating an appropriate chloride conductance in the plasma membrane. Acquired or hereditary conditions can alter the activity pattern of ion channels which may be compensated for or lead to a “*channelopathy*”, a disease caused by a malfunctioning ion channel. The effect may be further separated into a *gain-of-function* or *loss-of-function* of the respective channel. The threshold between health and disease is different for individual isoforms and — as shown for CLC-K/barttin — even different for each cell type the respective channel is expressed in. This strongly supports the notion that the surrounding environment of ion channels plays a critical role in determining physiology and pathophysiology.

### 3.1 Contribution from Our Studies

Barttin is the obligatory  $\beta$ -subunit of CLC-K channels<sup>[7,95]</sup>. Mutations of *BSND* that strongly attenuate or abolish CLC-K function cause Bartter syndrome type IVa, which is clinically characterized by a combination of renal failure and deafness. Interestingly, two *BSND* mutations, I12T<sup>[35]</sup> and V33L<sup>[96]</sup> have been reported to only cause deafness but not renal disease. In the first part of this thesis we characterized the V33L mutation in an immortalized renal cell line. We found that, in comparison with the wild type protein, V33L barttin was less effective in promoting CLC-K surface membrane insertion while single channel properties were not significantly altered. This partial loss-of-function of this mutation resembles the phenotype of the previously reported I12T mutation<sup>[35]</sup>. It was suggested that inner ear function is more sensitive to a loss of the CLC-K chloride conductance than kidney function. Therefore, our characterization of this second *BSND* mutation in cases of selective deafness provides the much needed support for this hypothesis.

In the second part of this thesis, we characterized several naturally occurring mutations of *CLCN2* in patients with familial primary hyperaldosteronism. We characterized the effects of these mutations in heterologous expression systems, studying ClC-2-mediated currents using patch-clamp. From our results we concluded that a constitutive increase of ClC-2 function in zona glomerulosa cells was responsible for aldosteronism probably via a  $\text{Ca}^{2+}$ -signaling pathway. Our work helped to identify and characterize a novel familial hyperaldosteronism-causing gene and provided a significant insight about the pathophysiology of this very prevalent disease.

## 3.2 Genetic Mutations Impair Behavior and Phenotype of ClC-K/barttin and ClC-2 Ion Channels

Naturally-occurring mutations in genes may have a number of effects: *First*, a mutation can change the expression of a gene. Such kind of mutations may take place in the noncoding area of a gene, resulting in altered transcription, splicing and cleavage of mRNA precursor or translation. *Second*, the nucleotide sequence encoding a protein may be changed by substitution, insertion, deletion or DNA fragment expansion or deletion. These mutations may be silent, in which case the change in DNA does not affect the amino acid sequence of the protein, or non-silent mutations, resulting in a change to the protein sequence. In this part I would like to talk about how non-silent, disease-causing mutations change the channel behavior of ClC-K/barttin or ClC-2, and how such changes alter the physiological function of an organ and lead to a certain disease phenotype.

### 3.2.1 Loss of Channel Activity and Phenotype

Disease causing mutations may reduce the function of a protein in various manners. The effect may be on the single channel activity itself, reducing the voltage-dependent open probability or affecting the single channel conductance. Such effects are the basis of many reported loss-of-function mutations in ClC-K/barttin or ClC-2<sup>[41,59,97-99]</sup>. Alternatively, the number of active channels in the plasma membrane may be reduced, either due to a reduction of expression of the protein through reduced transcription or translation. Closely related may be a decrease in protein stability, either via impaired protein folding or by facilitated protein degradation<sup>[100]</sup>, both reducing the overall amount of active proteins. In addition, alteration of protein trafficking and sorting to the right subcellular compartments may also reduce the number of functional proteins at their intended destination, especially important for the proper flow of electrolytes in epithelia<sup>[100]</sup>.

The barttin V33L mutation studied in this thesis, similar to the previously characterized I12T mutation, reduces the efficiency of surface membrane insertion of the channel complex, resulting in a smaller membrane chloride conductance. For both mutations, the

co-expressed V33L barttin/CIC-Ka and -Kb-mediated peak currents in whole cell patch-clamp were ~20% and ~60% preserved in the heterologous expression system, when compared with recordings of channels combined with wild type barttin<sup>[35,37]</sup>. Normalizing these currents for protein expression as indicated by the intensity of a linked fluorescent protein, suggested that the impact of V33L barttin on CIC-Ka might be more severe than indicated by patch-clamp experiments alone, reducing normalized CIC-Ka currents more than tenfold. The “next most severe” (as indicated by the magnitude of the remaining CIC-K/barttin currents) group of mutations in barttin encompasses the barttin G47R mutation which similarly decreases CIC-Ka currents to approximately ~10% when compared to wild type but attenuating CIC-Kb currents much stronger to ~15% of their wild type controls, respectively<sup>[100]</sup>. The G47R barttin mutation thus severely reduces the channel activity of both CIC-Ka and CIC-Kb yet retains enough currents so that the homozygous carrier patients develop typical clinical symptoms of antenatal BSND with only moderate severity. Patients carrying the V33L or I12T barttin mutations did not show any signs of typical Bartter syndrome kidney affection, neither later nor in the prenatal period<sup>[35,96]</sup>. Furthermore, mutations in barttin that result in the complete loss of CIC-K function result in a very pronounced, prenatal, Bartter syndrome<sup>[41,97-99]</sup>. Such a comparison supports the idea that the magnitude of loss-of-function is strongly correlated with severity of disease phenotype in BSND<sup>[29]</sup>, similar to the findings for mutations of CIC-Kb mutations in Bartter syndrome type III<sup>[101]</sup>.

However, the degree of the loss of channel activity does not always correlate with the severity of the disease phenotype. When compared with two disease causing mutations in CIC-Kb, P124L and V170M<sup>[101,102]</sup>, the V33L barttin mutation preserves similar levels of CIC-Kb channel activity, yet the CIC-Kb mutations lead to renal disease while V33L barttin does not. One explanation could be that biophysical characterizations under *in vitro* conditions only show the response to a small subset of possible stimuli and conditions which may not completely cover the native situation. As for P124L and V170M, the authors found that these two CIC-Kb mutants became less active when exposed to pH 8.5 or 20 mM extracellular Ca<sup>2+</sup>. Those conditions do not represent physiological conditions of basolateral CIC-Kb/barttin channels, but still signify how a study in more native environments may be critical to explain the true behavior of ion channels. Another aspect is that mutations of CIC-K or barttin may not only reduce macroscopic currents, but also affect other behaviors of the channel, for example, protein sorting. The E88X barttin mutation truncates two thirds of the total amino acids, but surprisingly leaves CIC-K ion conduction unaffected. However, CIC-K/barttin complexes are no longer sorted to the correct epithelial surface, showing equal insertion to the apical and basolateral side leading to a loss of directed transepithelial movement of chloride<sup>[100]</sup>. Consequently, the patient carrying barttin E88X suffered from the full range of BSND symptoms as if barttin had been totally removed<sup>[97]</sup>. No such case has been described for mutations in CIC-Ka or -Kb so far but polar insertion of CIC-K channels has rarely been studied, so far. Our unpublished data suggested that the basolateral sorting of the channel was not changed by the V33L mutation, however.

### 3.2.2 Gain-of-Function

It appears that epithelial transport proteins have been optimized during evolution for maximum transport efficiency. Further increase of conductance is thus unlikely to result in immediate disease, rendering the human body likely more tolerant to gain-of-function than loss-of-function mutations such as those of *ClC-K* in our case. One example, the naturally occurring T481S mutation of *ClC-Kb* is known to increase the channel activity, and may be linked to salt-dependent hypertension in specific communities<sup>[103,104]</sup>, but additionally lowers the hearing threshold of the carrier individuals, having a potentially beneficial effect on mutation carriers<sup>[105]</sup>.

Nevertheless, when it comes to *ClC-2*, the story is different, because *ClC-2* has different roles from *ClC-K*. In this thesis, we have found several mutations (M22K, Y26N, R172Q, Lys362del and S865R) that slightly increase the activity of *ClC-2* with the outcome of excessive production of aldosterone by zona glomerulosa cells. In contrast, a similarly small change in  $\text{Cl}^-$  conductance through epithelial *ClC-K/barttin* channels would likely not produce any symptoms.

In order to understand this difference in sensitivity to the change in protein function, one needs to be reminded of the nature of zona glomerulosa cells. As stated in the introduction, the cells within the zona glomerulosa have been demonstrated to be electrically excitable<sup>[106]</sup>. Similar to other electrical excitable tissues, the resting potential is determined by a  $\text{K}^+$  conductance<sup>[107]</sup>. The processes governing depolarization are not completely uncovered yet, but definitely require the presence of  $\text{Ca}_v3.2$  T-type  $\text{Ca}^{2+}$  channels. Repolarization likely requires  $\text{Ca}^{2+}$ -activated  $\text{K}^+$ -channels, so called “BK-channels”<sup>[108]</sup>.

One of the *ClC-2* mutations associated hyperaldosteronism, R172Q, studied in this thesis increased the basal membrane potential of the human adrenocortical cell line HAC15. This particular cell line is close to the physiological zona glomerulosa cell in that it contains the necessary enzymes for aldosterone production as well as TASK/TREK background potassium channels<sup>[109]</sup>. Typically, the resting plasma membrane potential is mainly set by the reversal potential of  $\text{K}^+$  ions. If  $\text{Cl}^-$  was only passively distributed between the intra- and extracellular space, the  $\text{Cl}^-$  ion distribution on both sides of the plasma membrane would be equilibrated according to the electrochemical potential set by  $\text{K}^+$  ions. However, many cells actively transport  $\text{Cl}^-$  across the cellular membrane, for example, via the ubiquitous Na-K-2Cl co-transporter (NKCC1), resulting in a shift of the  $\text{Cl}^-$  reversal potential away from the membrane potential. The difference between the Nernst potential for  $\text{Cl}^-$  and the membrane potential generates a driving force for  $\text{Cl}^-$  to move passively out or into the cell via active chloride channels. A transient increase of  $\text{Cl}^-$  permeability via the activation of chloride channels in the plasma membrane shifts the membrane potential towards the reversal potential of  $\text{Cl}^-$ , therefore can be either depolarizing or hyperpolarizing. A prime example for this mechanism is the activation of  $\text{GABA}_A$  channels in neurons which transiently opens a chloride channel that, due to the low intracellular  $\text{Cl}^-$  concentration in adult neurons, hyperpolarizes the cell, thereby inhibiting neuronal excitability.

We have found that expression of the R172Q ClC-2 mutant led to more depolarized membrane potentials in HAC15 cells when compared to the expression of wild type ClC-2. Combined with the knowledge of higher open probabilities in R172Q ClC-2, we have to assume that the Cl<sup>-</sup> permeability of these cells increases. We can infer that the reversal potential of Cl<sup>-</sup> in HAC15 cells must be more positive than the membrane potential as determined by the electrochemical gradient of K<sup>+</sup>. Therefore, we have to assume that Cl<sup>-</sup> ions are actively transported into the cells, possibly via the ubiquitously expressed NKCC1. HAC15 cells therefore end up with an accumulation of Cl<sup>-</sup> in the cell and a Cl<sup>-</sup> reversal potential higher than the membrane potential. This mirrors the situation in murine zona glomerulosa cells where we determined the intracellular [Cl<sup>-</sup>] in acute slice preparations to be at a level of approximately 75 mM. Our hypothesis is that, due to the increase in chloride permeability in cells expressing ClC-2 mutations, the membrane potential rises constitutively and Ca<sup>2+</sup> is likely to enter the cell in greater amount due to the activation of voltage dependent calcium channels. As stated in the introduction, Ca<sup>2+</sup> is the main intracellular stimulus for the production of aldosterone<sup>[63]</sup>, explaining the link between changes in ClC-2 function and an increase of aldosterone synthesis.



# Bibliography

- [1] T. J. Jentsch, *CLC chloride channels and transporters: from genes to protein structure, pathology and physiology.*, vol. 43 (2008).
- [2] D. C. Gadsby, P. Vergani, L. Csanády, *Nature* **440**, 477 (2006).
- [3] R. W. Olsen, T. M. DeLorey, *GABA Receptor Physiology and Pharmacology*. In: Siegel GJ, Agranoff BW, Albers RW, et al., editors. *Basic Neurochemistry: Molecular, Cellular and Medical Aspects*. 6th edition (Philadelphia: Lippincott-Raven, 1999).
- [4] A. Dereeper, et al., *Nucleic Acids Research* **36**, W465 (2008).
- [5] A. Dereeper, S. Audic, J.-M. Claverie, G. Blanc, *BMC Evolutionary Biology* **10**, 8 (2010).
- [6] T. J. Jentsch, K. Steinmeyer, G. Schwarz, *Nature* **348**, 510 (1990).
- [7] R. Estévez, et al., *Nature* **414**, 558 (2001).
- [8] K. Steinmeyer, C. Ortland, T. J. Jentsch, *Nature* **354**, 301 (1991).
- [9] A. Thiemann, S. Gründer, M. Pusch, T. J. Jentsch, *Nature* **356**, 57 (1992).
- [10] X. Li, T. Wang, Z. Zhao, S. A. Weinman, *American Journal of Physiology-Cell Physiology* **282**, C1483 (2002).
- [11] J. J. Matsuda, et al., *American Journal of Physiology-Cell Physiology* **294**, C251 (2008).
- [12] A. Picollo, M. Pusch, *Nature* **436**, 420 (2005).
- [13] I. Neagoe, T. Stauber, P. Fidzinski, E.-Y. Bergsdorf, T. J. Jentsch, *Journal of Biological Chemistry* **285**, 21689 (2010).
- [14] L. Leisle, C. F. Ludwig, F. A. Wagner, T. J. Jentsch, T. Stauber, *The EMBO Journal* **30**, 2140 (2011).
- [15] C. Miller, *Philosophical transactions of the Royal Society of London. Series B, Biological sciences* **299**, 401 (1982).
- [16] R. Dutzler, E. B. Campbell, M. Cadene, B. T. Chait, R. MacKinnon, *Nature* **415**, 287 (2002).
- [17] L. Feng, E. B. Campbell, Y. Hsiung, R. MacKinnon, *Science* **330**, 635 (2010).

- [18] E. Park, E. B. Campbell, R. MacKinnon, *Nature* **541**, 500 (2016).
- [19] A. Bateman, *Trends in Biochemical Sciences* **22**, 12 (1997).
- [20] S. Markovic, R. Dutzler, *Structure* **15**, 715 (2007).
- [21] G. Q. Martinez, M. Maduke, *PLoS ONE* **3**, e2746 (2008).
- [22] G. Stölting, S. Bungert-Plümke, A. Franzen, C. Fahlke, *Journal of Biological Chemistry* **290**, 30406 (2015).
- [23] S. Hebeisen, *et al.*, *Journal of Biological Chemistry* **279**, 13140 (2004).
- [24] S. Hebeisen, C. Fahlke, *Biophysical Journal* **89**, 1710 (2005).
- [25] G. Stölting, *et al.*, *Pflügers Archiv European Journal of Physiology* **465**, 1423 (2013).
- [26] B. Bennetts, Y. Yu, T. Y. Chen, M. W. Parker, *Journal of Biological Chemistry* **287**, 25808 (2012).
- [27] T. Yamada, M. Krzeminski, Z. Bozoky, J. D. Forman-Kay, K. Strange, *Biophysical Journal* **111**, 1876 (2016).
- [28] S. Kieferle, P. Fong, M. Bens, A. Vandewalle, T. J. Jentsch, *Proceedings of the National Academy of Sciences of the United States of America* **91**, 6943 (1994).
- [29] C. Fahlke, M. Fischer, *Frontiers in physiology* **1**, 155 (2010).
- [30] S. Waldegger, *et al.*, *Pflügers Archiv : European journal of physiology* **444**, 411 (2002).
- [31] K. Kobayashi, S. Uchida, S. Mizutani, S. Sasaki, F. Marumo, *Journal of the American Society of Nephrology : JASN* **12**, 1327 (2001).
- [32] U. Scholl, *et al.*, *Proceedings of the National Academy of Sciences of the United States of America* **103**, 11411 (2006).
- [33] B. K. Krämer, T. Bergler, B. Stoelcker, S. Waldegger, *Nature clinical practice. Nephrology* **4**, 38 (2008).
- [34] G. Stölting, M. Fischer, C. Fahlke, *Pflügers Archiv - European Journal of Physiology* pp. 2191–2204 (2014).
- [35] S. Riazuddin, *et al.*, *American journal of human genetics* **85**, 273 (2009).
- [36] M. Fischer, A. G. H. Janssen, C. Fahlke, *Journal of the American Society of Nephrology : JASN* **21**, 1281 (2010).
- [37] H. Tan, S. Bungert-Plümke, C. Fahlke, G. Stölting, *Frontiers in Physiology* **8** (2017).
- [38] D. B. Simon, R. P. Lifton, *Current opinion in cell biology* **10**, 450 (1998).
- [39] D. B. Simon, *et al.*, *Nature Genetics* **14**, 152 (1996).
- [40] D. B. Simon, *et al.*, *Nat Genet* **17**, 171 (1997).

- [41] R. Birkenhäger, *et al.*, *Nature genetics* **29**, 310 (2001).
- [42] K. P. Schlingmann, *et al.*, *New England Journal of Medicine* **350**, 1314 (2004).
- [43] R. Vargas-Poussou, *et al.*, *Journal of the American Society of Nephrology : JASN* **13**, 2259 (2002).
- [44] S. Watanabe, *et al.*, *The Lancet* **360**, 692 (2002).
- [45] F. C. Bartter, P. Pronove, J. R. Gill, R. C. MacCardle, *The American Journal of Medicine* **33**, 811 (1962).
- [46] S. C. Hebert, *Current opinion in nephrology and hypertension* **12**, 527 (2003).
- [47] G. Rickheit, *et al.*, *The EMBO journal* **27**, 2907 (2008).
- [48] F. Nin, *et al.*, *Proceedings of the National Academy of Sciences* **109**, 9191 (2012).
- [49] S. K. Boshier, R. L. Warren, *Proceedings of the Royal Society B: Biological Sciences* **171**, 227 (1968).
- [50] T. Konishi, P. E. Hamrick, P. J. Walsh, *Acta Oto-Laryngologica* **86**, 22 (1978).
- [51] N. Jeck, *et al.*, *PEDIATRICS* **108**, e5 (2001).
- [52] Y. Matsumura, *et al.*, *Nature genetics* **21**, 95 (1999).
- [53] E. M. Schwiebert, *et al.*, *Proceedings of the National Academy of Sciences of the United States of America* **95**, 3879 (1998).
- [54] A. Sík, R. L. Smith, T. F. Freund, *Neuroscience* **101**, 51 (2000).
- [55] M. Catalán, M. I. Niemeyer, L. P. Cid, F. V. Sepúlveda, *Gastroenterology* **126**, 1104 (2004).
- [56] I. Rinke, J. Artmann, V. Stein, *The Journal of neuroscience : the official journal of the Society for Neuroscience* **30**, 4776 (2010).
- [57] K. Staley, R. Smith, J. Schaack, C. Wilcox, T. J. Jentsch, *Neuron* **17**, 543 (1996).
- [58] C. Saint-Martin, *et al.*, *Human Mutation* **30**, 397 (2009).
- [59] C. Depienne, *et al.*, *The Lancet Neurology* **12**, 659 (2013).
- [60] U. I. Scholl, *et al.*, *Nature Genetics* (2018).
- [61] M. R. Bösl, *et al.*, *The EMBO Journal* **20**, 1289 (2001).
- [62] M. B. Hoegg-Beiler, *et al.*, *Nature Communications* **5**, 3475 (2014).
- [63] C. D. Clyne, P. C. White, W. E. Rainey, *Endocrine research* **22**, 485 (1996).
- [64] C. D. Clyne, *et al.*, *Molecular Endocrinology* **11**, 638 (1997).
- [65] M. Choi, *et al.*, *Science* **331**, 768 (2011).

- [66] U. I. Scholl, *et al.*, *eLife* **4** (2015).
- [67] U. I. Scholl, *et al.*, *Nature genetics* **45**, 1050 (2013).
- [68] M. Pusch, K. Steinmeyer, T. Jentsch, *Biophysical Journal* **66**, 149 (1994).
- [69] C. Saviane, F. Conti, M. Pusch, *The Journal of general physiology* **113**, 457 (1999).
- [70] T. J. Jentsch, *CLC Chloride Channels and Transporters: From Genes to Protein Structure, Pathology and Physiology*, vol. 43 (2008).
- [71] T. T. Chen, *et al.*, *Neurology* **80**, 1078 (2013).
- [72] E. Seong, *Molecular Biology of the Cell* **16**, 128 (2004).
- [73] F. J. Miller, *et al.*, *Circulation Research* **101**, 663 (2007).
- [74] Z. Zhao, X. Li, J. Hao, J. H. Winston, S. A. Weinman, *Journal of Biological Chemistry* **282**, 29022 (2007).
- [75] R. E. Guzman, E. Miranda-Laferte, A. Franzen, C. Fahlke, *Journal of Biological Chemistry* **290**, 25851 (2015).
- [76] R. E. Guzman, M. Grieschat, C. Fahlke, A. K. Alekov, *ACS Chemical Neuroscience* **4**, 994 (2013).
- [77] S. M. Stobrawa, *et al.*, *Neuron* **29**, 185 (2001).
- [78] Y. Yu, L. Ye, Y.-G. Li, D. J. Burkin, D. D. Duan, *International Journal of Cardiology* **214**, 218 (2016).
- [79] M. A. van Slegtenhorst, *et al.*, *Human molecular genetics* **3**, 547 (1994).
- [80] T. Friedrich, T. Breiderhoff, T. J. Jentsch, *The Journal of biological chemistry* **274**, 896 (1999).
- [81] G. Orhan, C. Fahlke, A. K. Alekov, *Biophysical Journal* **100**, 1233 (2011).
- [82] R. E. Guzman, S. Bungert-Plümke, A. Franzen, C. Fahlke, *Journal of Biological Chemistry* **292**, 19055 (2017).
- [83] H. Hu, *et al.*, *Molecular Psychiatry* **21**, 133 (2016).
- [84] E. E. Palmer, *et al.*, *Molecular Psychiatry* **23**, 222 (2018).
- [85] K. Steinmeyer, B. Schwappach, M. Bens, a. Vandewalle, T. J. Jentsch, *The Journal of biological chemistry* **270**, 31172 (1995).
- [86] T. Suzuki, *et al.*, *Journal of Cellular Physiology* **206**, 792 (2006).
- [87] M. Hara-Chikuma, Y. Wang, S. E. Guggino, W. B. Guggino, A. Verkman, *Biochemical and Biophysical Research Communications* **329**, 941 (2005).
- [88] B. Maranda, *et al.*, *Journal of Biological Chemistry* **276**, 18540 (2001).

- [89] N. Piwon, W. Günther, M. Schwake, M. R. Bösl, T. J. Jentsch, *Nature* **408**, 369 (2000).
- [90] O. M. Wrong, A. G. Norden, T. G. Feest, *QJM : monthly journal of the Association of Physicians* **87**, 473 (1994).
- [91] M. Poet, *et al.*, *Proceedings of the National Academy of Sciences* **103**, 13854 (2006).
- [92] D. Kasper, *et al.*, *The EMBO Journal* **24**, 1079 (2005).
- [93] P. F. Lange, L. Wartosch, T. J. Jentsch, J. C. Fuhrmann, *Nature* **440**, 220 (2006).
- [94] S. Weinert, *et al.*, *Science (New York, N.Y.)* **328**, 1401 (2010).
- [95] S. Waldegger, *et al.*, *Pflügers Archiv : European journal of physiology* **444**, 411 (2002).
- [96] S. Shafique, *et al.*, *PloS one* **9**, e100146 (2014).
- [97] F. Ozlu, *et al.*, *Pediatric Nephrology* **21**, 1056 (2006).
- [98] R. P. Bhamkar, a. Gajendragadkar, *Indian journal of nephrology* **19**, 23 (2009).
- [99] L. A. Plumb, *et al.*, *The Lancet* **388**, 631 (2016).
- [100] A. G. H. Janssen, *et al.*, *Journal of the American Society of Nephrology : JASN* **20**, 145 (2009).
- [101] O. Andrini, *et al.*, *American Journal of Physiology - Renal Physiology* **308**, F1324 (2015).
- [102] O. Andrini, *et al.*, *Pflügers Archiv - European Journal of Physiology* **466**, 1713 (2014).
- [103] N. Jeck, *et al.*, *Hypertension* **43**, 1175 (2004).
- [104] S. Sile, *et al.*, *Journal of hypertension* **27**, 298 (2009).
- [105] A. Frey, *et al.*, *Hearing Research* **214**, 68 (2006).
- [106] C. Hu, C. G. Rusin, Z. Tan, N. A. Guagliardo, P. Q. Barrett, *Journal of Clinical Investigation* **122**, 2046 (2012).
- [107] G. Czirják, P. Enyedi, *Molecular endocrinology (Baltimore, Md.)* **16**, 621 (2002).
- [108] P. Q. Barrett, *et al.*, *The Journal of Physiology* **594**, 5851 (2016).
- [109] J. Parmar, R. E. Key, W. E. Rainey, *The Journal of Clinical Endocrinology & Metabolism* **93**, 4542 (2008).



# Zusammenfassung

Die Familie der CLC Chlorid-Kanäle ist verantwortlich für den Transport des am häufigsten vorkommenden Anions im menschlichen Körper,  $\text{Cl}^-$ . Sie sind an vielen physiologischen Funktionen beteiligt, wie etwa der Einstellung und Aufrechterhaltung des Ruhemembranpotentials, der intrazellulären oder vesikulären Chloridkonzentration sowie des pH-Wertes, wie auch der Erregbarkeit der Skelettmuskulatur. In der Vergangenheit konnten viele Mutationen in CLC-Genen genetischen Erkrankungen zugeordnet werden. Dieses Wissen um die Pathophysiologie konnte letztlich häufig auch helfen, Verständnis für die Physiologie dieser Proteine zu entwickeln. In dieser Arbeit konnten wir verschiedene, natürlich vorkommende Mutationen in CLC-K/Barttin und CLC-2 Kanälen beschreiben.

CLC-Ka- und -Kb-Kanäle finden sich vorwiegend in den Epithelien des Nephrons und in den Marginalzellen der Innenohren. Sie spielen daher eine zentrale Rolle für die Nierenfunktion und das Hören. Barttin ist die  $\beta$ -Untereinheit von CLC-K, essentiell für die Reifung, die richtige Sortierung und das Gating des Kanals. Ein Funktionsverlust von barttin führt ebenfalls zu einem Verlust der Funktion von CLC-K und führt zum Bartter-Syndrom Typ IV mit Symptomen wie Nierenversagen und Taubheit. Im ersten Teil dieser Arbeit charakterisierten wir die Mutante barttin V33L, die in einer pakistanischen Familie nur Taubheit, aber keine Nierenerkrankung verursachte. Wir folgerten, dass die nur teilweise verminderte CLC-K-Membranleitfähigkeit für den Phänotyp verantwortlich sein könnte.

CLC-2 wird im Körper weit verbreitet exprimiert. Der Kanal ist wichtig für die Aufrechterhaltung der intrazellulären  $\text{Cl}^-$  Konzentrationen und des Ruhemembranpotentials. Im zweiten Teil dieser Arbeit haben wir einige Mutationen in CLC-2 untersucht, welche bei Patienten mit Hyperaldosteronismus identifiziert werden konnten. Wir fanden heraus, dass diese Mutationen die Offen-Wahrscheinlichkeit des Kanals in HEK293T-Zellen erhöhten. In HAC15 Zellen, welche mutierte CLC-2 Kanäle exprimierten, war das Ruhemembranpotential erhöht sowie die Expression der Aldosteron-Synthase erhöht. Wir schlossen daraus, dass der Funktionsgewinn dieser CLC-2-Mutanten das Ruhepotential von Zona glomerulosa Zellen erhöht und zu einer übermäßigen und unregulierten Produktion von Aldosteron führt.



# ERKLÄRUNG

Ich versichere an Eides statt, dass die Dissertation von mir selbständig und ohne unzulässige fremde Hilfe unter Beachtung der "Grundsätze zur Sicherung guter wissenschaftlicher Praxis an der Heinrich-Heine-Universität Düsseldorf" erstellt worden ist. Die Dissertation wurde in der vorgelegten oder in ähnlicher Form noch bei keiner anderen Institution eingereicht. Ich habe bisher keine erfolglosen Promotionsversuche unternommen.

Hua TAN \_\_\_\_\_ Jülich, \_\_\_\_\_